ANALYSIS AND DESIGN OF NONLINEAR FIBER OPTIC COMMUNICATION SYSTEMS

ANALYSIS AND DESIGN OF NONLINEAR FIBER OPTIC COMMUNICATION SYSTEMS

BY

ELHAM BIDAKI, M.A.Sc.

A THESIS

SUBMITTED TO THE DEPARTMENT OF ELECTRICAL AND COMPUTER ENGINEERING

AND THE SCHOOL OF GRADUATE STUDIES

OF MCMASTER UNIVERSITY

IN PARTIAL FULFILMENT OF THE REQUIREMENTS

FOR THE DEGREE OF

DOCTOR OF PHILOSOPHY

Doctor of Philosophy (2020) McMaster University

(Department of Electrical and Computer Engineering) Hamilton, Ontario, Canada

TITLE:	Analysis and Design of Nonlinear Fiber Optic Communication Systems
AUTHOR:	Elham Bidaki M.A.Sc., (Electrical and Computer Engineering) Iran University of Science and Technology, Tehran, Iran
SUPERVISOR:	Prof. Shiva Kumar
NUMBER OF PAGES:	xvii, 125

Abstract

Fiber-optic systems represent the backbone of the communication networks, carrying most of the world's data traffic. The main bottleneck in today's fiber-optic communication systems has roots in the inherent nonlinearity of the fiber. Hence, developing new transmission schemes that are compatible with the nonlinear behavior of the optical fiber has become necessary.

To utilize the full transmission capacity of an optical fiber, this thesis investigates two different techniques—compensation-based method and nonlinear Fourier transform (NFT).

For the purpose of suppressing the nonlinear distortion in real time, an optical back propagation (OBP) technique using Raman pumped dispersion compensating fibers (DCF). OBP, as an all-optical signal processing technique, can compensate for both intra- and inter-channel nonlinear impairments in real time in point-to-point systems as well as in optical networks. The proposed inline OBP module consists of an optical phase conjugator (OPC), amplifiers and a Raman pumped DCF. In order to suppress the nonlinear effects of the transmission fiber, the power in the OBP fiber should increase exponentially with distance. This can be approximately achieved by using Raman pumping of the backpropagation fiber. Simulation results show that this technique provides 7.7 dB performance improvement in Q-factor over conventional systems.

The second part of this thesis is dedicated to the NFT as a promising framework to exploit the inherent nonlinearity of optical fiber rather than treating it as an undesirable effect and using perturbation and approximation-based methods to mitigate it. A novel

multistage perturbation technique to realize the NFT as a cascade of linear discrete Fourier transforms is developed. The linear Fourier transform can be easily implemented in the optical domain using a time lens or discrete photonic components, which can be implemented in silicon photonics. The proposed technique provides a promising way to implement NFT in the optical domain, which will fully utilize the potential of NFT for wavelength-division multiplexed fiber-optic systems in the optical domain.

Moreover, a nonlinear frequency-division multiplexed (NFDM) transmission scheme with midpoint OPC is investigated. The proposed mid-OPC NFDM system offers a degree of freedom to have a flexible power normalization factor, P_n to minimize the signal-noise mixing in NFT processing for a specific launch power, resulting in significant system performance improvement up to 5.6 dB in Q-factor over conventional NFDM systems. Another advantage of the proposed scheme is that the mid-OPC NFDM system extends the transmission reach without having to increase the guard interval, which leads to higher spectral efficiency.

To my beloved parents

Fatemeh and Hassan

Acknowledgments

I would like to express my sincere appreciation to my supervisor, Prof. Shiva Kumar, for all his consistent support and technical guidance during the running of this project. Without his persistent help, the goal of this project would not have been realized. I am also extremely grateful for all his endless efforts and patience to revise and improve my academic papers.

I would like to thank my supervisory committee, Prof. Xun Li and Prof. Mohamed Bakr, for their valuable feedbacks and technical supports during my study. I would also like to express my gratitude to my external examiner, Prof. Frank Kschischang, for his careful reading of the dissertation and his constructive suggestions.

I am very thankful to all my colleagues and friends, who made my Ph.D. journey enjoyable and smooth. I would also like to thank all the administrative staff at the Department of Electrical and Computer Engineering, in particular Cheryl Gies for providing all the convenience and assistance I have needed.

I would like to give special thanks to my high school math teacher, Shekoofeh Kaveh, whose inspirational words of encouragement ring in my ears.

Finally, I must express my very profound gratitude to my mother, my father, and my siblings for providing me with unfailing support and continuous encouragement throughout my studies, without which all my achievements would have simply been impossible.

Contents

List of Figures

List of Tables

Abbreviations

ADC	Analog-to-Digital Converter
ADC	Analog-to-Digital Converter
AL	Ablowitz-Ladik
ASE	Amplified Spontaneous Emission
AWGN	Additive White Gaussian Noise
BER	Bit Error Rate
BPF	Band Pass Filter
CS	Continuous Spectrum
DBP	Digital Back Propagation
DCF	Dispersion Compensating Fiber
DDF	Dispersion Decreasing Fiber
DFT	Discrete Fourier Transform
DMUX	Demultiplexer
DP	Dual Polarization
DPC	Digital Phase Conjugator

DSP	Digital Signal Processing
DVF	Dispersion-varying Fiber
EDC	Electronic Dispersion Compensation
FBG	Fiber Bragg Grating
FEC	Forward Error Correction
FFT	Fast Fourier Transform
FIR	Finite Impulse Response
FT	Fourier Transform
FWM	Four-wave Mixing
GI	Guard Interval
GN	Gaussian Noise
GVD	Group Velocity Dispersion
HDF	High-Dispersion Fiber
HNLF	Highly Nonlinear Fiber
IDFT	Inverse Discrete Fourier Transform
IFWM	Intra-Channel Four Wave Mixing
INFT	Inverse Nonlinear Fourier Transform
ISI	Inter-Symbol Interference
IST	Inverse Scattering Transform
IXPM	Intra-Channel Cross-Phase Modulation

LPA	Lossless Path-averaged
Mod	Modulator
MUX	Multiplexer
NFDM	Nonlinear Frequency-Division Multiplexing
NFT	Nonlinear Fourier Transform
NLSE	Nonlinear Shrödinger Equation
NZDSF	Non-Zero Dispersion-Shifted Fiber
OBP	Optical Back Propagation
OBPF	Optical Backpropagation Fiber
OFDM	Orthogonal Frequency-Division Multiplexing
OPC	Optical Phase Conjugator
OSNR	Optical Signal-to-Noise Ratio
PDM	Polarization Division Multiplexing
PMD	Polarization Mode Dispersion
PM	Polarization Multiplexing
QAM	Quadrature Amplitude Modulation
RIN	Relative Intensity Noise
ROADM	Reconfigurable Optical Add-Drop Multiplexer
Rx	Receiver
SBS	Stimulated Brillouin Scattering

SE	Spectral Efficiency
SNR	Signal-to-Noise Ratio
SPM	Self-Phase Modulation
SRS	Stimulated Raman Scattering
SSFS	Split-Step Fourier Scheme
SSMF	Standard Single-Mode Fiber
TF	Transmission Fiber
TIB	Toeplitz Inner Boarding
Tx	Transmitter
WDM	Wavelength Division Multiplexing
WDM-PON	Wavelength Division Multiplexing-Passive Optical Network
XPM	Cross-Phase Modulation

Chapter 1

Introduction and Problem Statement

1.1 Fiber-optic Communication Systems

Optical fibers have revolutionized the world of telecommunication due to their extremely large bandwidth, low loss, resistance to electromagnetic interference, their small size and light weight. Several Tera bits of information within a second (10^{12} bps) can be sent (Agrawal, 2012). Nowadays, more than 80% of world long distance traffic is carried over fiber-optics (Kumar and Deen, 2014). In fact, fiber-optic systems are the main backbone of today's communication systems worldwide, and it is of significant importance to get a thorough understanding of their characteristics and performance.

A fiber-optic communication system is an optical communication system that uses an optical fiber as the transmission channel (Agrawal, 2012). A typical wavelength division multiplexed (WDM) fiber-optic system is illustrated in Fig. 1.1. In a WDM system, multiple optical carriers of different wavelengths are modulated by independent electrical data. The modulated signals are multiplexed together and sent into the channel. The channel is made of several spans of optical fibers and optical amplifiers. At the end of the fiber-optic link, the signals are demultiplexed and the information is retrieved by a bank of receivers (RXs).

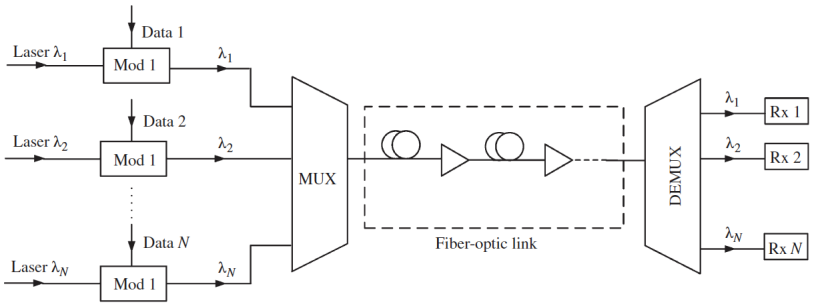

Figure 1.1: A typical fiber-optic communication system (Kumar and Deen, 2014).

1.1.1 Impairments in Fiber-optic Links

Despite all the advantages, fiber propagation loss, chromatic dispersion and Kerr nonlinearity are the major limiting factors, restricting fiber-optic systems capacity and realization (Agrawal, 2012; Essiambre *et al.*, 2010). These characteristics, by either acting alone or interacting with each other, cause performance degradation which needs to be dealt with.

First of all, optical fibers are lossy, i.e., the power of the optical signal decreases during propagation (with a typical attenuation coefficient of 0.2 dB/km) (Agrawal, 2012). Therefore, in long-haul transmission systems, it is essential to amplify the optical signal using Erbium doped amplifiers (EDFA) which, unfortunately, add amplified spontaneous emission (ASE) noise. Distributed Raman amplification is a viable alternative to EDFAs which amplifies the signal along the fiber link. Distributed Raman amplification also introduces ASE noise and relative intensity noise (RIN). However, due to the distributed nature of amplification, the transmission performance is better than that of systems with EDFA.

Chromatic Dispersion (CD) is a fiber impairment that tends to broaden the signal propagating along the optical fiber due to the dependence of refractive index of the fiber on wavelength. Different frequency components within the same pulse travel at different velocities, leading to signal distortion causing inter-symbol interference (ISI) (Agrawal, 2012; Kumar and Deen, 2014). There are different techniques to compensate for dispersion. Special dispersion compensating fibers (DCF) (Antos and Smith, 1994) and fiber brag grating (FBG) (Hill *et al.*, 1994) have been developed to be used as optical means to compensate

for the dispersion, which provides an all-optical, fiber-based solution to the dispersion problem. With the advent of coherent detection, since the receiver has access to the complex optical field envelope, electronic dispersion compensation (EDC) techniques can also be used to compensate for fiber dispersion (Li, 2009). Dispersion is usually described by the group velocity dispersion (GVD) parameter β_2, which is measured in ps^2/km, or by the dispersion parameter $D = -2\pi c\beta_2/\lambda^2$ in ps/(nm.km), where c and λ are the speed of light and wavelength, respectively.

Once both loss and dispersion effects are compensated, Kerr nonlinearity becomes the limiting factor (Agrawal, 2012). In 1875, John Kerr discovered the effect that now bears his name. Kerr effect is an electro optic effect that the refractive index, n of the material is changed by an amount proportional to the applied optical intensity, i.e., $n(\omega, I) = n_0(\omega) + n_2 I$, where n_0, n_2 and I are linear refractive index, Kerr coefficient, and optical intensity, respectively (Agrawal, 2012). Kerr coefficient n_2 is measured in m^2/W. This means that as the optical intensity increases, the induced phase delay in the fiber gets larger. This intensity dependence of the refractive index causes numerous nonlinear interactions: One of the consequences of the Kerr effect is self-phase modulation (SPM). Since the change in refractive index due to the Kerr effect translates into a phase shift, the signal phase is modulated by its power distribution, which is known as SPM. SPM is the most common nonlinear effect in single mode fibers (SMF). Further, the phase of a signal is modulated not only by its power i.e., SPM, but also by other signals, which is known as cross phase modulation (XPM).

The nonlinear interaction among pulses of the same channel is known as intra-channel nonlinear effects (Kumar and Deen, 2014; Essiambre *et al.*, 1999). In a single channel fiber-optic link, the Kerr effect results in self-phase modulation (SPM), intra-channel cross-phase modulation (IXPM), and intra-channel four wave mixing (IFWM). SPM and IXPM mean the intensity dependent nonlinear phase shifts added to an optical pulse due to the presence of the same pulse and a neighboring pulse, respectively. Nonlinear interaction among signal

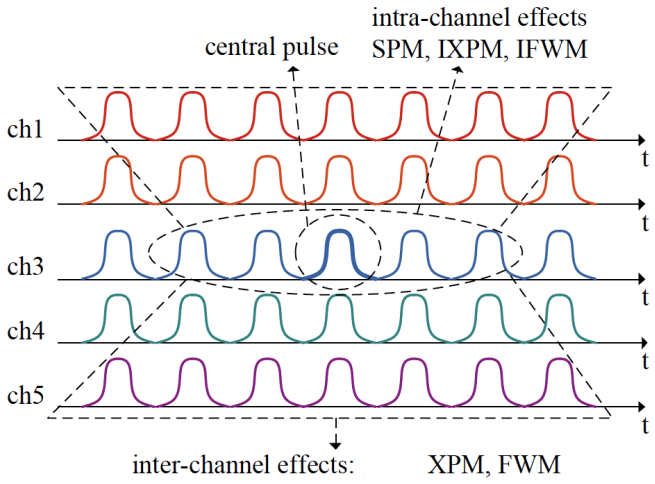

Figure 1.2: Intra-channel and inter-channel nonlinear effects.

.

pulses centered at t_1, t_2 and t_3 leads to echo pulses centered at $(t_1+t_2\pm t_3)$ which is known as IFWM. As shown in Fig. 1.2, the intra-channel effects are due to the nonlinear interactions of optical pulses of a same channel (e.g. ch3).

In a WDM system, the nonlinear interactions between pulses of different channels are called inter-channel nonlinear effects (Agrawal, 2012; Kumar and Deen, 2014). Inter-channel nonlinear effects can be divided into cross-phase modulation (XPM), and four wave mixing (FWM). XPM and FWM correspond to the nonlinear interactions of two and three WDM channels, respectively. In the case when multiple signal channels co-propagate in a single fiber, the power fluctuations of one signal channel produce a phase shift to another channel, which is due to the XPM effect (Mollenauer and Evangelides, 1990). Nonlinear interactions between channels of center frequencies f_1, f_2, and f_3 results in new frequency components at $f_1 + f_2 - f_3$, $f_1 - f_2 + f_3$, and $-f_1 + f_2 + f_3$ which is known as FWM (Inoue *et al.*, 1994; Tkach *et al.*, 1995). The new frequency components generated through FWM act as noise on channels centered at those frequencies.

Moreover, nonlinear interaction between signal and ASE noise leads to nonlinear phase noise, known as the Gordon-Mollenauer effect (Gordon and Mollenauer, 1990). The instantaneous signal power fluctuates due to ASE noise and it is translated into phase shift due to

the Kerr nonlinear effect. Hence, the phase changes randomly, which is known as nonlinear phase noise. In the absence of fiber dispersion, nonlinear phase noise can lead to significant performance degradation in the coherent fiber-optic systems (Gordon and Mollenauer, 1990; Mecozzi, 1994). However, in the presence of moderate to large dispersion, nonlinear phase noise is significantly reduced (Kumar, 2005).

1.1.2 Nonlinear Schrödinger Equation

Owing to the Kerr effect, signal propagation in fiber is described by the stochastic nonlinear Schrödinger equation (NLSE):

$$\frac{\partial q(t,z)}{\partial z} + j\frac{\beta_2}{2}\frac{\partial^2 q(t,z)}{\partial t^2} - j\gamma|q(t,z)|^2 q(t,z) + \frac{\alpha}{2}q(t,z) = N(t,z), \tag{1.1}$$

where $q(t,z)$ is the optical field envelope, and β_2, α and γ are the dispersion, attenuation and nonlinear coefficients of the transmission fiber, respectively. The Nonlinear coefficient is related to the Kerr coefficient n_2 by $\gamma = 2\pi n_2/(\lambda A_{eff})$ where A_{eff} and ω are the effective area of the fiber and angular frequency of the optical carrier, respectively (Kumar and Deen, 2014).

The second term in NLSE represents dispersion which causes pulse broadening during propagation, while the third term accounts for Kerr nonlinearity, which can cause signal-signal nonlinear interaction such as self-phase modulation (SPM), cross-phase modulation (XPM), and four-wave mixing (FWM) as well as signal-noise nonlinear interaction such as nonlinear phase noise. Finally, the fourth term accounts for propagation loss. $N(t,z)$ represents the amplified spontaneous emission (ASE) noise, added by optical amplifiers.

1.2 Capacity Limits of Fiber-optic Systems

Figure 1.3 illustrates the achievable information rates as a function of signal-to-noise ratio (SNR) for various transmission distance. According to Shannon formula for an additive

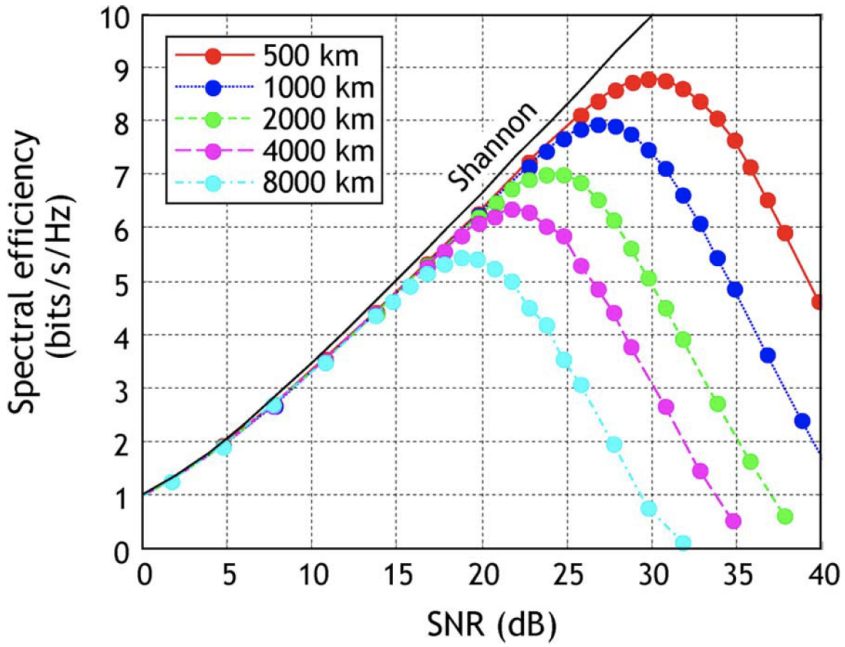

Figure 1.3: Spectral efficiency as a function of SNR for various distance (Essiambre *et al.*, 2010). SNR: signal-to-noise ratio.

white Gaussian noise (AWGN) channel (Shannon, 1948), capacity increases monotonically with SNR (the solid black line). However, in optical communication systems, the spectral efficiency starts to fall at higher SNRs for optical channels of various transmission distance. Moreover, the spectral efficiency falls at lower SNR as the distance increases. It can be stated that the fiber channel capacity, represented by the colored curves in Fig. 1.3, depends on both the launch power and the transmission distance (Essiambre *et al.*, 2010).

The fiber Kerr nonlinearity is a key impairment that leads to a decrease in the spectral efficiency at high SNR, whereas at lower SNR, transmission performance is limited by ASE noise. In fact, achieving higher spectral efficiency requires higher-order modulation formats, which in turn requires higher SNR. However, higher optical power activates fiber Kerr nonlinearity that reduces the signal quality. Consequently, the spectral efficiency is decreasing at higher SNR for a fixed transmission distance. In addition, since the fiber Kerr nonlinearity degrades the signal quality as the fiber distance increases, the spectral efficiency is further decreasing for a longer fiber.

In order to enhance the information-carrying capacity of optical fiber, two main approaches have been followed up to now: the first one treats the fiber nonlinearity as a perturbation that needs to be mitigated by compensation techniques in conventional transmission schemes, originally developed for linear communication systems. An alternate approach is to exploit the nonlinear channel by taking into account the fiber nonlinearity as an essential element in the system's design. This approach is based on the use of nonlinear Fourier transform (NFT) where information is encoded on the nonlinear spectrum that evolves in a simple multiplicative way along the nonlinear fiber channel. We will introduce these two approaches in the following.

1.3 Nonlinear Compensation Techniques

Several optical and digital compensation techniques have been investigated to partially or fully compensate for the nonlinear impairments due to the interplay between the chromatic dispersion and nonlinearity in the transmission fiber. In this section, the most relevant techniques i.e., digital back propagation (DBP), midpoint optical phase conjugation (OPC) and optical back propagation (OBP) are introduced.

1.3.1 Digital Back Propagation

Digital back propagation (DBP) principles originate directly from NLSE which governs the optical signal propagation forward along the physical transmission fiber (TF). DBP–the most commonly used technique–can compensate for the dispersion and deterministic nonlinear impairments due to the TF by propagating backward the received digital signals along a virtual fiber modeled by the inverse NLS equation (Kumar and Deen, 2014). In other words, after coherent detection and analog to digital conversion (ADC), the distorted received signal passes through a virtual fiber whose loss, dispersion and nonlinear coefficients have the opposite signs of those of the TF.

The main challenge in DBP is finding algorithms to reduce the computational cost of numerical implementation of the NLSE (Yamazaki *et al.*, 2011). Attempts have been made to introduce new fast methods of solving NLSE numerically which mostly rely on split-step Fourier method (SSFM). Split-step Fourier method is a pseudo-spectral numerical method that is used to solve nonlinear partial differential equations like NLSE. This method breaks the fiber length into smaller segments and compute the solution for each segment, and also treats linear and nonlinear parts separately. This technique is an approximation and is accurate for very small step size.

Further, in optical networks with add-drop nodes, although DBP can compensate for intra-channel nonlinear impairments, it cannot compensate for inter-channel nonlinear impairments since the receiver at a node requires the knowledge of all channels including those ones dropped at previous nodes. It also cannot undo the impact of ASE, and nonlinearity–ASE coupling.

Coherent detection plays a vital role for DBP algorithm as it provides necessary information about the signal phase. Concepts on backward propagation were first introduced by Paré *et al.* (1996); Tsang *et al.* (2003); Essiambre and Winzer (2005). In (Tsang *et al.*, 2003), a digital reverse propagation technique is proposed for reversing the femtosecond pulse propagation in an optical fiber to obtain the input pulse shape by numerically compensating for both dispersion and nonlinear effects, whereas, in (Paré *et al.*, 1996), a dispersive medium with a negative nonlinear refractive-index coefficient is used to mitigate the dispersion and the nonlinearity. First important studies on compensation of nonlinear impairments by DBP for modern optical communication systems and coherent detection were reported by Li *et al.* (2008); Ip and Kahn (2008). In (Li *et al.*, 2008), DBP is implemented by finite impulse response (FIR) filters for the dispersion step and a parallel architecture for real-time implementation. In (Ip and Kahn, 2008), a non iterative asymmetric split-step Fourier scheme (SSFS) for solving the inverse NLSE in DBP is investigated. It is shown through simulations

that three-times oversampling is required for DBP to achieve good numerical accuracy. Mateo *et al.* (2008) investigated the impact of XPM and FWM in a coherent WDM system with DBP at the receiver. In their work, coupled NLSE and total field NLSE are used to compensate for XPM and XPM+FWM, respectively. The results show that the impact of FWM is weak compared to XPM, and DBP based on coupled NLSE is sufficient to compensate for most nonlinearities in long-haul systems with large accumulated dispersion. In (Savory *et al.*, 2010), a 112 Gb/s nonreturn-to-zero dual-polarization WDM transmission system is experimentally investigated and it is shown that the nonlinear compensation algorithm i.e., DBP can increase the reach by 23% in a 100 GHz spacing WDM system, whereas the reach enhances by 46% for the single-channel systems. When the channel spacing is reduced to 50 GHz, the reach improvement is minimal due to the uncompensated inter-channel nonlinear distortions. Investigations show that in point-to-point WDM systems, optimum performance using DBP is obtained by using 2, 4 and 8 steps per fiber span for 14 GBaud, 28 GBuad and 56 GBaud, respectively (Asif *et al.*, 2011). Advanced split-step methods to reduce the computational cost of DBP for single-polarization and polarization-division multiplexed (PDM) WDM systems are presented in (Mateo *et al.*, 2010) and (Mateo *et al.*, 2011), respectively. The modification is based on including the effect of inter-channel walk-off in the nonlinear step of the split-step method. In (Saavedra *et al.*, 2017), the performance and complexity of DBP on Raman-pumped- and EDFA-based transmission links is numerically studied using the Gaussian noise (GN)-model. The distributed nature of backward pumped Raman amplification allows for an improved performance in both studied scenarios, with and without the use of nonlinearity compensation. Galdino *et al.* (2017) investigated the impact of transceiver noise on the performance of DBP.

In order to avoid the need for large electrical bandwidth and high computational cost, all-optical compensation techniques such as optical phase conjugation (OPC) and, recently optical back propagation (OBP) have been proposed.

1.3.2 Midpoint Optical Phase Conjugation

The principles of midpoint OPC rely on inverting the sign of the signal phase due to the dispersion and nonlinearity in the middle of the transmission link by OPC. As the signal propagates to the end of the link, the accumulated phase distortions will be removed if there is a perfect symmetry with respect to the OPC location. In other word, OPC acts like a temporal mirror i.e., the temporal object placed at the transmitter (i.e., input signal) has an image at the receiver that is identical to the object except for phase conjugation, provided the fiber-optic link is exactly symmetric with respect to the location of the OPC.

Due to the propagation loss, it is hard to realize the symmetric power profile which limits the performance of the midpoint OPC technique. In addition, the performance of this technique is limited by its strong dependency on the exact position of the OPC which could be hard to be found especially in optical networks due to the fact that amplifier spacings vary randomly.

Pepper and Yariv (1980) showed theoretically that the nonlinear impairments in a lossless optical fiber can be compensated by the use of a phase conjugation. Extending this work, Fisher *et al.* (1983) showed that the combined effect of chromatic dispersion and self-phase modulation can be compensated by conjugating the signal near the midpoint of the fiber-optic. In a WDM system, Watanabe (1994) investigated the compensation of FWM using midpoint OPC. For fiber-optic communication systems using lumped amplification such as EDFA, the power profile with respect to the OPC is not symmetric, which limits the compensation performance of OPC. Power profile can be made symmetric using Raman amplification to some extent. In (Solis-Trapala *et al.*, 2014), it is experimentally demonstrated that midpoint OPC brings a significant performance improvement in WDM system with dispersion-flattened non-zero dispersion-shifted fibers (NZDSFs) and bidirectional Raman amplification.

1.3.3 Optical Back Propagation

An alternative technique for real-time compensation of nonlinear impairment is realizing back propagation in the optical domain i.e. optical back propagation (OBP). OBP compensates for the chromatic dispersion and nonlinearity by introducing real photonic devices inline or at the receiver instead of the virtual fibers of DBP (e.g., Kumar and Yang, 2011; Liang and Kumar, 2016). The basic idea of OBP is to optically implement backward propagation i.e., solve the inverse NLSE, using optical devices with the opposite sign of loss, dispersive and nonlinear coefficients which compensate for the nonlinear transmission impairments due to the TF. However, fibers with negative nonlinear coefficients do not exist which makes it harder to realize OBP.

Kumar and Yang (2011) proposed a technique to realize an effective negative nonlinear coefficient using two highly nonlinear fibers (HNLF), which can be used to implement OBP. The proposed OBP module consisting of DCFs and nonlinearity compensators is placed at the end of fiber-optic link to compensate for dispersion and nonlinear effects. This OBP scheme provides good transmission performance, but it requires pumps and polarization alignment of the pumps with signal, which increases the complexity of the receiver. In (Shao and Kumar, 2012), an improved OBP technique that does not require pumps is presented. The OBP module consists of an OPC followed by short lengths of high-dispersion fibers (HDFs) and HNLFs, concatenated to implement split-step Fourier scheme (SSFS) used for solving the NLSE. The HDF provides the accumulated dispersion that is the same as the corresponding transmission fiber section and the set of HDF and HNLF provides a nonlinear phase shift that is equal to the corresponding transmission fiber section. It is shown that the proposed OBP provides better performance as compared to midpoint OPC in the presence of loss. Extending this OBP scheme, in (Kumar and Shao, 2013), an OBP scheme consisting of an optical phase conjugator, fiber Bragg gratings (FBGs), and HNLFs is introduced. Transmission fiber dispersion is compensated by the FBGs and the nonlinearity is compensated by HNLFs. The optimum accumulated dispersion of each section of the FBG and the optimum

nonlinear phase shift of the each section of the the OBP scheme are calculated to find an optimal step size for OBP. The proposed OPB scheme provides significant reach enhancement as compared to uniform spacing for a given step size in (Shao and Kumar, 2012). An ideal OBP scheme to compensate for nonlinear impairments in WDM systems is proposed in (Liang *et al.*, 2013). The scheme consists of an optical phase conjugator (OPC), N spans of dispersion decreasing fibers (DDFs) and amplifiers, placed at the end of the fiber-optic link. The performance of the proposed OBP scheme is compared with DBP and midpoint OPC and simulation results show that the transmission reach can be significantly enhanced using the OBP with DDF. This technique is further investigated to compensate for nonlinear impairments in fiber-optic communication systems with reconfigurable optical add-drop multiplexers (ROADMs) in (Liang and Kumar, 2016). Kaminski *et al.* (2019) experimentally demonstrated a receiver-side OBP scheme using FBG for dispersion matching, polarization-insensitive OPC for chirp reversal and short spool of standard single mode fiber (SSMF) for nonlinearity cancellation. Improvement of 1.98 dB in SNR and 12% of reach extension are reported for a dual-polarization WDM 16-QAM unrepeated transmission systems.

1.4 Nonlinear Frequency Division Multiplexing

Current approaches to the design of fiber-optic communication systems treat fiber nonlinearity as an undesirable effect or perturbation and using compensation techniques to mitigate or suppress it without considering the fact that the modulation, coding and transmission schemes are developed for a linear channel. Mastering the nonlinear fiber channel requires a paradigm shift and development of alternative transmission schemes which take the nonlinear nature of the channel into account as an essential design element.

The NLSE belongs to the unique class of integrable equations that can be solved using nonlinear Fourier transform (NFT). Similar to the linear Fourier transform that translates dispersive effects into a simple phase rotation in the frequency domain, the NFT transforms

the effects of both nonlinearity and dispersion into a simple multiplicative evolution of the nonlinear spectral data. An immediate application is a transmission scheme that is the nonlinear analog of orthogonal frequency division multiplexing (OFDM), called nonlinear frequency division multiplexing (NFDM), which modulates the nonlinear spectra using NFT (Yousefi and Kschischang, 2014; Cartledge *et al.*, 2017).

The idea of including the fiber nonlinearity into the design of a fiber-optic communication system is introduced with soliton communication (Hasegawa and Tappert, 1973; Nakazawa *et al.*, 1991; Mollenauer and Smith, 1988). Indeed, by properly adjusting the power of the transmitted optical signal, it is possible to generate a solitary pulse i.e., soliton, whose shape is intact as it propagates in the nonlinear fiber channel due to the perfect balance between chromatic dispersion and Kerr nonlinearity. Extending the idea of the soliton communications, Hasegawa and Nyu (1993) proposed eigenvalue communication in which discrete eigenvalues (corresponding to solitons), emerging from the NFT, are employed to encode and transmit information, as they are a set of parameters that are invariant during the transmission of the optical signal in the fiber. Conventional soliton communication system which corresponds to the case of one eigenvalue is a particular case of eigenvalue communication. However, soliton-based communications lost the competition to existing WDM systems in the late 1990s due to the effects such as soliton-to-soliton collisions, inter-channel cross-talk, and Gordon-Haus timing jitter (Hasegawa and Matsumoto, 2003).

The recent revival of coherent detection in combination with high-speed digital signal processing (DSP) allows the modulation of not only the eigenvalues, but also the amplitude and the phase of the scattering coefficients associated to the both discrete eigenvalues (solitary modes) and continuous part of nonlinear spectrum (dispersive mode), to enhance the system spectral efficiency (SE). This has resulted in a renewed and growing interest in NFT-based communication systems as a new paradigm in optical communications (Terauchi and Maruta, 2013; Prilepsky *et al.*, 2013; Turitsyna and Turitsyn, 2013; Yousefi and Kschischang, 2014). Exploiting the integrability of the nonlinear Schrödinger (NLS) equation, a

nonlinear frequency-division multiplexed (NFDM) transmission scheme which directly modulates the non-interacting degrees of freedom of a signal under NLS propagation is proposed and actively investigated (Turitsyn *et al.*, 2017). Conceptually, NFDM is in close analogy to its linear counterpart, OFDM in which interference is avoided in linear frequency domain by properly allocating transmission modes with the help of Fourier transform. More specifically, data is encoded on the multiple orthogonal subcarriers i.e., Fourier coefficients using standard modulation formats. Similarly, NFDM is a signal multiplexing technique in which data is encoded on the nonlinear spectrum (discrete and continuous part) which propagates in a simple way over the nonlinear fiber channel.

Several NFDM schemes have been proposed for modulating the continuous spectrum (e.g., Le *et al.*, 2014; Prilepsky *et al.*, 2014; Le *et al.*, 2015), the discrete spectrum (e.g., Terauchi and Maruta, 2013; Buelow *et al.*, 2016; Dong *et al.*, 2015; Gui *et al.*, 2017), or both parts of the nonlinear spectrum (Tavakkolnia and Safari, 2015; Aref *et al.*, 2016; Le *et al.*, 2017).

A number of proof-of-concept experiments for NFDM transmission have been carried out (e.g., Bulow, 2014, 2015; Aref *et al.*, 2015; Le *et al.*, 2016a; Buelow *et al.*, 2016; Aref *et al.*, 2016; Le *et al.*, 2017, 2018b; Aref *et al.*, 2018; Yangzhang *et al.*, 2019b).

In (Gui *et al.*, 2017), with the modulation of the discrete part (eigenvalue transmission), data rates up to 24 Gb/s at 4 Gbaud (6 bits/symbol) is reported. By modulating the continuous spectrum only, 32 Gb/s transmission with 64 modulated subcarriers is designed and tested for 1464 km link in (Le and Buelow, 2017), providing 1.3 dB performance advantage over the conventional OFDM transmission. Using both continuous and discrete spectrum, an NFDM system with 65 Gb/s is experimentally investigated which outperforms OFDM in terms on nonlinearity tolerance (Le *et al.*, 2017). Combining the modulation of both the discrete and continuous parts is a natural method of increasing the SE and data rate but in the presence of ASE noise, the nonlinear interaction between continuous and discrete nonlinear spectral components hinders the benefit of this approach (Le, 2019). By employing

a pre-compensation technique, while increasing the number of modulated nonlinear subcarriers up to 222, the transmission rate of 125 Gb/s with spectral efficiencies of 2.3 bit/s/Hz for a EDFA-based NFDM system is achieved when transmission distance is almost 1000 km and the continuous spectrum is employed (Le *et al.*, 2018b). However, it is experimentally observed in (Le *et al.*, 2018b) and theoretically predicted in (Derevyanko *et al.*, 2016; Civelli *et al.*, 2017) that increasing the number of modulated nonlinear subcarriers degrades significantly the system performance and the achievable SE, because of the signal–noise mixing in NFT processing. Hence, to improve the performance of NFDM transmission systems, developing techniques to reduce the signal-noise interaction through NFT-processing is necessary. A 100 Gb/s b-modulated nonlinear frequency division multiplexed (NFDM) transmission using 132 subcarriers is demonstrated in (Le *et al.*, 2018a), showing a gain up to 1.5 dB over the conventional OFDM system. A dual polarization NFDM transmission achieving a record net data rate of 400 Gb/s based on b-modulation is demonstrated in (Yangzhang *et al.*, 2018). It offers 1 dB Q-factor improvement over conventional $\tilde{q}$-modulation scheme.

The highest data rate of 220 Gb/s with a spectral efficiency (SE) of 4 bits/s/Hz, reported so far for the NFT-based transmission method, is achieved for a high-capacity dual polarization (DP)-NFDM transmission system with b-modulation (Yangzhang *et al.*, 2019a), which is recently experimentally validated (Yangzhang *et al.*, 2019b). It is also shown that the SE of the b-modulated system achieved 1.2 bits/s/Hz higher SE than $\tilde{q}$-modulated system (Yangzhang *et al.*, 2019a).

Despite the several important advances and the potential of the NFT-based methods, there are still many challenges associated with NFDM systems based on vanishing boundary conditions (Turitsyn *et al.*, 2017). NFDM suffers from limited SE mainly due to the large guard intervals between the two adjacent burst signals, required for the NFT boundary conditions and for avoiding burst interaction due to the dispersion (Yangzhang *et al.*, 2019a).

One solution to this problem is to consider a system based on the NFT with periodic boundary conditions and use a cyclic prefix rather than long guard intervals (Wahls and Poor, 2015; Kamalian *et al.*, 2016a,b). However, despite its potential to increases the spectral efficiency (SE) significantly, the NFT with periodic signals is mathematically more complicated. The pre-dispersion compensation (PDC) technique is another proposed solution which can effectively reduce the required guard interval duration by a factor of 2 (Tavakkolnia and Safari, 2016; Le *et al.*, 2017; Civelli *et al.*, 2017; Le *et al.*, 2018b). PDC can also reduce the peak-to-average-power ratio (PAPR) in the time domain and consequently, the required number of samples (Yangzhang *et al.*, 2018).

In addition, with vanishing boundary, the signal $q(t)$ generated by $\tilde{q}(\lambda)$ is not confined in time and its tail is slowly decaying to zero. To lower the truncation error, the tail is appended to the guard interval. To address this issue, a modified continuous spectrum modulation scheme, b-coefficient modulation based on the NFT for vanishing signals is proposed which offers tight control over the duration of the NFT-generated signals at the transmitter (e.g., Wahls, 2017; Gui *et al.*, 2018; Le *et al.*, 2018a; Yangzhang *et al.*, 2018; Shepelsky *et al.*, 2020). This scheme reduces the impact of tail truncation and noise, but has marginal impact on the SE (Le, 2019). Shepelsky *et al.* (2020) theoretically showed how to embed discrete solitary modes into the b-modulation without violating the exact localization of the time-domain signal.

NFT method is based on the integrability property of the lossless nonlinear Schrödinger equation. In most cases, it is assumed that the fiber loss is perfectly compensated by Raman amplification. To address the loss problem, non-integrable lossy model with periodic lumped amplification is successfully approximated to an integrable lossless model by applying the path-average rule (Le *et al.*, 2015). In (Le *et al.*, 2015), it is shown that mismatch between the path-averaged NLSE model and practical fiber link with lumped amplification grows linearly with distance and the energy of the signal. It is also shown in (Yangzhang *et al.*, 2018) that NFDM in path-averaged model is subject to a more phase distortion compared with NFDM

in the ideal integrable model. Kamalian *et al.* (2017) showed that by an optimum shift in the amplifier locations in the link, the accuracy of the path-average model can be improved. To avoid the approximation error from the path-average model, Bajaj *et al.* (2020) proposed the idea of using dispersion decreasing fiber (DDF) in NFDM systems.

Another source of perturbation in NFT-based communications which breaks the integrability property of the lossless NLS model is noise. Noise models for nonlinear frequencies and spectral amplitudes are proposed in (Zhang and Chan, 2015; Civelli *et al.*, 2018). The probability distribution of the noise in the nonlinear Fourier domain is studied in (Kazakopoulos and Moustakas, 2008) for some special cases. The impact of noise and perturbations on NFT is analyzed in (Civelli *et al.*, 2017; Yangzhang *et al.*, 2018; Aref *et al.*, 2017; Jones *et al.*, 2018). An important characteristic of the channel in the nonlinear spectral domain is the strong signal dependency of noise (Tavakkolnia and Safari, 2015). In (Tavakkolnia and Safari, 2017), it is shown that the signal dependency of noise leads to peak-power-limited signal space, resulting in the channel capacity saturation at high powers.

1.5 Thesis Contributions

The main goal of this thesis is to overcome the problems arising in an optical fiber communication system due to the interplay between dispersion, Kerr nonlinearity, and noise which are the main barriers to increase the capacity and/or transmission reach of the system. To achieve this goal, this thesis explores two different strategies:

(i) Optical signal processing to compensate for the nonlinear impairments due to the interplay between dispersion, Kerr nonlinearity and noise. An optical back propagation technique using Raman amplification to compensate for nonlinear impairments in wavelength division multiplexed (WDM) systems in real time is proposed. Simulation results show that this technique provides significant performance improvement as compared to DBP ($\approx$ 7 dB advantage in Q-factor).

(ii) Nonlinear Fourier transform (NFT) to exploit the nonlinear fiber channel. A novel nonlinear discrete Fourier transform algorithm to realize the NFT in digital as well as optical domain is developed. The proposed technique provides a promising way to implement NFT in optical domain, which will fully utilize the potential of NFT for WDM systems. In addition, an NFDM transmission system is developed to address one major problem in NFT-based transmission systems: signal-noise mixing in NFT processing. Simulation results shows the performance improvement of 4.5 dB in Q-factor. The proposed technique also reduces the duration of guard interval and thereby, enhances the spectral efficiency.

This thesis has been prepared in accordance with the regulations for a "sandwich-style" format, with each technical chapter representing a published or submitted journal article. These articles represent the independent work of the author of this thesis, Elham Bidaki. In each of the journal articles, the problem formulations were conceived, the mathematical analysis was performed, and the numerical simulations were carried out by Elham Bidaki under the supervision of Prof. Shiva Kumar. The first draft of each article was written by Elham Bidaki, and was revised in conjunction with Prof. Kumar.

1.5.1 Chapter 2: A Raman-Pumped Dispersion and Nonlinearity Compensating Fiber for Fiber-optic Communications

This chapter seeks to develop an optical back propagation (OBP) technique to compensate for the dispersion and nonlinearity of the transmission fibers in real time. The proposed scheme consists of an optical phase conjugator (OPC), amplifiers and a Raman pumped dispersion compensating fiber (DCF). We have identified the conditions under which the nonlinear effects (both intra- and inter-channel nonlinearities) can be fully compensated and obtained an analytical expression for the power profile of the signal, propagating in Raman pumped DCF which provides the exact compensation for nonlinear impairments. Power profile required by the ideal OBP condition can be approximately achieved by using forward/backward Raman pumping of the DCF. Two possible configurations to implement

the OBP are introduced and compared. Numerical simulations show that the proposed OBP can enhance the maximum transmission reach of a long-haul WDM system significantly as compared to DBP.

This work has resulted in the following publication:

- Bidaki, E. and Kumar, S. (2020). A Raman-pumped dispersion and nonlinearity compensating fiber for fiber optic communications. *IEEE Photonics Journal*, **12**(1), 1–17.

1.5.2 Chapter 3: Nonlinear Fourier Transform

Chapter 3 provides some useful preliminary information required to define an NFDM communication system with a particular focus on the channel model and the nonlinear Fourier transform (NFT) theory. The simple fiber model provided by the noiseless and lossless nonlinear Schrödinger equation (NLSE) is one of a very special class of integrable nonlinear equations which can be solved by using the NFT technique. The inverse scattering method based on this channel is introduced and the key concepts of nonlinear spectrum and its multiplicative evolution are presented. Next, a generalized channel model that takes into account fiber losses is also presented. Finally, NFDM systems which employ the NFT to modulate the nonlinear spectra is introduced.

1.5.3 Chapter 4: Nonlinear Fourier Transform using Multistage Perturbation Technique for Fiber-optic Systems

We develop perturbation techniques to compute NFT and compare the accuracy and computational cost of single stage second-order and third-order perturbation techniques and find that the accuracy of the single-stage perturbation approach decreases as the amplitude and/or the duration of the signal increases. We also find that as the order of the perturbation technique increases, the accuracy improves, but the computational cost becomes extensive. Hence, for the first time to our knowledge, we develop a multistage perturbation technique

for NFT. The multistage perturbation technique realizes the NFT as a cascade of linear Fourier transforms (FT). An advantage of the proposed approach in digital domain is that the computation can be split into fast Fourier transform (FFT) of smaller lengths, which can be processed on parallel processors.

To utilize the full advantage of NFT-based systems and avoid the interference associated with the WDM, channels should be multiplexed/demultiplexed nonlinearly using INFT and NFT, respectively, which calls for the optical domain implementation of NFT. With the recent development of all-optical DFT operating at Tb/s on a silicon photonics chip, our proposed approach offers a promising way to realize NFT in the optical domain by using the cascade of linear Fourier transform.

This work has resulted in the following publications:

- Bidaki, E. and Kumar, S. (2018). Multi-stage perturbation technique based nonlinear Fourier transform for fiber optic systems. In *2018 Photonics North (PN)*, pages 1–2.

- Bidaki, E. and Kumar, S. (2018). Nonlinear Fourier transform using multistage perturbation technique for fiber-optic systems. *Journal of the Optical Society of America B*, **35**(9), 2286–2293.

1.5.4 Chapter 5: Enhanced-Power NFDM Transmission System with Midpoint Optical Phase Conjugation

Adopting a different philosophy to treat nonlinearity and dispersion as essential elements in the design of fiber communication systems, we developed an NFDM transmission scheme with midpoint OPC. In NFDM systems, non-integrable fiber channel due to the loss and noise introduces nonlinear interaction, leading to system performance degradation. Currently, NFDM systems provide only small performance improvement ($\approx$ 1 dB in Q-factor) over their linear counterparts, OFDM, mainly because the launch power to the fiber cannot be increased without suffering a penalty from the signal and noise mixing in the NFT block at

the receiver. We investigate the combination of NFDM transmission scheme with midpoint OPC, and show that midpoint OPC introduces a power enhancement by compensating for nonlinear impairments. It offers a degree of freedom to have a flexible power normalization factor, P_n to minimize the signal-noise mixing in NFT processing for a specific launch power, resulting in improving the system performance significantly. We also show how dispersion map can help to improve the performance of the system. Using the midpoint OPC, our simulation results have shown significant performance improvement (about 4.5 dB in Q-factor) as compared to the conventional NFDM system without OPC.

This work has resulted in the following publication:

- Bidaki, E. and Kumar, S. (2020). Enhanced-power NFDM transmission system with midpoint optical phase conjugation. *Optics Letters*, **45**(17), 4682–4685.

Chapter 2

A Raman-Pumped Dispersion and Nonlinearity Compensating Fiber for Fiber Optic Communications

2.1 Abstract

An optical back propagation (OBP) technique using Raman pumped dispersion compensating fibers (DCF) is investigated to compensate for nonlinear impairments in WDM systems in real time. The proposed inline OBP module consists of an optical phase conjugator, amplifiers and a Raman pumped DCF. In order to suppress the nonlinear effects of the transmission fibers exactly, the power in the backpropagation fiber should increase exponentially with distance. This can be approximately achieved by using forward/backward Raman pumping of the DCF. We introduce two configurations to realize the OBP. In this chapter, we show that the OBP with forward/backward pumping provides 2.45 dB Q-factor gain as compared to single-channel digital back propagation (DBP) when transmission distance is 1500 km for a WDM system with QAM-64. To minimize the variation of effective

gain coefficient of the Raman pumped DCF as a function of distance, a bidirectional pumping scheme which can provide the signal power profile closest to that required by the ideal OBP condition is proposed. The bidirectional pumping scheme provides a superior performance over forward/backward pumping and wideband DBP (i.e., DBP is applied on the entire WDM signal). Our numerical simulation results show that the bidirectional pumping scheme provides 7.6 dB and 5 dB advantage in Q-factor as compared to single-channel DBP and wideband DBP, respectively at a transmission distance of 5000 km. The maximum achievable reach of a long haul WDM system can be enhanced by 225% using a bidirectional pumping scheme as compared to wideband DBP.

2.2 Introduction

The maximum reach of a fiber-optic system is mainly limited by fiber nonlinear impairments which can be divided into two types: (i) deterministic (although symbol pattern dependent) nonlinear impairments that depend only on dispersion and nonlinearity such as self-phase modulation (SPM) (Agrawal, 2012), intra-channel cross-phase modulation (IXPM) and four wave mixing (IFWM) (Essiambre *et al.*, 1999; Mecozzi *et al.*, 2000; Kumar, 2001), and inter-channel cross-phase modulation (XPM) and four wave mixing (FWM) (Agrawal, 2012; Poggiolini, 2012; Kumar and Deen, 2014) (ii) stochastic nonlinear impairments that depend on the interplay between nonlinearity, amplified spontaneous emission (ASE) and dispersion (Gordon and Mollenauer, 1990; Kumar, 2005; Mecozzi, 1994). The compensation of these impairments can be divided into three types: (i) digital (Essiambre and Winzer, 2005; Roberts *et al.*, 2006; Ip and Kahn, 2008; Li *et al.*, 2008; Mateo *et al.*, 2008; Du and Lowery, 2010; Tao *et al.*, 2011; Shao *et al.*, 2013; Oyama *et al.*, 2014; Y. Fan *et al.*, 2014; Gao *et al.*, 2014; Liang and Kumar, 2014; Liang *et al.*, 2014; Liang and Kumar, 2015), (ii) optical (Pepper and Yariv, 1980; Watanabe and Shirasaki, 1996; Minzioni *et al.*, 2006; Morshed *et al.*, 2013; Pelusi, 2013; Solis-Trapala *et al.*, 2014; Liang *et al.*, 2013; Liang and Kumar, 2016;

Liang and Kumar, 2017) and (iii) optoelectronic (Foo *et al.*, 2016; Foo *et al.*, 2018).

In digital back propagation (DBP), virtual fibers with negative dispersion, loss and nonlinear coefficients are realized in digital domain (Essiambre and Winzer, 2005; Roberts *et al.*, 2006; Ip and Kahn, 2008; Li *et al.*, 2008; Mateo *et al.*, 2008). Although the DBP can compensate for deterministic nonlinear impairments, it cannot compensate for stochastic nonlinear impairments. Besides, it is currently limited to compensate for intra-channel nonlinear distortions only since in an optical network, a receiver does not have access to other channels that are dropped at other nodes (Liang and Kumar, 2016). In principle, the DBP can be used to compensate for inter-channel nonlinear distortion in a WDM point-to-point system (Li *et al.*, 2008). However, it has not been implemented in real time due to limitations on computational resources and challenges to combine the outputs of many coherent receivers.

In contrast, optical back propagation (OBP) can compensate for both intra-channel and inter-channel nonlinear impairments of a WDM system in real time (Liang *et al.*, 2013; Liang and Kumar, 2016; Liang and Kumar, 2017). In OBP, virtual fibers of DBP are replaced by real fibers/photonic devices. Since fibers with negative nonlinear coefficients do not exist, the optical phase conjugation (OPC) is used. An advantage of OBP technique is that it can partially compensate for stochastic nonlinear impairments if inline OBP is used (Liang and Kumar, 2016). However, there are a few hurdles to realize OBP in practical systems. First, photonic devices of OBP introduce losses and to compensate for losses, amplifier gain has to be increased leading to reduction in optical signal-to-noise ratio (OSNR). Second, in (Liang *et al.*, 2013; Liang and Kumar, 2016; Liang and Kumar, 2017) dispersion decreasing fiber (DDF)/dispersion varying fiber (DVF) is proposed to realize ideal OBP. Although DDF-/DVF- based OBP provides significant performance improvement, the fabrication of DDF/DVF is difficult since dispersion of such fibers should vary as a function of propagation distance.

In this chapter, we propose a Raman amplified dispersion and nonlinearity compensating fiber to compensate for dispersion and nonlinearity of the transmission fiber. Unlike the

DDF/DVF of (Liang *et al.*, 2013; Liang and Kumar, 2016; Liang and Kumar, 2017), the dispersion of the proposed fiber does not change as a function of its length; in fact, the commercially available dispersion compensating fiber (DCF) can be used for this purpose. The required signal power profile to mitigate the transmission fiber nonlinearity is achieved by adjusting the Raman pump power. We introduce two configurations. In configuration A, an inline OPC is used after the transmission fiber (TF), which is followed by a Raman-pumped DCF. As a result, the signal power in the DCF increases nearly exponentially with distance. To enhance the OSNR, a second configuration is proposed in which the Raman-pumped DCF is placed as the first span followed by an OPC and the TF. The configuration B requires a fewer photonic devices and outperforms configuration A slightly. We also compare three types of pumping schemes: (i) forward, (ii) backward, and (iii) bidirectional. In the case of forward/backward pumping, the OBP scheme does not provide the exact nonlinearity compensation since the signal power evolution in the DCF deviates from the requirement of ideal OBP condition. This scheme provides a moderate performance improvement ($\approx$ 2.45 dB) as compared to single-channel DBP at a transmission distance of 1500 km. However, when the bidirectional pumping is used, we found that the signal power evolution in the DCF is nearly the same as that required by ideal OBP condition. Our results show that the OBP scheme based on bidirectional pumping outperforms that based on forward/backward pumping by 6.8 dB in Q-factor when the reach is 5000 km. We also find that this bidirectional pumping OBP scheme outperforms single-channel DBP and wideband DBP by 7.7 dB and 5 dB in Q-factor, respectively. The superior performance of the proposed scheme over DBP is due to the fact that it partially compensates for stochastic nonlinear impairments as well. It is well-known that midpoint OPC can mitigate fiber dispersion and nonlinear impairments (Pepper and Yariv, 1980; Watanabe and Shirasaki, 1996) and it has been demonstrated experimentally (Minzioni *et al.*, 2006; Solis-Trapala *et al.*, 2014).

We note that the proposed scheme differs from midpoint OPC for the following reason. In midpoint OPC systems, the transmission fibers after the OPC mitigates the dispersion

and nonlinearity effects of the fibers preceding the OPC, if there is a power symmetry about the point of phase conjugation. Although the midpoint OPC can provide significant performance improvement in point-to-point systems such as transoceanic systems, the performance improvement is marginal in optical networks due to the fact that amplifier spacings in North America vary from 50 km to 150 km randomly. As a result, the fibers following the OPC cannot mitigate the nonlinear effects of the fibers preceding the OPC exactly. Hence, there is a need to introduce a dedicated photonic device at each node (or inline) to compensate for the nonlinear impairments of the transmission fiber. The Raman amplified DCF proposed in this chapter achieves this goal and the parameters of this sub-system can be tuned to achieve the desired nonlinearity compensation for the transmission fiber of arbitrary lengths.

Raman amplification in DCF has drawn significant attention in the past (Hansen *et al.*, 1998; Emori *et al.*, 1998; Vasilyev *et al.*, 2002; Nicholson, 2003) owing to the fact that Raman gain efficiency of DCF is 7 to 10 times higher than standard single-mode fiber (SSMF). The Raman pumped DCF acts as an amplifier as well as the dispersion compensator (Nicholson, 2003). The proposed Raman pumped DCF may be interpreted as an amplifier and compensator for both dispersion and nonlinearity.

The rest of the chapter is organized as follows. In Section 2.3, conditions for ideal OBP are derived and Section 2.4 discusses how to satisfy the OBP conditions using the Raman pumped DCF. The optimal pump ratio for the bidirectional pumping is calculated. Section 2.5 provides two system configurations and in Section 2.6, numerical simulation of these configurations for various pumping schemes is carried out. The Q-factor of the proposed schemes are compared with single-channel DBP and wideband DBP. A summery of the chapter is provided in Section 2.7.

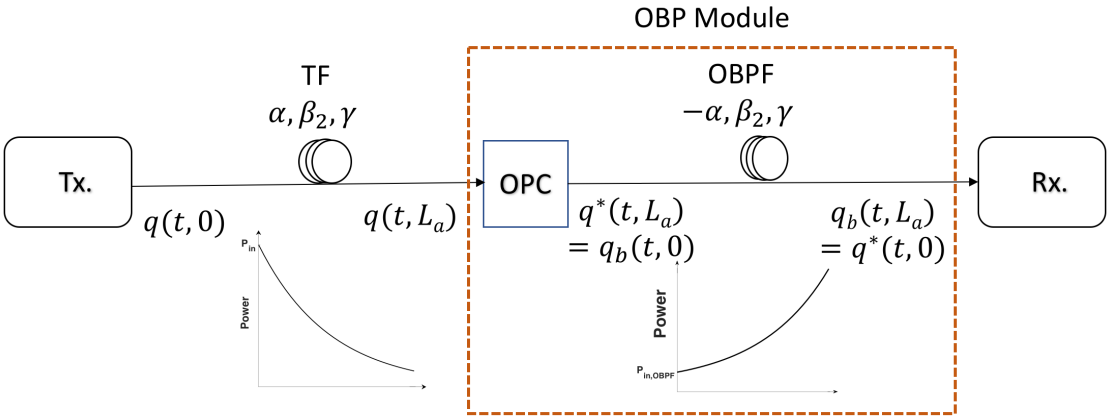

Figure 2.1: A single-span fiber optic system with OBP using an ideal optical backpropagation fiber with negative loss coefficient. Tx: transmitter; TF: transmission fiber; OPC: optical phase conjugator; OBPF: optical backpropagation fiber; Rx: receiver.

2.3 OBP Theory

2.3.1 Ideal Optical Back Propagation

Consider a single span of a transmission fiber (TF) of length L_a. The propagation of the field envelope in a fiber in the absence of noise is described by the nonlinear Schrödinger equation (NLSE):

$$\frac{dq}{dz} = i[D(t) + N(t,z)]q(t,z), \tag{2.1}$$

where

$$D(t) = -\frac{\beta_2}{2}\frac{\partial^2}{\partial t^2} + i\frac{\alpha}{2}, \tag{2.2}$$

$$N(t,z) = \gamma|q(t,z)|^2. \tag{2.3}$$

D and N denote the linear and nonlinear operators, respectively. Here, β_2, α and γ represent dispersion, loss and nonlinear coefficients, respectively. The formal solution of Eq. (2.1) is

$$q(t,L_a) = Mq(t,0), \tag{2.4}$$

where M is the propagation operator,

$$M = e^{i\int_0^{L_a}[D(t)+N(t,s)]\,ds}. \tag{2.5}$$

Suppose the output signal of the transmission fiber which is described by Eq. (2.4) passes through an optical phase conjugator (OPC) (see Fig. 2.1). The conjugated signal becomes

$$q^*(t, L_a) = e^{-i\int_0^{L_a}[D^*(t)+N(t,z)]\,dz} q^*(t, 0) = M^* q^*(t, 0). \tag{2.6}$$

Let the conjugated signal propagate through an OBP fiber (OBPF) with a propagation operator M'. The purpose of OBPF is to compensate exactly for dispersive and nonlinear distortions caused by the TF. The output of OBPF,

$$q_b(t, L_a) = M' q^*(t, L_a), \tag{2.7}$$

is identical to the conjugated input signal $q^*(t, 0)$ only if $M'M^* = I$ where I is the identity operator. Hence,

$$M' = (M^*)^{-1} = e^{i\int_0^{L_a}[D^*(t)+N(t,s)]\,ds}, \tag{2.8}$$

where

$$D^*(t) = -\frac{\beta_2}{2}\frac{\partial^2}{\partial t^2} - i\frac{\alpha}{2}. \tag{2.9}$$

Thus, the OBP fiber is identical to the transmission fiber except its loss coefficient is $-\alpha$. The input field envelope can be retrieved by taking the complex conjugate of the received signal in the electrical domain at the receiver. Equation (2.7) with the propagation operator of M' given by Eq. (2.8) is equivalent to

$$\frac{\partial q_b}{\partial z_b} = i[D^*(t) + N(t, z_b)]q_b(t, z_b), \tag{2.10}$$

with $q_b(t,0) = q^*(t, L_a)$ and z_b is the distance in OBPF. Equation (2.10) describes the evolution of the optical signal in OBPF. Let

$$q_b(t, z_b) = \sqrt{P_{\text{in,OBPF}}} e^{\frac{\alpha z_b}{2}} u_b(t, z_b), \tag{2.11}$$

where $P_{\text{in,OBPF}}$ is the power launched to OBPF,

$$P_{\text{in,OBPF}} = P_{\text{in}}\, e^{-\alpha L_a}, \tag{2.12}$$

and P_{in} is the launch power to the TF. The reason for the exponential function in Eq. (2.11) is that the signal power in the OBP fiber increases exponentially with distance. Also, for later convenience, we use the following transformation

$$dz_b' = \beta_2 dz_b. \tag{2.13}$$

Using Eqs. (2.11) and (2.13), Eq. (2.10) may be rewritten as

$$i\frac{\partial u_b}{\partial z_b'} - \frac{1}{2}\frac{\partial^2 u_b}{\partial t^2} + \frac{\gamma P_{\text{in}}}{\beta_2} e^{-\alpha(L_a - z_b)} |u_b|^2 u_b = 0. \tag{2.14}$$

Equation (2.14) describes the field propagation in an ideal fiber with a negative loss coefficient α (or equivalently the power increasing with distance) which exactly compensates for dispersion and nonlinearity of the TF.

We note that this ideal fiber (OBPF) with negative loss coefficient does not exist. In (Liang *et al.*, 2013), the characteristics of the ideal fiber is realized using a DDF. In this chapter, we investigate the possibility of realizing it using a DCF with distributed Raman amplification.

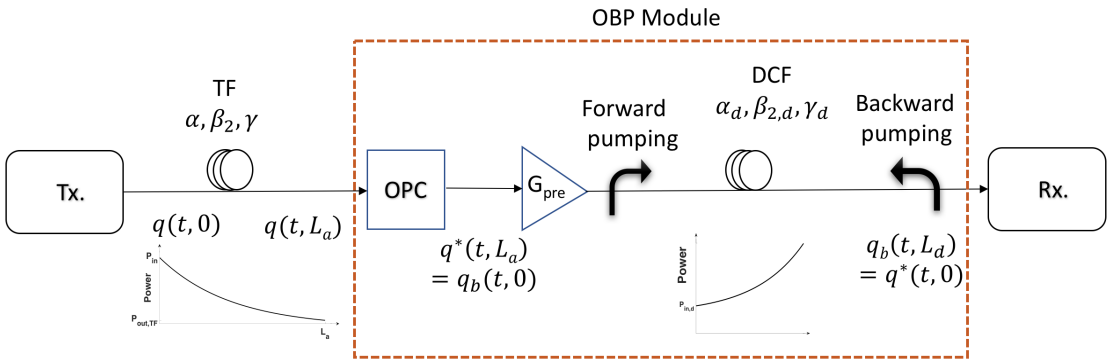

Figure 2.2: A single-span fiber optic system with OBP using a Raman pumped DCF and amplifiers. Tx: transmitter; TF: transmission fiber; OPC: optical phase conjugator; OBPF: optical backpropagation fiber; Rx: receiver.

2.3.2 Ideal OBP using Distributed Amplification

To derive an equivalent way of realizing the ideal back propagation equation (Eq. (2.14)), let the output signal of the OPC, $q_b(t,0) = q^*(t,L_a)$, propagate through a DCF whose effective loss profile is a function of distance $\alpha_d(z_d)$, where z_d is the distance in DCF (see Fig. 2.2).

Using transformations

$$q(z_d,t) = \sqrt{P_{\text{in,d}}}e^{-\frac{1}{2}\int_0^{z_d}\alpha_d(z')\,dz'}u_b, \tag{2.15}$$

and

$$dz'_d = \beta_{2,d}dz_d, \tag{2.16}$$

Eq. (2.1) that describes the optical field envelope in this fiber can be rewritten as

$$i\frac{\partial u_b}{\partial z'_d} - \frac{1}{2}\frac{\partial^2 u_b}{\partial t^2} + \frac{\gamma_d P_{\text{in,d}}}{\beta_{2,d}}e^{-\int_0^{z_d}\alpha_d(z')dz'}|u_b|^2u_b = 0, \tag{2.17}$$

where $\beta_{2,d}$ and γ_d are the dispersion and nonlinear coefficients of the DCF, respectively, and $P_{\text{in,d}}$ is the launch power to the DCF.

Equations (2.17) and (2.14) are identical only if

$$dz'_b = dz'_d, \tag{2.18}$$

and

$$\frac{\gamma P_{\text{in}}}{\beta_2} e^{-\alpha(L_a - z_b)} = \frac{\gamma_d P_{\text{in,d}}}{\beta_{2,d}} e^{-\int_0^{z_d} \alpha_d(z')dz'}. \tag{2.19}$$

Substituting Eqs. (2.16) and (2.13) in Eq. (2.18), we obtain

$$\frac{dz_d}{dz_b} = \frac{\beta_2}{\beta_{2,d}}, \tag{2.20}$$

$$z_d = \frac{\beta_2}{\beta_{2,d}} z_b + c, \tag{2.21}$$

where c is a constant. Putting $z_d = 0$ when $z_b = 0$ yields $c = 0$.

Integrating Eq. (2.21), we find the length of the DCF as

$$L_d = \frac{\beta_2}{\beta_{2,d}} L_a. \tag{2.22}$$

It may be noted that the length of the ideal OBPF is the same as that of the TF (i.e., L_a), whereas the length of the DCF (i,e., L_d) could be much smaller if $|\beta_{2,d}| \gg |\beta_2|$.

Next, the constraints of Eq. (2.19) may be broken down into the following two constraints,

$$e^{\alpha z_b} = e^{-\int_0^{z_d} \alpha_d(z')dz'}, \tag{2.23}$$

$$P_{\text{in,d}} = \frac{\gamma}{\gamma_d} \frac{\beta_{2,d}}{\beta_2} P_{\text{in}} e^{-\alpha L_a}. \tag{2.24}$$

From Eq. (2.24), we see that if $\beta_{2,d} = \beta_2$ and $\gamma_d = \gamma$, the launch power to the DCF is simply the output of the TF.

Equation (2.23) can be satisfied only if α_d is constant, i.e.,

$$\alpha z_b = -\alpha_d z_d. \tag{2.25}$$

Using Eq. (2.21), we obtain an expression for the effective loss coefficient of DCF to have the ideal OBP as

$$\alpha_d = -\alpha \frac{\beta_{2,d}}{\beta_2}. \tag{2.26}$$

In Section 2.4, we discuss how to realize the effective loss/gain coefficient α_d of DCF for various pumping configurations. For simplicity, we have based our analysis on the scalar nonlinear Schrödinger equation (NLSE). However, the results are also applicable for the case of dual polarization when the polarization mode dispersion (PMD) is ignored. In fact, our simulations in Section 2.6 consider dual polarizations.

2.4 Raman Pumping

2.4.1 Forward Raman Pumping

The evolution of the signal and pump powers in the DCF for the forward pumping scheme is governed by (Agrawal, 2012; Kumar and Deen, 2014)

$$\frac{dP_s}{dz_d} = \frac{g_R P_p P_s}{A_p} - \alpha_s P_s, \tag{2.27a}$$

$$\frac{dP_p}{dz_d} = -\frac{\omega_p}{\omega_s}\frac{g_R P_p P_s}{A_s} - \alpha_p P_p, \tag{2.27b}$$

where g_R is the Raman gain coefficient; P, A, α and ω denote the power, effective cross-section, loss coefficient and angular frequency, respectively, and the subscripts p and s denote the pump and the signal, respectively. If the depletion of the pump due to the transfer of power to the signal (first term on the right hand side of Eq. (2.27b)) is ignored, the solution

of Eq. (2.27b) under this approximation is

$$P_p(z_d) = P_p^+(0)e^{-\alpha_p z_d}, \tag{2.28}$$

where $P_p^+(0)$ is the input pump power. Substituting Eq. (2.28) in Eq. (2.27a) and solving for P_s, we find (Agrawal, 2012; Kumar and Deen, 2014)

$$P_s(z_d) = P_s(0)\exp\left[-\alpha_s z_d + \frac{g_R P_p^+(0)}{A_p} z_{eff}^+\right], \tag{2.29}$$

where

$$z_{eff}^+(z_d) = \frac{1-\exp(-\alpha_p z_d)}{\alpha_p}. \tag{2.30}$$

Equation (2.29) may be rewritten as

$$P_s(z_d) = P_s(0)\exp[-g_{eff}(z_d)z_d], \tag{2.31}$$

where

$$g_{eff}(z_d) = \alpha_s - \frac{g_R P_p^+(0)}{A_p}\frac{z_{eff}^+}{z_d}. \tag{2.32}$$

At $z_d = L_d$, the effective gain coefficient is

$$g_{eff}(L_d) = \alpha_s - \frac{g_R P_p^+(0)}{A_p}\frac{L_{eff}}{L_d}, \tag{2.33}$$

where $L_{eff} = z_{eff}^+(L_d)$. When $z_b = L_a$, $z_d = L_d$ and from Eq. (2.23), we find that one of the requirements for the ideal OBP is

$$e^{\alpha L_a} = e^{-g_{eff}(L_d)L_d}. \tag{2.34}$$

Simplifying Eq. (2.34), we find an expression for the input pump power as

$$P_{p0}^{+} \equiv P_{p}^{+}(0) = (\alpha L_a + \alpha_s L_d)\frac{A_p}{g_R L_{eff}}. \tag{2.35}$$

Taylor expansion of Eq. (2.30) yields

$$z_{eff}^{+} = z_d - \frac{\alpha_p z_d^2}{2!} + \frac{\alpha_p^2 z_d^3}{3!} + \dots. \tag{2.36}$$

If $\alpha_p z_d \ll 1$, we find $z_{eff}^{+} \approx z_d$. Under this approximation, we have

$$g_{eff}(z_d) \approx \alpha_s - \frac{g_R P_{p0}^{+}}{A_p}. \tag{2.37}$$

Equation (2.26) provides the effective loss coefficient required for the ideal OBP. Hence, equating Eqs. (2.37) and (2.26), we obtain

$$g_{eff} = -\frac{\alpha \beta_{2,d}}{\beta_2}. \tag{2.38}$$

If $\alpha_p L_d \ll 1$, the variation of g_{eff} as a function of z_d is very small and the ideal OBP condition of Eq. (2.38) can be approximately realized. So, to make this approximation more accurate, we would like to keep the length of DCF, L_d small. If we choose the DCF that has larger $|\beta_{2,d}|$ as compared to that of the TF, the required length L_d becomes smaller (see Eq. (2.22)).

In our simulations (see Section 2.6), we have used $L_d = 3.077$ km and for such a short length, we found that the signal power evolution given by Eq. (2.29) obtained by the undepleted pump approximation is reasonably accurate. We have solved the nonlinear coupled Eqs. (2.27a) and (2.27b) numerically, and found that the maximum discrepancy between the signal power obtained by the numerical solution and Eq. (2.29) is ≈ 0.18 dB.

Due to the difference in dispersion and nonlinear coefficients between TF and DCF, the

launch power to the DCF should be adjusted in accordance with Eq. (2.24). So, we introduce a pre-amplifier with gain G_{pre} (see Fig. 2.2) which can be adjusted so that the one of the OBP conditions (Eq. (2.24)) is satisfied.

2.4.2 Backward Raman Pumping

Under the undepleted pump approximation, the evolution of the signal and pump powers in the DCF are given by (Agrawal, 2012)

$$P_p(z_d) = P_{p0}^{-} \exp\left[-\alpha_p(L_d - z_d)\right], \tag{2.39}$$

$$P_s(z_d) = P_{s0} \exp\left[-\alpha_s z_d + \frac{g_R P_{p0}^{-} e^{-\alpha_p L_d}}{Ap} z_{eff}^{-}\right], \tag{2.40}$$

$$z_{eff}^{-}(z_d) = \frac{e^{\alpha_p z_d} - 1}{\alpha_p}, \tag{2.41}$$

where P_{s0} is the signal power at $z_d = 0$ and P_{p0}^{-} is the pump power injected at $z_d = L_d$. Proceeding as before, the required pump power P_{p0}^{-} is found to be the same as that for forward pumping case (see Eq. (2.35)). If $\alpha_p z_d \ll 1$, $z_{eff}^{-} \approx z_d$ and in this case the effective gain coefficient becomes constant as required by the ideal OBP condition (Eq. (2.26)).

2.4.3 Bidirectional Pumping

We assume that there are two pumps, one co-propagating with the signal and the other counter-propagating (see Fig. 2.2). Under the undepleted pump approximation, the evolution of the signal is given by

$$P_s(z_d) = P_{s0} \exp\left[-\alpha_s z_d + \frac{g_R}{A_p}(P_{p0}^{+} z_{eff}^{+} + P_{p0}^{-} e^{-\alpha_p L_d} z_{eff}^{-})\right], \tag{2.42}$$

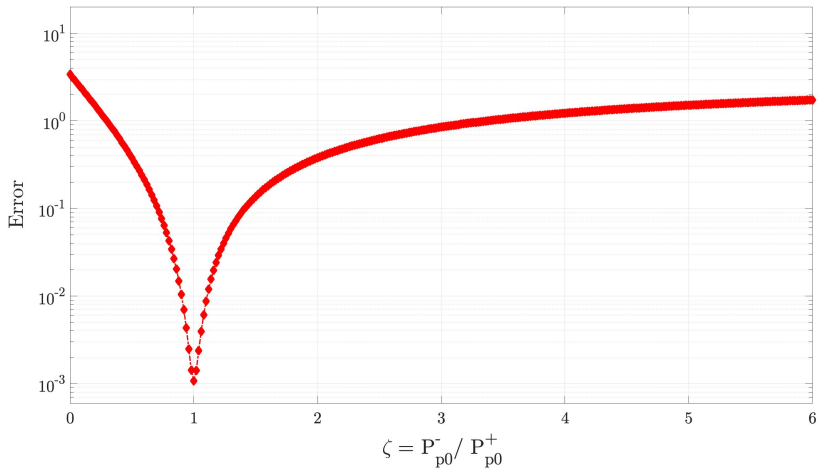

Figure 2.3: Deviation of the power profile from the ideal power profile as a function the pump power ratio.

where $P^{+}_{p0} = P^{+}_{p}(0)$ is the input power of the co-propagating pump and $P^{-}_{p0} = P^{-}_{p}(L_d)$ is the input power of the counter-propagating pump.

Using Eqs. (2.23), (2.25), (2.30) and (2.41), one of the requirements for the ideal OBP is

$$e^{\alpha L_a} = e^{-\alpha_s L_d + g_R L_{eff}(P^{+}_{p0}+P^{-}_{p0})/A_p}, \tag{2.43}$$

where $L_{eff} = \frac{1-\exp(-\alpha_p L_d)}{\alpha_p}$. Simplifying Eq. (2.43), we obtain

$$P_{p0} \equiv P^{+}_{p0} + P^{-}_{p0} = (\alpha L_a + \alpha_s L_d)\frac{A_p}{g_R L_{eff}}, \tag{2.44}$$

where P_{p0} is the total input pump power. Comparing Eqs. (2.35) and (2.44), we find that the sum of the input pump powers is the same as the input pump power of the case of the forward (or backward) pumping only.

Let the ratio of the input backward and forward pump powers be ζ, i.e., $\zeta = P^{-}_{p0}/P^{+}_{p0}$. Since the total input pump power P_{p0} is fixed (it should satisfy Eq. (2.44)), we have only one degree of freedom in the design of bidirectional pumping scheme, namely, the pump power ratio, ζ, which is optimum if the deviation of signal power profile from the ideal case (as

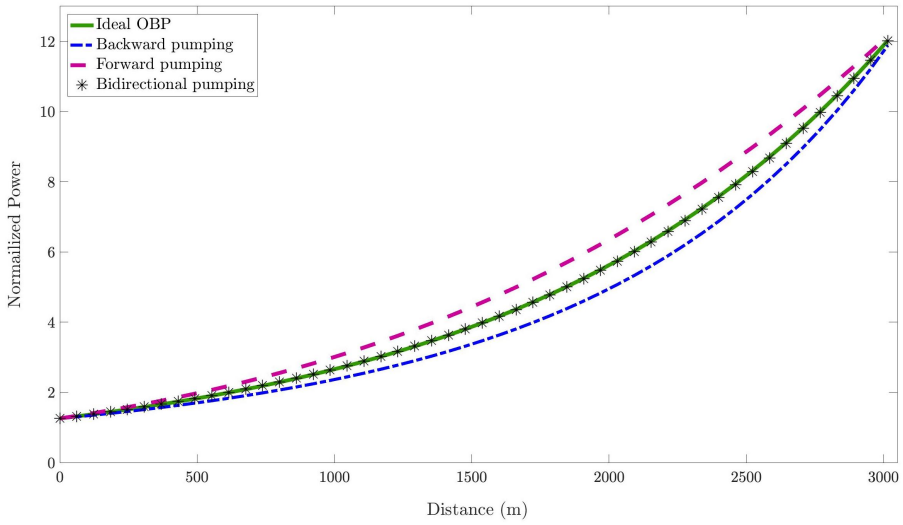

Figure 2.4: Normalized power profile of the signal along the DCF. For bidirectional pumping, $\zeta = 1$. Length of the DCF = 3.077 km.

required by the ideal OBP conditions, Eqs. (2.25) and (2.26)) is minimized. So, we consider the following optimization problem,

$$\underset{\zeta}{\text{minimize}} \quad e(\zeta)$$

where the error e is

$$e(\zeta) = \int_o^{L_d} |P_s^{ideal}(z_d) - P_s(z_d)|\, dz_d, \qquad \zeta = \frac{P_{p0}^-}{P_{p0}^+},$$

$P_s(z_d)$ is given by Eq. (2.42) and

$$P_s^{ideal}(z_d) = P_s(0) \exp\left(\frac{\alpha\beta_{2,d}}{\beta_2} z_d\right). \tag{2.45}$$

Figure 2.3 shows the error as a function of ζ. As can be seen, the error i.e., the deviation of the actual power profile from the ideal power profile is minimum when the input forward and backward pump powers are equal ($\zeta = 1$). Figure 2.4 shows the normalized signal power profile for forward/backward pumping only and bidirectional pumping cases. In the case of bidirectional pumping, we assume that the pump power ratio, ζ to be unity. As the length of the DCF is short, signal power profiles are close to exponential profiles. However,

for the longer length of a Raman pumped fiber (e.g., $L_d = 50$ km), for example, using the forward pumping scheme, signal power increases nearly exponentially at the beginning and then starts decreasing due to the signal loss and pump depletion. Figure 2.4 also shows the evolution of the signal power corresponding to the ideal case as required by OBP condition (Eq. (2.26)). As can be seen, in the case of forward power pumping, the power in the DCF exceeds that required by the ideal OBP, whereas in the case of backward pumping, it is lower than that required by the ideal OBP. When bidirectional pumping with an optimum power ratio $\zeta = 1$ is used, the power profile is closest to that required by the ideal OBP.

When $\zeta = 1$, Eq. (2.42) may be written as

$$P_s(z_d) = P_{s0} \exp\left[-\alpha_s z_d + \frac{g_R P_p(0)}{A_p} z_{eff}\right], \tag{2.46}$$

where

$$z_{eff} = \frac{1}{2}\left(\frac{1 - e^{-\alpha_p z_d}}{\alpha_p} + \frac{e^{-\alpha_p (L_d - z_d)} - e^{-\alpha_p L_d}}{\alpha_p}\right). \tag{2.47}$$

Next, we show that the second order term in z_d in the expansion of the z_{eff} can be made significantly smaller using bidirectional pumping with $\zeta = 1$ so that z_{eff} is nearly equal to z_d, which is the requirement for the ideal OBP. Expanding exponential functions in Eq. (2.47) using Taylor series yields

$$\begin{aligned} z_{eff} = &\left(1 - \frac{x}{2} + \frac{x^2}{4} - \frac{x^3}{12} + ...\right) z_d \\ &+ \left(-\frac{x}{4} + \frac{x^2}{8} - \frac{x^3}{24} + ...\right) \alpha_p z_d^2 \\ &+ \left(\frac{1}{6} - \frac{x}{12} + \frac{x^2}{24} + ...\right) \alpha_p^2 z_d^3, \end{aligned} \tag{2.48}$$

where $x = \alpha_p L_d$. For example, when $\alpha_p = 0.138$ km^{-1}, $L_d = 3.077$ km and $x = 0.425$. The coefficient of $\alpha_p z_d^2$ in Eq. (2.48) is -0.087, whereas it is -0.5 for the case of of the forward pumping (see Eq. (2.36)). Thus, there is a 82% reduction in the second order term in z_d using the bidirectional pumping. Hence, we expect that the OBP with bidirectional pumping

shows better performance. In the Section 2.6, we find that the transmission performance improvement brought by OBP depends mainly on how close the signal power profile is to the ideal profile.

Xia *et al.* (2014) used bidirectional Raman pumps for 400 Gb/s PM-16QAM transmission over 1504 km over Verizon network fiber deployed around Dallas. The backward Raman module consists of pump wavelengths in the range of 1420 nm to 1500 nm and the forward Raman module includes 3 pump wavelengths (1420 nm—1480 nm). Multiple pump wavelengths are used for the purpose of gain flattening. Iqbal *et al.* (2018) demonstrated the bidirectional distributed Raman amplification scheme for 83.32 km SSMF in which the backward Raman pump is at 1365 nm and the forward Raman pump module consists of two pumps at 1365 nm and 1455 nm which are combined with the signal using a WDM coupler. The pump at 1455 nm is obtained by backward pumping a separate 10 km SSMF with a 1365 nm pump. Wang *et al.* (2008) implemented the bidirectional Raman pumping scheme over 84 km NZDSF in a WDM-PON system. Both forward and backward Raman pump modules use two pump wavelengths 1450 nm and 1460 nm, and provide a gain of $\approx$ 20 dB.

Generally, WDM couplers are used for multiplexing the pumps and the signal at the fiber input and output ends, and isolators are placed at both ends. More details on the implementation of bidirectional pumping can be found in (Xia *et al.*, 2014; Iqbal *et al.*, 2018; Wang *et al.*, 2008).

2.5 OBP Configurations

We consider two OBP configurations (see Fig. 2.5). In configuration A, the OBP module post-compensates the dispersive and nonlinear effects of the TF, whereas in configuration B, the OBP module pre-compensates it. Eq. (2.24) may be written as

$$P_{\mathrm{in,d}}(\mathrm{dBm}) = P_{\mathrm{in,TF}}(\mathrm{dBm}) - F_{\mathrm{TF}}(\mathrm{dB}) + G_{pre}(\mathrm{dB}), \tag{2.49}$$

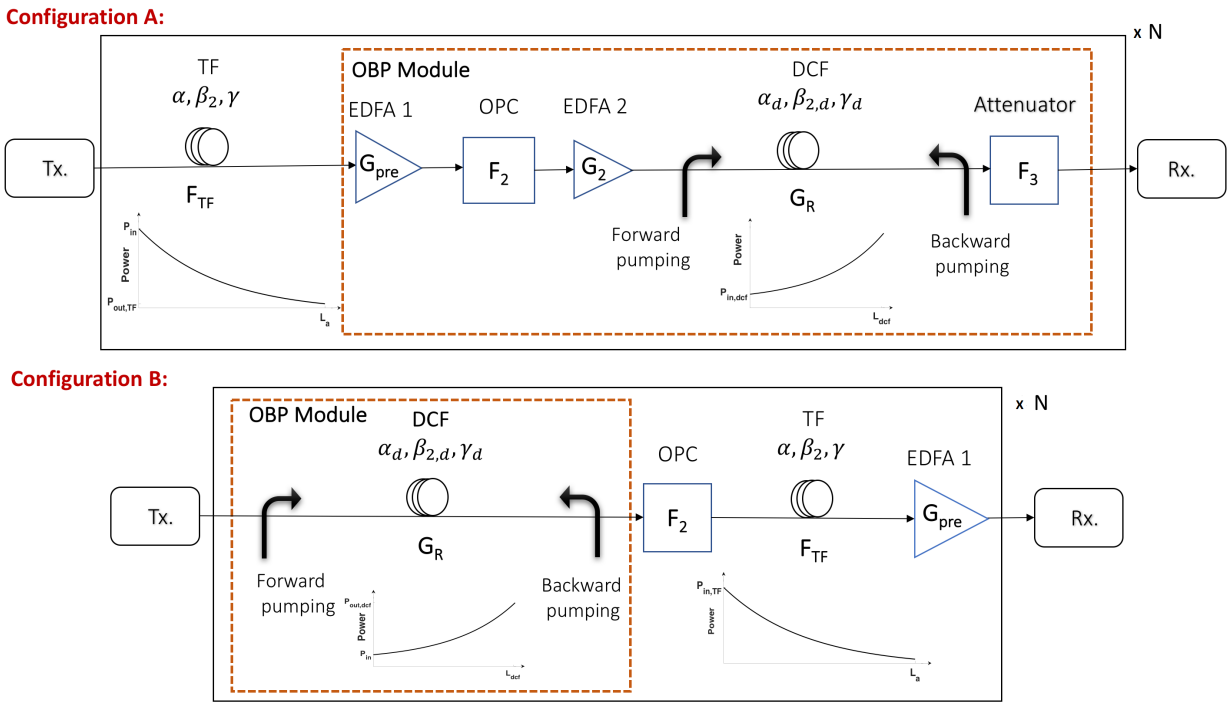

Figure 2.5: Configuration A and B: N-span fiber optic system with OBP using a Raman pumped DCF and amplifiers. Tx: transmitter; TF: transmission fiber; OPC: optical phase conjugator; DCF: dispersion compensating fiber; Rx: receiver.

where F_{TF} is the loss due to the TF and

$$G_{pre} = 10 \times \log_{10} \frac{\gamma}{\gamma_d} \frac{\beta_{2,d}}{\beta_2}. \tag{2.50}$$

From Eq. (2.49), we see that the launch power to the DCF, $P_{\mathrm{in,d}}$ should be larger than the output of the TF. As a result, in configuration A, we need to amplify the output of the TF by G_{pre}. Besides, OPC introduces a loss around 8 dB (Liang and Kumar, 2016). So, we need an amplifier, EDFA 2 with gain G_2 to compensate for the OPC loss (F_2). In order to meet the requirement of the ideal OBP, the Raman pumped DCF should provide a gain that is equal to loss of the TF. So, we are forced to introduce an attenuator, F_3 to compensate for the gain of the pre-amplifier (EDFA 1). So, the additional amplification by EDFA 1 to satisfy the OBP condition and the subsequent attenuation to compensate for it, leads to degradation in OSNR. This problem can be solved by using configuration B in

which the Raman pumped DCF precedes the TF. The theory of OBP developed in Section 2.3 is applicable to this configuration as well.

Next, we consider the power evolution in configuration B. Since the loss due to the TF (F_{TF}) is equal in magnitude to the net gain provided by the Raman amplification (G_R), but opposite in sign, Eq. (2.49) may be rewritten as

$$\begin{aligned} P_{\mathrm{out,d}}\,(\mathrm{dBm}) &= P_{\mathrm{in,d}}\,(\mathrm{dBm}) + F_{\mathrm{TF}}\,(\mathrm{dB}) \\ &= P_{\mathrm{in,TF}}\,(\mathrm{dBm}) + G_{pre}\,(\mathrm{dB}), \end{aligned} \tag{2.51}$$

where $P_{\mathrm{out,d}}$ is the output of DCF. From Eq. (2.51), we see that the input of the TF should be lower than the output of DCF by G_{pre} (dB). This means that we need to introduce attenuation after the DCF. Since the OPC introduces a loss which is of the order of G_{pre} (dB), it acts as the required attenuation and thereby, eliminates the need for the pair of amplification and attenuation required in configuration A.

The OSNR in configuration A is calculated as follows:

$$\mathrm{OSNR} = \frac{P_{\mathrm{in}}}{\sum_{j=1}^{3} P_{N,j}}, \tag{2.52}$$

where P_{in} is the output power of transmitter,

$$P_{N,j} = N n_{\mathrm{sp,EDFA}} G_R F_3 (G_j - 1) h f \Delta f, \quad j = 1, 2, \tag{2.53}$$

$n_{\mathrm{sp,EDFA}}$ is the spontaneous factor of EDFA, G_1, G_2, G_R and F_3 are the gains of EDFA 1, EDFA 2, Raman amplification and the loss due to the attenuator, respectively, and $\Delta f =$ 12.49 GHz.

$$P_{N,3} = N n_{sp,R} F_3 h f \Delta f \sum_{k=1}^{N_R} [(G_k - 1) \prod_{i=k+1}^{N_R} G_i], \tag{2.54}$$

where $n_{sp,R}$ is the spontaneous factor of Raman amplifier. We have modeled distributed Raman amplification as a superposition of N_R discrete tiny amplifiers with gain G_k (see

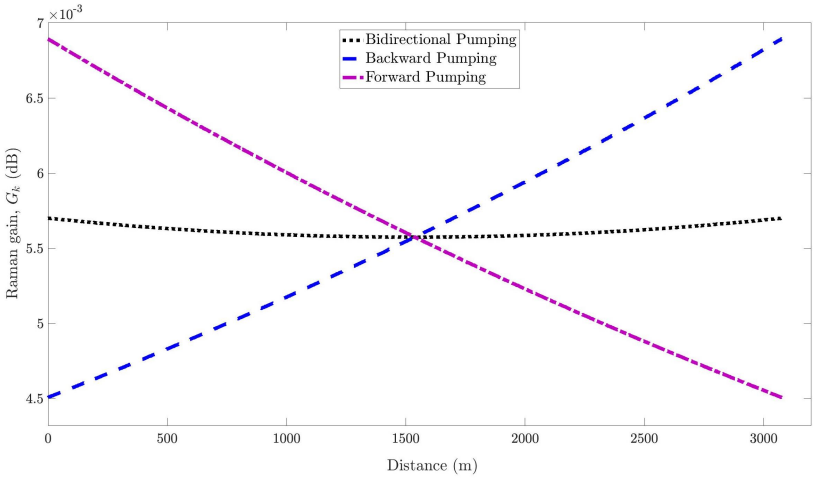

Figure 2.6: Gain evolution over the length of the DCF due to Raman amplification. For bidirectional pumping, $\zeta = 1$. Number of Raman tiny amplifiers, $N_R = 2000$, total Raman gain = 11.23 dB and length of the DCF = 3.077 km.

Section 2.6). The OSNR in scheme B is also calculated as follows:

$$\text{OSNR} = \frac{P_{\text{in}}}{\sum_{j=1}^{2} P_{N,j}}, \tag{2.55}$$

where

$$P_{N,1} = N n_{sp,R} F_{\text{TF}} h f \Delta f \sum_{k=1}^{N_R} [(G_k - 1) \prod_{i=k+1}^{N_R} G_i], \tag{2.56}$$

and

$$P_{N,2} = N n_{\text{sp,EDFA}} (G_{pre} - 1) h f \Delta f. \tag{2.57}$$

For example, when transmitter output power, $P_{\text{in}} = -10$ dBm, OSNR after $N = 30$ spans is 19.1 dB and 22.8 dB for configuration A and configuration B, respectively. Therefore, we expect the configuration B to show better performance over configuration A in the linear regime. However, in nonlinear regime (higher launch power), we cannot conclude which which configuration works better. Hence, we perform the numerical simulation of various OBP schemes in the next section.

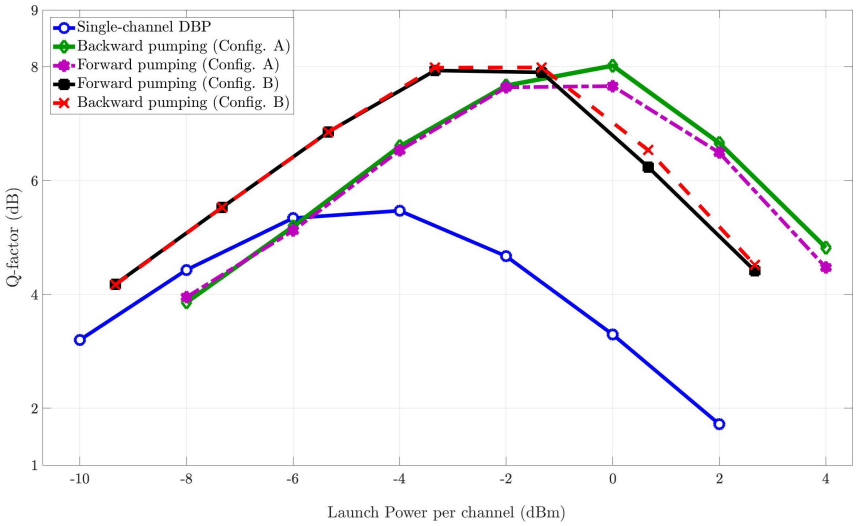

Figure 2.7: Q-factor versus transmitter output power per channel for different schemes when transmission distance is 1500 km.

2.6 Simulation Results

A 5-channel dual-polarization (DP) WDM fiber-optic system is simulated using the following parameters: channel spacing = 50 GHz, symbol rate per channel = 28 Gsymbols/s, modulation = 64 quadrature amplitude modulation (QAM). The raised cosine pulses with a roll-off factor 0.2 is used. Number of symbols/channel simulated is 4096 and the computational bandwidth = 560 GHz. The transmission fiber is Corning's Metrocor fiber whose dispersion, loss and nonlinear coefficients are $\beta_2 = 8$ ps^2/km, $\alpha = 0.2$ dB/km and $\gamma = 2.2$ W^{-1} km^{-1}, respectively. TF length, $L_a = 50$ km. For the DCF, $\beta_{2,d} = 130$ ps^2/km, loss coefficient at signal wavelength (1550 nm), $\alpha_s = 0.4$ dB/km, $\gamma_d = 4.86$ W^{-1} km^{-1}, and $L_d = 3.077$ km. For the proposed technique, it is required that dispersion coefficient of TF and DCF have the same sign. The commercially available DCFs have large normal dispersions and hence Corning's Metrocor fiber is used as a transmission fiber whose dispersion is normal. The proposed approach could be adapted to anomalous dispersion regime without any changes if DCFs with large anomalous dispersion coefficients are available. It may be possible to fabricate DCFs with large anomalous dispersion, but it was not attempted mainly because the standard single-mode fibers (SSMF) have anomalous dispersion in the C-band. It may

also be possible to develop Silicon photonics based nonlinear waveguides with very large anomalous dispersion which could be a substitute for the DCF in the proposed technique.

The pre-amplifier gain, $G_{pre} = 8.67$ dB. We assume the signal loss due to OPC is 8 dB. The OPC can be realized by four-wave mixing (FWM), stimulated Brillouin scattering (SBS) or stimulated Raman scattering (SRS). The OPC is typically realized using highly nonlinear fibers (HNLF) with one or two laser pumps. The nonlinear mixing of the signal and the pumps produces a four wave mixing sideband which is proportional to the signal conjugate. More details about the OPC modeling can be found in (Liang and Kumar, 2016), in which the non-ideal effects are also considered. The noise figure of EDFA (i.e., inline amplifiers/pre-amplifiers) is 4.77 dB. For a Raman pump, loss coefficient at pump wavelength (1450 nm), $\alpha_p = 0.6$ dB/km, $g_R/A_p = 2.2$ W^{-1} km^{-1}, and spontaneous noise factor $n_{sp,R} = 1.1$. Total input Raman pump power, $P_{p0} = 26.7$ dBm which is fixed for all three pumping schemes. The pumps have a RIN of -155 dB/Hz (Namiki *et al.*, 2004). The DCF is divided into $N_R = 2000$ segments, which corresponds to a step size of 1.5 m. The Raman gain over a segment is determined by Eqs. (2.29), (2.40) and (2.42) for forward, backward and bidirectional, respectively. A tiny discrete amplifier is introduced at the end of the segment k with ASE power spectral density given by $\rho_{\text{ASE,R}} = n_{sp,R}hf(G_k - 1)$, where G_k is the gain of the kth discrete amplifier. As a sanity check, we changed the step size to 1 m and 0.5 m, and found that the BER remains constant. Figure 2.6 shows the gain of the tiny amplifiers, G_k as a function of the DCF length. As can be seen, the gain is nearly constant as a function of length for the bidirectional scheme (as required by the OBP condition, Eq. (2.26)). This can be qualitatively understood as follows. For the case of forward pumping, the gain is higher at the beginning ($z_d \approx 0$) and it decreases at larger distance due to pump attenuation. In contrast, for backward pumping, the gain is higher near the end ($z_d \approx L_d$). When bidirectional pumping is used, the gain becomes nearly equal throughout the length of DCF. Total gain provided by the Raman amplifier is 11.23 dB.

We do not intend to make a rigorous modeling of Raman amplifier taking into account

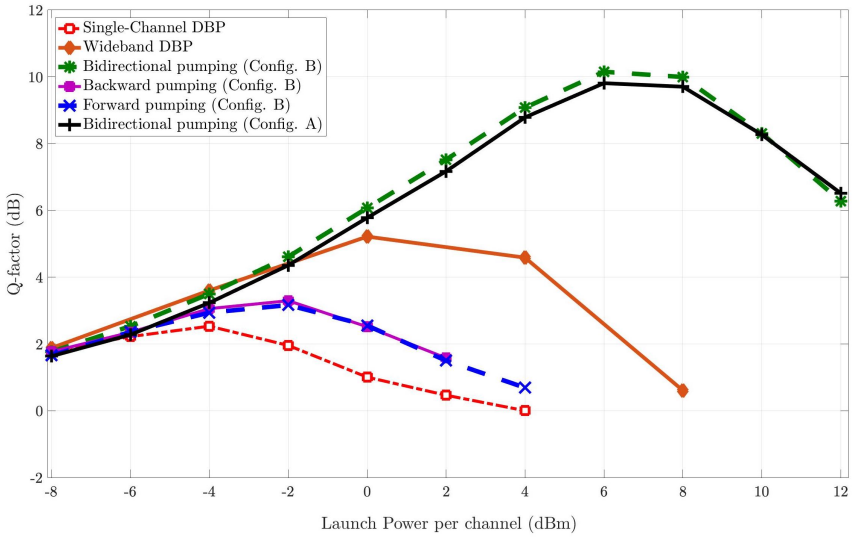

Figure 2.8: Q-factor versus launch power to the TF per channel for different schemes when transmission distance is 5000 km.

the effects such as reflection and single/double Rayleigh scattering which may cause the weakly reflected light oscillating and amplified between two pumping points (in the case of bidirectional pumping) since our primary focus is to model the entire fiber-optic link; instead, we focused only on the dominant effects such as gain and ASE. This is similar to our EDFA modeling which includes only gain and ASE.

The signal propagation in fiber is modeled by Manakov equation (Wai and Menyak, 1996). The well-known split-step Fourier technique (Agrawal, 2012; Kumar and Deen, 2014) is used to solve Manakov equation.

To compare the performance of the schemes discussed in Sec. 2.4, we study the performance in terms of Q-factor. The Q-factor is calculated using (Kumar and Deen, 2014),

$$Q = 20 \log_{10} \left[\sqrt{2}\, \text{erfcinv}(2 \times \text{BER}) \right], \tag{2.58}$$

where the BER is the bit error rate computed by the error counting. We compute the mean BER of 10 statistical runs of the fiber-optic system and use it in Eq. (2.58) to calculate the Q-factor.

Figure 2.7 shows the Q-factor of the central channel as a function of transmitter output

power when the transmission distance is 1500 km. At low powers, configuration B shows performance advantage over configuration A which can be attributed to higher OSNR. We can also see that both forward and backward pumping schemes show almost the same performance in the linear region which is due to the fact that for a short length of Raman pumped fiber, overall noise figure is almost the same for both pumping schemes, although for a longer length of the fiber, overall noise figure depends on the pumping scheme (Isoe *et al.*, 2013). From Fig. 2.7, it can be seen that for both configurations, backward pumping has a slightly better performance than forward pumping in the nonlinear region (≥ 0 dBm). This can be explained as follows. The compensation of the nonlinear distortions caused at the beginning of the transmission fiber span ($z \approx 0$) is more important than at the end of the span ($z \approx L_a$) since the power is higher at the beginning. The end section of the DCF ($z_d \approx L_d$) is responsible for the compensation of the nonlinear distortions occurring at the beginning of the TF ($z \approx 0$). As shown in Fig. 2.4, the signal power for the case of forward pumping is higher than the required power (as required by the ideal OBP condition) at the end section ($z_d \approx L_d$) and hence, it introduces more nonlinearity which leads to performance degradation as compared to backward pumping scheme. Both configurations provide roughly 2.5 dB Q-factor gain compared to single-channel DBP. At this distance, we find that the BER of a system with bidirectional pumping for a launch power of 2 dBm and above is below the detection limit; hence, we extend the reach further to be able to compare its performance with other compensation techniques.

Figure 2.8 shows the Q-factor of the central channel as a function of launch power to the TF when the transmission distance is 5000 km. In the case of single channel DBP, the central channel is demultiplexed at the receiver and the DBP is applied only to the central channel, whereas in the case of wideband DBP, full field DBP (Li *et al.*, 2008) is applied to all the channels and after the DBP, the central channel is demultiplexed. At the lower launch powers (-8 to -4 dBm), the OBP and DBP schemes provide roughly the same performance since nonlinear impairments are not significant. However, as the launch power increases, the

performance of forward/backward pumping schemes gets worse as compared to that of bidirectional Raman pumping scheme. This is because of the second and third order terms in z_d in Eq. (2.36) which makes the effective loss/gain coefficient α_d to deviate from the ideal OBP condition of Eq. (2.26). However, using the bidirectional pumping scheme, the performance can be significantly improved. From Fig. 2.8, we see that the configuration B brings 0.4 dB advantage in Q-factor as compared to the configuration A using bidirectional pumping at the optimum launch power. Using configuration B, the bidirectional pumping scheme (with ratio $\zeta = 1$) provides 6.8 dB improvement in Q-factor as compared to forward/backward pumping scheme. This significant improvement is attributed to the fact that the power profile in the bidirectional pumping scheme is close to the power profile required by the ideal OBP condition. The penalty due to RIN transfer from forward/bidirectional pumping can be neglected due to the high walkoff between pump and signal wavelength in the DCF (Fludger *et al.*, 2001).

As compared to single-channel DBP, OBP based on forward/backward pumping provides a performance advantage of 0.8 dB in Q-factor. At this distance, the wideband DBP has 2 dB performance advantage over OBP based forward/backward pumping scheme. However, wideband DBP requires extensive computational resources and there are technical challenges to combine the outputs of coherent receivers corresponding to different channels. Hence, wideband DBP is not implemented in real time in practical systems. Besides, although in principle, wideband DBP can be used in point-to-point systems, it cannot be implemented in optical networks (Liang and Kumar, 2016). In contrast, the OBP schemes provide performance improvements in both point-to-point systems and optical networks. From Fig. 2.8, we see that the OBP scheme with bidirectional Raman pumping provides 5 dB performance improvement over wideband DBP. This can be explained as follows.

Although the wideband DBP compensates for deterministic (signal-dependent) nonlinear impairments, it cannot compensate for stochastic signal-ASE nonlinear impairments such as Gordon-Mollenauer phase noise (Gordon and Mollenauer, 1990). However, the OBP scheme

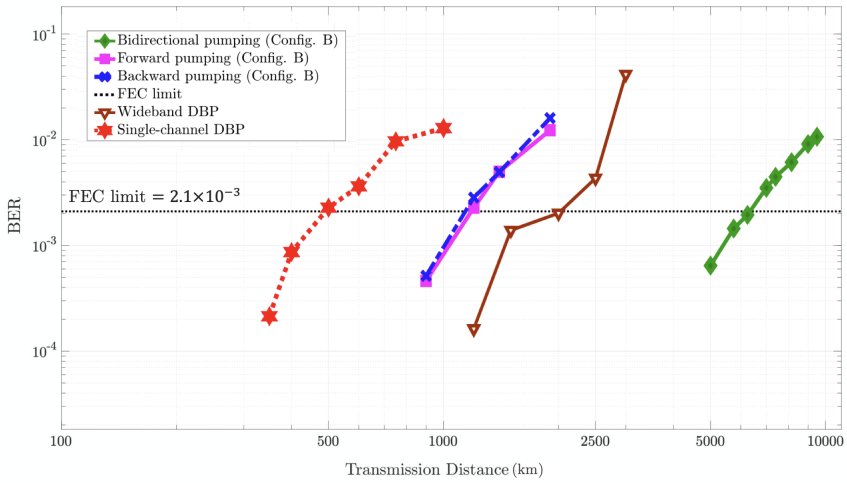

Figure 2.9: BER versus transmission distance.

with bidirectional Raman pumping provides partial compensation of stochastic signal-ASE nonlinear interactions, since the OPC partially compensates for nonlinear phase noise (Kumar and Liu, 2007a; Rahbarfam and Kumar, 2019).

Figure 2.9 shows the minimum BER as a function of transmission distance. The minimum BER is obtained by optimizing the launch power for each distance. At the BER of 2.1×10^{-3}, the transmission reach of single-channel DBP is about 500 km. OBP based forward/backward pumping scheme enhances the reach to 1150 km. The maximum achievable reach is further extended to 2000 km and 6500 km using wideband DBP and OBP based on bidirectional pumping, respectively.

2.7 Conclusion

We have investigated an optical back propagation technique to compensate for the dispersion and nonlinearity of the transmission fibers in real time. We have identified the conditions under which the nonlinear effects (both intra- and inter-channel nonlinearities) can be fully compensated and obtained an analytical expression for the power profile of the signal propagating in Raman pumped DCF which provides the exact compensation of intra-

and inter-channel signal-signal nonlinear impairments. Two possible configurations to implement the OBP are introduced and compared. We have studied a WDM system with 64-QAM format and showed that for 1500 km transmission distance, OBP based forward/backward Raman scheme brings 2.45 dB Q-factor gain as compared to single-channel DBP. However, wideband DBP (which compensates for all WDM channels) outperforms the OBP based on forward/backward pumping. This is because of the signal power profile in the DCF deviates from the ideal OBP condition due to the pump loss. Therefore, we proposed a third OBP scheme based on bidirectional pumping. We found that the signal power profile deviation from the ideal OBP profile is minimum when the forward and backward pump power are equal. Using this optimized pump powers, OBP based on bidirectional pumping outperforms that with forward/backward pumping. For 5000 km transmission distance, the performance of the proposed OBP schemes are compared with wideband DBP and single-channel DBP. Bidirectional pumping provides 5 dB performance advantage over wideband DBP. This is due to the fact that the OBP can also provide partial compensation for stochastic nonlinear impairments, whereas wideband DBP despite its high complexity cannot. Simulation results show that the transmission reach can be enhanced roughly by a factor of 2.4 using the OBP based on forward/backward pumping and by a factor of 13 using the OBP based on bidirectional pumping, as compared to single-channel DBP.

Chapter 3

Nonlinear Fourier Transform

The nonlinear Fourier transform (NFT) or inverse scattering transform (IST) is a mathematical method to solve initial value problems (IVP) associated with nonlinear partial differential equations that belong to a certain class of so-called integrable equations. It involves associating a given nonlinear equation to a pair of auxiliary linear operators i.e., a nonlinear partial differential equation can be written as the compatibility condition of two linear equations. In simple words, an integrable nonlinear equation is solved moving to another domain, the nonlinear frequency domain, where it is mapped into a linear equation. Consequently, the NFT can be viewed as the nonlinear analog of the linear Fourier transform (FT), which indeed, approximates the NFT at low power.

This chapter focuses on the fiber channel model and the nonlinear Fourier transform (NFT) theory. In Section 3.1, the integrable version of the NLSE and its normalized version are presented which will be later used to define the NFT. After a brief introduction about the NFT in Section 3.2, the NFT theory regarding the NLSE with vanishing boundary conditions and its concepts are reviewed in Section 3.3. Section 3.4 highlights the similarity between the NFT and linear Fourier method. It can help the reader understand the NFT. In Section 3.5, the non-integrable lossy fiber channel is approximated with a lossless integrable path-averaged model. Finally, Section 3.6 studies nonlinear frequency division multiplexing

(NFDM) as the possible application of the NFT in optical fiber communications.

3.1 Normalized Nonlinear Schrödinger Equation

The propagation of a narrowband optical wave over a lossless fiber is described by the so-called nonlinear Schrödinger equation (NLSE) (Agrawal, 2012)

$$\frac{\partial Q(\tau,l)}{\partial l} = -j\frac{\beta_2}{2}\frac{\partial^2 Q(\tau,l)}{\partial \tau^2} + j\gamma|Q(\tau,l)|^2 Q(\tau,l), \tag{3.1}$$

where $Q(\tau,l)$ is the complex envelope of the signal, l is the distance along the fiber, τ is the retarded time moving with the group velocity. β_2 and γ are dispersion and nonlinear coefficients, respectively. In order to remove the dependency of the channel model on fiber parameters, it is customary to work with the normalized NLSE by performing the following change of variables:

$$q = \frac{Q}{\sqrt{P_n}}, \quad z = \frac{l}{L_0}, \quad t = \frac{\tau}{T_0}, \tag{3.2}$$

with $L_0 = 2T_0^2/|\beta_2|$, power normalization factor $P_n = 2/(\gamma L_0)$, and T_0 is a free parameter. Using Eq. (3.2), the normalized NLSE becomes

$$jq_z(t,z) = q_{tt}(t,z) + 2\sigma|q(t,z)|^2 q(t,z), \tag{3.3}$$

where q, z and t represent the normalized signal envelope, space and time variables, respectively. The parameter $\sigma = -sign(\beta_2)$: the case with $\sigma = +1$ corresponds to the focusing regime while $\sigma = -1$ corresponds to the defocussing case. In this thesis only the focusing regime is considered.

The NLSE in the absence of loss and noise, Eq. (3.3) belongs to the class of integrable nonlinear systems that can be solved analytically by the NFT. This means given the initial value $q(t,0)$, the solution $q(t,z) \in L^1(\mathbb{R})$ with vanishing boundary condition i.e., $q(t,z) \to 0$ as $t \to \pm\infty$, can be obtained via the NFT. In fact, NFT allows effective diagonalization of the

nonlinear fiber channel by decomposing the nonlinear channel into the multiple independent channels in nonlinear spectral domain which propagate multiplicatively down the nonlinear channel.

3.2 Nonlinear Fourier Transform

The nonlinear Fourier transform (also known as the inverse scattering transform (IST)) as a method for solving nonlinear evolution equations was first discovered in the course of studying solutions to the Korteweg-deVries (KdV) equation, known in the study of water waves. Zabusky and Kruskal (1965) showed numerically the existence of a solitary wave solution whose shape is preserved (or varies periodically) during propagation, while, this solitary wave, for the first time, in 1834 was observed by J. Scott Russel in water canal (Russel, 1838). They surprisingly observed that when two such special solutions pass through each other, their shapes remain unchanged except for a relative phase shift. To reflect their particle-like nature, Kruskal and Zabusky named these solutions solitons.

Gardner, Greene, Kruskal and Miura (Gardner *et al.*, 1967), discovered that the eigenvalues of one-dimensional Schrödinger operator $L = \partial^2/\partial t^2 + u(t, z)$ remain invariant during the evolution in z if the potential $u(t, z)$ satisfies the KdV equation. They developed a method to recover the external potential $u(t, z)$ by solving the inverse scattering problem for L. This method, obtaining the potential from its scattering data, is now known as inverse scattering transform (IST).

Lax (1968) gave a mathematical formalization to generalize the method, by relating the nonlinear evolution equation to a pair of auxiliary operators with invariant eigenvalues–now called Lax pair. Once a Lax pair for a nonlinear evolution equations is found, the IST method can be applied to solve that equation. However, at that time a Lax pair was known only for the KdV equation. Not long afterwards, Zaharov and Shabat (1972) found a Lax pair for the NLSE and showed that NLSE can also be solved using the IST method. Later

this method for the NLS equation was referred to as the "nonlinear Fourier transform" due to its analogy with the linear Fourier transform (FT) by Ablowitz and Segur (1981) and others who further developed this method.

Mollenauer *et al.* (1980) announced the observation of solitons in nonlinear optical fibers earlier predicted by Hasegawa and Tappert (1973).

3.2.1 Lax Approach

A Lax pair (Yousefi and Kschischang, 2014) refers to a set of two linear operators (L, M) depending on the space coordinate z that together construct a given nonlinear evolution equation such that

$$\frac{dL}{dz} = [M, L] = ML - LM, \tag{3.4}$$

where $[M, L]$ represents the commutator of the operators L and M. This equation is called the Lax equation.

The process of finding L and M corresponding to a given nonlinear system of equations is generally non-trivial but once the corresponding suitable Lax pair is found, they can be used to solve the equation using the NFT method.

Example: The Lax pair associated with KdV equation is $L = D^2 + q$ and $M = [3D^3 + Dq + qD]/2$ where $D = \frac{\partial}{\partial t}$. By plugging this Lax pair into the Lax equation i.e., $L_z = [M, L]$, KdV equation can be recovered as $q_z = qq_t + q_{ttt}$.

The eigenvalues of the operator L, $\lambda \in \mathbb{C}$ such that

$$Lv = \lambda v, \tag{3.5}$$

are constant in an isospectral flow (as seen in Fig. 3.1) i.e., independent of z as a consequence of Lax equation, Eq. (3.4) (Lamb, 1980; Yousefi and Kschischang, 2014).

Taking the z derivative of Eq. (3.5) and using the Lax equation, the eigenfunction v evolves

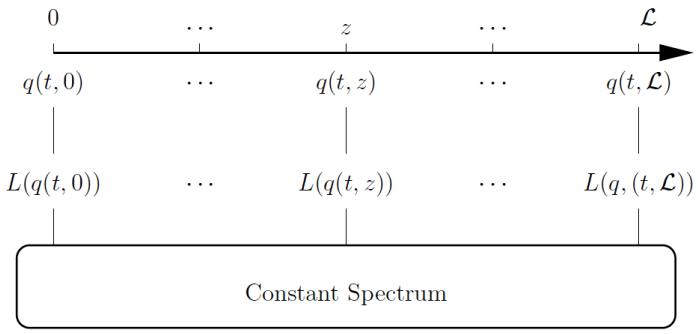

Figure 3.1: An isospectral flow: the spectrum of L remains unchanged upon spatial propagation (Yousefi and Kschischang, 2014).

in z according to the linear equation (Yousefi and Kschischang, 2014)

$$v_z = Mv. \tag{3.6}$$

Equation (3.5) can be rewritten, by differentiating with respect to t and after simple algebra, as

$$v_t = Pv, \tag{3.7}$$

where $P = \Sigma(L - \lambda I) + DI$ for some invertible Σ and $D = \frac{\partial}{\partial t}$ (Yousefi and Kschischang, 2014).

Using the equality of mixed derivatives i.e., $v_{zt} = v_{tz}$ and with $\partial\lambda/\partial z = 0$, the Lax equation Eq. (3.4) can be written as

$$P_z - M_t + [P, M] = 0, \tag{3.8}$$

which is called *zero-curvature condition* (Yousefi and Kschischang, 2014). Therefore, the given nonlinear evolution equation for a complex-value $q(t, z)$ can be viewed as a compatibility condition for the simultaneous linear equations. This implies that certain nonlinear equations hold a hidden linearity in the form of Eqs. (3.6) and (3.7).

3.3 Nonlinear Fourier Transform for the Nonlinear Schrödinger Equation

The Lax pair associated with the scalar NLSE is

$$L = j \begin{pmatrix} D & -q(t,z) \\ -\sigma q^*(t,z) & -D \end{pmatrix}, \tag{3.9}$$

and

$$M = \begin{pmatrix} 2j\lambda^2 - j\sigma|q(t,z)|^2 & -2\lambda q(t,z) - jq_t(t,z) \\ 2\lambda\sigma q^*(t,z) - j\sigma q_t^*(t,z) & -2j\lambda^2 + j\sigma|q(t,z)|^2 \end{pmatrix}, \tag{3.10}$$

with derivative operator $D = \frac{\partial}{\partial t}$.

Substituting Eqs. (3.9) and (3.10) in the Lax equation, Eq. (3.4), results in four equations, one for each matrix component. Performing calculation on the (1,2)-element of the matrix equation yields the integrable NLSE, Eq. (3.3).

Operator P for NLSE is

$$P = \begin{pmatrix} -j\lambda & q(t,z) \\ -\sigma q^*(t,z) & j\lambda \end{pmatrix}. \tag{3.11}$$

Using Eqs. (3.10) and (3.11), zero-curvature equation is also simplified to $jq_z(t,z) = q_{tt}(t,z) + 2\sigma|q(t,z)|^2 q(t,z)$. The equation with P i.e., $v_t = Pv$, for NLSE generally is known as *Zakharaov-Shabat* system.

3.3.1 Nonlinear Fourier Spectrum and Coefficients

To study the scattering data for NLSE, for a given eigenfunction $v(t) = (v_1(t), v_2(t))^T$ at a certain distance z, we can write Zakharaov-Shabat system, as the following two partial

differential equations (PDEs)

$$\frac{\partial v_1}{\partial t} = -j\lambda v_1(t) + q(t,z)v_2(t), \tag{3.12a}$$

$$\frac{\partial v_2}{\partial t} = -\sigma q(t,z)^* v_1(t) + j\lambda v_2(t), \tag{3.12b}$$

where $q(t,z)$ evolves according to the NLSE. The solution of Eq. (3.12) depends on the choice of boundary conditions. If $q(t,z)$ is a rapidly decaying smooth function i.e., $q(t,z) \to 0$ as $t \to \infty$, the Eq. (3.12) becomes

$$v_t \to \begin{pmatrix} -j\lambda & 0 \\ 0 & j\lambda \end{pmatrix} v \quad \text{as } t \to \infty, \tag{3.13}$$

which has a general solution:

$$v(\infty,\lambda) \longrightarrow (\alpha e^{-j\lambda t}, \beta e^{j\lambda t}),\ \alpha,\beta \in \mathbb{C}. \tag{3.14}$$

These solutions form a two-dimensional subspace E_λ of continuously differentiable 2×1 vector functions. A possible set of solutions of Eq. (3.12), called Jost solutions, are (Ablowitz *et al.*, 2004)

$$v^1(t,\lambda) = \begin{pmatrix} 0 \\ 1 \end{pmatrix} e^{j\lambda t}; \qquad \bar{v}^1(t,\lambda) = \begin{pmatrix} 1 \\ 0 \end{pmatrix} e^{-j\lambda t} \quad \text{as } t \to +\infty, \tag{3.15a}$$

$$v^2(t,\lambda) = \begin{pmatrix} 1 \\ 0 \end{pmatrix} e^{-j\lambda t}; \qquad \bar{v}^2(t,\lambda) = \begin{pmatrix} 0 \\ 1 \end{pmatrix} e^{j\lambda t} \quad \text{as } t \to -\infty. \tag{3.15b}$$

These four eigenfunctions $v^1(t,\lambda)$, $v^2(t,\lambda)$, $\bar{v}^1(t,\lambda)$ and $\bar{v}^2(t,\lambda)$, which are all elements of E_λ, are called canonical eigenfunctions. These solutions $\{v^1(t,\lambda), \bar{v}^1(t,\lambda)\}$ and $\{v^2(t,\lambda), \bar{v}^2(t,\lambda)\}$ form two linearly dependent bases corresponding to λ. By choosing $v^1(t,\lambda)$ and $\bar{v}^1(t,\lambda)$ as

a basis of E_λ, we can write

$$v^2(t,\lambda) = a(\lambda)\bar{v}^1(t,\lambda) + b(\lambda)v^1(t,\lambda), \tag{3.16a}$$

$$\bar{v}^2(t,\lambda) = \bar{b}(\lambda)\bar{v}^1(t,\lambda) + \bar{a}(\lambda)v^1(t,\lambda), \tag{3.16b}$$

where $a(\lambda) = \langle v^2, v^1\rangle$ and $b(\lambda) = \langle \bar{v}^1, v^2\rangle$; where for any u, w, $\langle u, w\rangle := u_1w_2 - u_2w_1$. $a(\lambda), \bar{a}(\lambda), b(\lambda)$ and $\bar{b}(\lambda)$ are known as scattering coefficients. Note, in order not to overburden the notation, the dependence on the space variable z is dropped.

The coefficients $a(\lambda)$ and $b(\lambda)$ and their barred version are time-invariant. This is a crucial property that allows computing them at any arbitrary time: $v^1(t,\lambda)$ and $\bar{v}^1(t,\lambda)$ are known from the vanishing boundary condition at $t \to +\infty$ (see Eq. 3.15a). The other two canonical eigenfunctions are scattered from $t = -\infty$ to $t = +\infty$, i.e., for example, $v^2(t,\lambda)$ propagates from $t = -\infty$ where it is known from the boundary condition, towards $t = +\infty$, while interacts with potential $q(t,z)$, according to $v_t^2 = P(\lambda, q)v^2$ (Yousefi and Kschischang, 2014). Therefore, these scattering coefficients (for all λ) contain complete information of the signal. Thus, from them, we can reconstruct $q(t,z)$ uniquely. This scattering process is known as nonlinear Fourier transform (NFT) which was originally called the inverse scattering transform.

From Eq. (3.16) and considering boundary conditions Eq. (3.15)

$$a(\lambda) = \lim_{t\to+\infty} v_1^2 e^{j\lambda t}, \tag{3.17a}$$

$$b(\lambda) = \lim_{t\to+\infty} v_2^2 e^{-j\lambda t}. \tag{3.17b}$$

where $v^2(t,\lambda)$ is a solution of $Lv = \lambda v$ under the boundary condition Eq. (3.15b) and v_j^2 refers to the jth element of v^2.

Continuous spectrum If $\lambda \in \mathbb{R}$, the Jost solutions are bounded, therefore Eq. (3.16)

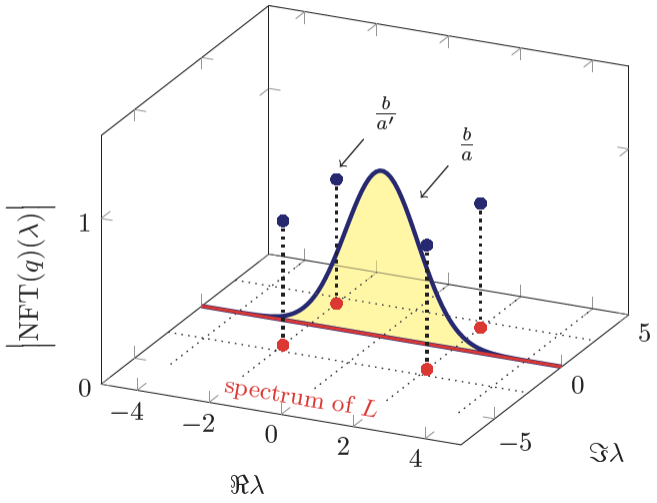

Figure 3.2: The continuous and discrete spectral amplitudes corresponding to the nonlinear frequencies and the discrete eigenvalues (Yousefi and Yangzhang, 2020).

are well-defined and consequently the scattering coefficients too. The continuous spectrum $\lambda \in \mathbb{R}$ corresponds to the non-solitonic (dispersive) components of the signal. They are often called nonlinear frequencies.

The continuous spectral amplitudes (also referred to as reflection coefficients (Ablowitz *et al.*, 2004)) based on scattering coefficients are defined as

$$\tilde{q}(\lambda) = \frac{b(\lambda)}{a(\lambda)}, \qquad \lambda \in \mathbb{R} \tag{3.18}$$

Discrete spectrum If λ is complex i.e., $\Im(\lambda) \neq 0$, either one of the Jost solutions $\{v^1(t,\lambda), \bar{v}^1(t,\lambda)\}$ diverge as $t \to +\infty$. If the upper half complex plane i.e., $\lambda \in \mathbb{C}^+$ is considered, in order to make sure that $v^2(t,\lambda)$ in Eq. (3.16a) is bounded, the condition $a(\lambda) = 0$ is needed. $a(\lambda)$ is an analytic function over the upper half complex plane (Ablowitz *et al.*, 2004; Yousefi and Kschischang, 2014) so that $a(\lambda)$ has a finite set of N_{DS} zeros corresponding to the discrete eigenvalues (λ_j) of Zakharov-Shabat system. These discrete eigenvalues correspond to solitons.

The discrete spectral amplitudes (also called norming constants) are defined as

$$C_j = \frac{b(\lambda_j)}{a'(\lambda_j)}, \quad j = 1, 2, \dots N_{DS}, \;\; \lambda_j \in \mathbb{C}^+ \tag{3.19}$$

where $a'(\lambda_j) = \frac{da(\lambda)}{d\lambda}|_{\lambda=\lambda_j}$ such that $a(\lambda_j) = 0$. Figure 3.2 shows the continuous and discrete nonlinear spectrum and their corresponding spectral amplitudes.

The inverse process i.e., reconstructing the time domain signal $q(t)$ from the nonlinear spectrum can be carried out by solving the Gelfand-Levitan-Marchenko equation (GLME) (Ablowitz *et al.*, 2003)

$$K(x, y) - \sigma F^*(x + y) + \sigma \int_x^{+\infty} \int_x^{+\infty} K(x, r) F(r + s) F^*(s + y)\, ds\, dr = 0, \tag{3.20}$$

where function $F(x)$ depends on the nonlinear spectrum and is defined as

$$F(x) = \frac{1}{2\pi} \int_{-\infty}^{+\infty} \tilde{q}(\lambda) e^{j\lambda x} d\lambda - j \sum_{j=1}^{N_{DS}} C_j e^{j\lambda_j x}. \tag{3.21}$$

When the discrete spectrum is empty, it reduces to

$$F(x) = \frac{1}{2\pi} \int_{-\infty}^{+\infty} \tilde{q}(\lambda) e^{j\lambda x} d\lambda, \tag{3.22}$$

which is just the inverse Fourier transform (IFT) of the continuous spectrum. The integral equation (3.20) is solved to find $K(x, y)$ and finally $q(t)$ is determined using $q(t) = -2K(t, t)$.

3.3.2 Evolution of Nonlinear Fourier Transform

As $q(t, z)$ propagates along z, the eigenvalues of L are constant and the eigenfunctions of L evolve in z according to Eq. (3.6). The spatial evolution of the scattering coefficients,

derived from Eq. (3.6), is given by (Ablowitz *et al.*, 2004)

$$a(\lambda, z) = a(\lambda, 0) \qquad \bar{a}(\lambda, z) = \bar{a}(\lambda, 0) \tag{3.23a}$$

$$b(\lambda, z) = b(\lambda, 0)e^{-4j\lambda^2 z} \qquad \bar{b}(\lambda, z) = \bar{b}(\lambda, 0)e^{4j\lambda^2 z} \tag{3.23b}$$

From the evolution of the scattering coefficients, the discrete and continuous spectral amplitudes propagate according to

$$\tilde{q}(\lambda, z) = e^{-4j\lambda^2 z}\tilde{q}(\lambda, 0), \tag{3.24a}$$

$$C_j(z) = e^{-4j\lambda_j^2 z}C_j(0), \tag{3.24b}$$

$$\lambda_j(z) = \lambda_j(0), \quad j = 1, 2, \ldots N_{DS}. \tag{3.24c}$$

Note, the nonlinear domain transfer function of the fiber channel modeled by the NLSE is a simple linear filter i.e.,

$$H(\lambda) = e^{-4j\lambda^2 z}, \tag{3.25}$$

very similar to the linear Fourier transform that maps $y(t) = x(t) * h(t)$ into a number of parallel scalar channels as $Y(f) = X(f) \cdot H(f)$.

3.4 Understanding the Nonlinear Fourier Transform

NFT can be understood as the nonlinear analog of the well-known procedure for solving the initial value problem (IVP) of linear PDEs using the Fourier transform (FT). This similarity can be understood as follows.

For example, the evolution of an optical pulse over a purely dispersive fiber is governed by

$$\frac{\partial q(t, z)}{\partial z} = -j\frac{\partial^2 q(t, z)}{\partial t^2}. \tag{3.26}$$

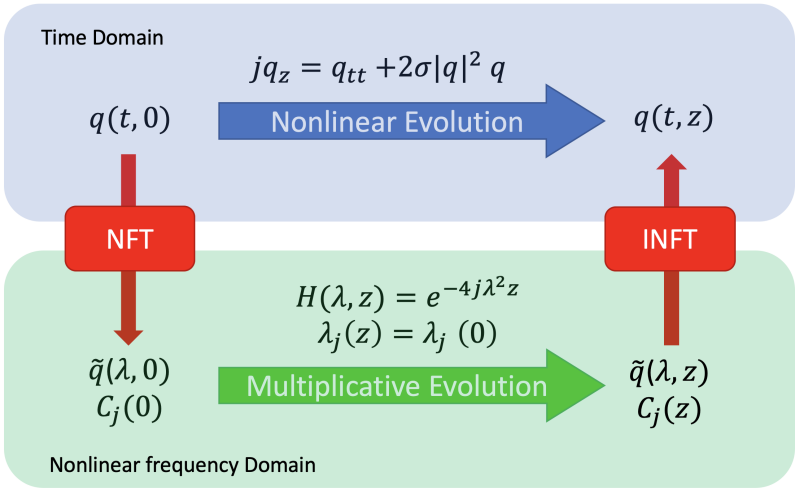

Figure 3.3: Solving an IVP problem associated with the NLSE using nonlinear Fourier transform.

Given the initial waveform $q(t, z = 0)$, the goal is to find the waveform $q(t, z)$ for some specific spatial coordinate z. This linear IVP can be straightforwardly solved in the Fourier domain.

The first step is to transfer the evolution in the Fourier domain as

$$\frac{\partial Q(f,z)}{\partial z} = j(2\pi f)^2 Q(f,z), \quad Q(f, z = 0) = Q_0(f) \tag{3.27}$$

where $Q(f,z) = \int_{-\infty}^{+\infty} q(t,z)e^{-j2\pi ft}\,dt$ is the FT of the signal $q(t,z)$. Then the spatial evolution of $Q(f,z)$ for each component f can be obtained by integrating over the spatial coordinate z as

$$Q(f,z) = \exp(j4\pi^2 f^2 z)Q_0(f), \tag{3.28}$$

where $\exp(j4\pi^2 f^2 z)$ is the channel response in linear frequency domain. In the linear frequency domain, each frequency component evolves independently, implying that FT diagonalizes the linear dispersive channel.

Finally, the solution $q(t,z)$ of the IVP is obtained by performing the inverse FT (IFT) of $Q(f,z)$ i.e., $q(t,z) = \int_{-\infty}^{+\infty} Q(f,z)e^{j2\pi ft}\,df$. This approach can be extended to solve the IVP

of nonlinear PDEs such as the NLSE using nonlinear Fourier transform (NFT). The method to solve a given nonlinear evolution equation using the NFT is conceptually similar to the linear Fourier method, despite the fact that a compact formula does not exist for computing the NFT or the inverse NFT (INFT).

The solution $q(z,t)$ of the NLSE, given by

$$jq_z(t,z) = q_{tt}(t,z) + 2\sigma|q(t,z)|^2 q(t,z), \qquad q(t,z=0) = q_0(t) \tag{3.29}$$

can be found, as shown in Fig 3.3, through the following steps:

1. Direct scattering problem: obtain the nonlinear Fourier spectrum $\tilde{q}(\lambda,0)$ and $C_j(0)$ of $q_0(t)$ by performing the NFT.

2. Propagate the nonlinear spectrum according to Eq. (3.24) to obtain the nonlinear spectrum $\tilde{q}(\lambda,z)$ and $C_j(z)$. Similar to the Fourier transform, the spatial evolution of the spectral data is transformed into a simple phase rotation in the transform domain, which indicates the linear propagation of spectral data.

3. Inverse scattering problem: perform the INFT of the nonlinear spectrum to obtain the time domain signal $q(t,z)$ at distance z.

3.5 Nonlinear Schrödinger Equation in the Presence of Loss

For optical links with EDFA-based lumped amplification, the channel model is given (that is, in-between two consecutive amplifiers)

$$\frac{\partial Q(\tau,l)}{\partial l} = -j\frac{\beta_2}{2}\frac{\partial^2 Q(\tau,l)}{\partial \tau^2} + j\gamma|Q(\tau,l)|^2 Q(\tau,l) - \frac{\alpha}{2}Q(\tau,l) + N(\tau,l), \tag{3.30}$$

where $N(\tau, l)$ is band-limited white Gaussian amplified spontaneous emission (ASE) noise and α is the fiber loss coefficient. The presence of these two terms makes Eq. (3.30) non-integrable so that the inverse scattering method cannot provide exact analytical solutions anymore.

This non-integrable lossy channel model Eq. (3.30) can be approximated by an integrable lossless path-averaged (LPA) model where the nonlinear coefficient γ is replaced with its average value over the fiber length. This approach, earlier introduced by Hasegawa and Kodama (1990) for soliton communications, is used in (Le *et al.*, 2015) to address the loss problem in NFT-based systems.

Using transformation

$$Q(\tau, l) = e^{-\frac{1}{2}\int_0^l \alpha dz} u(\tau, l), \tag{3.31}$$

Equation (3.30) can be rewritten as

$$\frac{\partial u(\tau, l)}{\partial l} = -j\frac{\beta_2}{2}\frac{\partial^2 u(\tau, l)}{\partial \tau^2} + j\gamma(l)|u(\tau, l)|^2 u(\tau, l) + N(\tau, l), \tag{3.32}$$

where $\gamma(l) = \gamma e^{-\int_0^l \alpha dz}$.

By averaging this parameter over one span length L_a as

$$\gamma_{eff} = \frac{1}{L_a}\int_0^{L_a} \gamma(l) dl, \tag{3.33}$$

we arrive to the lossless path-averaged (LPA) NLSE as

$$\frac{\partial u(\tau, l)}{\partial l} = -j\frac{\beta_2}{2}\frac{\partial^2 Q(\tau, l)}{\partial \tau^2} + j\gamma_{eff}|u(\tau, l)|^2 u(\tau, l) + N(\tau, l). \tag{3.34}$$

For an EDFA amplified system with equally spaced amplifiers and the loss is exactly compensated by gain $G = e^{\alpha L_a}$, the average value becomes

$$\gamma_{eff} = \gamma\frac{(1 - e^{-\alpha L_a})}{\alpha L_a}. \tag{3.35}$$

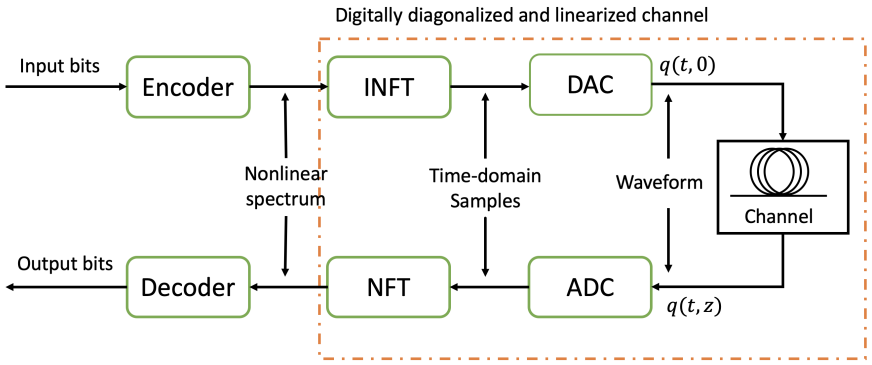

Figure 3.4: A typical NFDM scheme.

Since the LPA-NLSE is an approximate model, its accuracy generally depends on the signal power, bandwidth and transmission distance (Le *et al.*, 2015). Note, the inverse scattering method can be applied to solve LPA-NLSE, but the obtained solutions are only approximations of the real solutions of Eq. (3.30).

3.6 Nonlinear Frequency Division Multiplexing

Nonlinear frequency division multiplexing (NFDM) is introduced as the nonlinear analog of orthogonal frequency division multiplexing (OFDM) to encode (and decode) data on (from) the nonlinear spectrum of optical signal, propagating multiplicatively over the fiber (Yousefi and Kschischang, 2014). In this scheme, the ideal channel model is given by

$$\tilde{q}(\lambda, z) = H(\lambda)\tilde{q}_0(\lambda), \tag{3.36a}$$

$$C_j(z) = H(\lambda_j)C_j(0), \tag{3.36b}$$

where $\tilde{q}_0(\lambda)$ and $C_j(0)$ are continuous and discrete spectrum at the input of the channel, respectively. $\tilde{q}(\lambda, z)$ and $C_j(z)$ are the nonlinear spectra of the signal at the output of the channel and the channel filter is $H(\lambda) = e^{-4j\lambda^2 z}$.

Figure 3.4 shows the block diagram of an NFDM system. At the transmitter, data is modulated in nonlinear frequency domain, according to a specific constellation, onto the nonlinear

spectra $\big(\tilde{q}_0(\lambda), C_j(0)\big)$. Next, the time domain signal is generated by performing the INFT as

$$q(t,0) = \mathrm{INFT}\big(\tilde{q}_0(\lambda), C_j(0)\big), \tag{3.37}$$

and is transmitted through the fiber channel. There are several algorithms introduced to compute the INFT such as Darboux transformation (Gu *et al.*, 2005), Riemann-Hilbert system and Gelfand-Levitan method (GLM)(FaddeevLeon and Takhtajan, 2007). At the receiver, the NFT is applied

$$\big(\tilde{q}(\lambda, z), C_j(z)\big) = \mathrm{NFT}\big(q(t,z)\big). \tag{3.38}$$

After channel compensation (i.e., removal of the phase rotation, see Eq. (3.24)), the spectra are compared against the input spectra using some metric. While the time domain signal and its linear spectrum are distorted due to the interplay between dispersion and fiber nonlinearity, the nonlinear spectrum evolves multiplicatively along fiber with no interaction with other spectral components.

Several techniques to compute the NFT such as Layer-peeling method, Crank-Nicolson method and Ablowitz-Ladik algorithm are introduced. Details on each method can be found in (Yousefi and Kschischang, 2014).

3.7 Conclusion

In this chapter, we reviewed the NFT theory pertaining to the NLSE with vanishing boundary conditions and highlighted its concepts that are important for their application for communication. NFT provides non-interacting degrees of freedom for encoding data in a signal in the nonlinear fiber channel. The NFDM scheme which employs the NFT to master fiber nonlinearity is introduced.

Chapter 4

Nonlinear Fourier Transform using Multistage Perturbation Technique for Fiber-optic Systems

4.1 Abstract

In nonlinear frequency division multiplexed systems, the inverse nonlinear Fourier transform (INFT) and nonlinear Fourier transform (NFT) are applied at the transmitter and receiver, respectively, so as to minimize the impact of fiber nonlinear effects. Typically, the INFT is applied at the digital signal processing of the transmitter to the individual channels of a wavelength division multiplexed (WDM) system, and these channels are linearly multiplexed using the wavelength-division multiplexer. Hence, currently, NFT-based systems suffer from nonlinear impairments due to other channels of a WDM system. This problem can be alleviated if the signals are nonlinearly multiplexed/demultiplexed using INFT and NFT in the optical domain, which is hard to achieve. In this chapter, we develop a novel multistage perturbation technique to realize the NFT as the cascade of linear discrete Fourier transforms. Since all-optical discrete Fourier transforms have been implemented in silicon photonics,

the proposed approach provides a promising way to implement the NFT in the optical domain. The other challenge in real time implementation of the NFT-based system is the computational complexity of the NFT. In this chapter, we develop a novel nonlinear discrete Fourier transform algorithm to realize NFT. When the signal energy is small, the NFT can be evaluated by single stage second- or third-order perturbation methods. However, as the signal energy increases, we show that the single stage technique is not accurate and the multistage perturbation technique provides reasonably accurate results for high energy signals. The number of stages required depends on the signal energy and desired accuracy. Modifying the fast Fourier transform (FFT) algorithm, the computational cost of the NFT based on the multistage perturbation technique is found to be $O(KN \log_2 N/K)$, where N is the number of signal samples and K is the number of stages. An advantage of the proposed approach is that the computation can be split into FFTs of smaller lengths, which can be processed on K parallel processors. The computational cost per processor is $O(N \log_2 N/K)$.

4.2 Introduction

Recently the application of the nonlinear Fourier transform (NFT) for fiber optic communication systems has drawn significant attention (Hasegawa and Nyu, 1993; Yousefi and Kschischang, 2014; Prilepsky *et al.*, 2014; Le *et al.*, 2014; Yousefi and Yangzhang, 2020; Le *et al.*, 2016b). For a linear orthogonal frequency division system, the inverse discrete Fourier transform (IDFT) and discrete Fourier transform (DFT) are used to multiplex (at the transmitter) and demultiplex (at the receiver), respectively. Similarly, in a nonlinear fiber optic system, the inverse nonlinear Fourier transform (INFT) is used to multiplex at the transmitter and the NFT is used at the receiver to demultiplex (Yousefi and Kschischang, 2014; Prilepsky *et al.*, 2014; Le *et al.*, 2014). If IDFT and DFT are used in the nonlinear fiber optic system, subcarrier orthogonality is destroyed by the fiber nonlinearity, leading to performance degradations. However, when INFT and NFT are used, nonlinear impairments

can be significantly suppressed. Successful transmission of 10 Gb/s using the NFT pairs has been achieved (Le *et al.*, 2016b). NFT-based signal processing has been used successfully in other fields such as laser characterization in dissipative systems (Sugavanam *et al.*, 2017; Ryczkowski *et al.*, 2018).

Various algorithms for computing the NFT have been proposed (Yousefi and Kschischang, 2014; Turitsyn *et al.*, 2017; Ablowitz and Ladik, 1976; Ablowitz and Herbst, 1990; Frumin *et al.*, 2015; Burtsev *et al.*, 1998; Wahls and Poor, 2015). One of the widely used methods is the Ablowitz–Ladik (AL) discretization method (Ablowitz and Ladik, 1976). Ablowitz and Ladik (1976) introduced a discrete integrable version of the nonlinear Schrödinger equation. The AL discretization of the Zakharov–Shabat system is robust to noise (Ablowitz and Herbst, 1990). In (Yousefi and Kschischang, 2014), a layer peeling method is used to evaluate NFT, which benefits from the causality property of NFT to estimate the nonlinear spectrum of the signal by assuming the signal to be piece-wise constant. Another efficient method is the direct Toeplitz inner bordering method (TIB) (Frumin *et al.*, 2015). In this method, the continuous nonlinear spectrum was computed by using the Toeplitz matrix transformations. In (Frumin *et al.*, 2015), the TIB was compared with the T-matrix method (Burtsev *et al.*, 1998), and it was found that the TIB is more efficient and its calculation speed is higher.

One of the challenges of NFT-based communication systems is the computational complexity of the implementation of NFT. While the complexity of most methods to compute the nonlinear spectrum is $O(N^2)$ (Yousefi and Kschischang, 2014; Turitsyn *et al.*, 2017) where N is the number of samples, a fast NFT with a polynomial approach to the Zakharov–Shabat system was introduced by Wahls and Poor (2015) which requires about $O(N(\log N)^2)$ flop.

When the signal amplitude is weak, a Zakharov–Shabat system can be solved by perturbation techniques. The single stage third-order perturbation technique for computing the reflection coefficient was first developed by Prilepsky *et al.* (2013). In this chapter, we develop perturbation techniques to compute NFT and compare the accuracy and computational cost of single stage second-order and third-order perturbation techniques and find that

the accuracy of the single-stage perturbation approach decreases as the amplitude and/or the duration of the signal increases. We also find that as the order of the perturbation technique increases, the accuracy improves, but the computational cost becomes extensive. Hence, for the first time to our knowledge, we develop a multistage perturbation technique for NFT. In each stage, a first-order perturbation technique is used which is computationally inexpensive. The output of the kth stage is used as the input of the $(k+1)$th stage. The cascade of two stages with each stage using the first-order technique roughly provides the accuracy of the single stage second-order perturbation technique. However, the computational cost of the two stage perturbation technique is significantly lower than the single stage second-order technique. In this chapter, we develop new algorithms to reduce the computational complexity of the multistage perturbation technique so that it has the structure of a fast Fourier transform (FFT). We find that the computational cost of the multistage perturbation technique is $O(KN \log_2 N/K)$ for $K < N$, where K is the number of stages. The computational cost can be reduced by decreasing K; however, the error increases. The number of stages should be chosen depending on the desired accuracy. The advantage of the proposed approach is that the N-point FFT required at each block is split into several M-point FFTs ($M = N/K$ is the number of samples per block) which can be processed in parallel, and these computations can be carried out simultaneously on K parallel processors. Hence, the computational cost per processor becomes $O(N \log_2 M)$.

Another challenge of NFT-based systems is that the inter-channel nonlinear impairments in a wavelength division multiplexing system cause penalty. The reason is that INFT is applied to the signal of each channel in the digital domain and multiple channels are multiplexed linearly using a wavelength division multiplexer. Hence, currently, in NFT-based systems, intra-channel impairments such as intra-channel cross phase modulation and intra-channel four wave mixing (Kumar and Deen, 2014) pose no problem. However, inter-channel nonlinear impairments such as classical four wave mixing and cross phase modulation arising due to the nonlinear interaction between channels cause performance degradation. In

fact, in practical systems, the nonlinear impairments due to other channels is much stronger than intra-channel nonlinear impairments (which can be removed by the digital domain NFT-based systems). This problem can be alleviated if the signal is nonlinearly multiplexed/demultiplexed in the optical domain using INFT/NFT. However, realization of NFT in the optical domain is hard, although the linear Fourier transform (FT) can be easily implemented in the optical domain using a time lens (Lohmann and Mendlovic, 1992; Yang and Kumar, 2009; Hirooka and Nakazawa, 2006; Guan *et al.*, 2017) or discrete photonic components (Lee *et al.*, 2008; Hillerkuss *et al.*, 2010), which can be implemented in silicon photonics (Nejadriahi *et al.*, 2017). Since the multistage perturbation technique realizes the NFT as a cascade of linear FTs, the proposed technique provides a promising way to implement NFT in the optical domain, although there could still be hurdles to realize it in experiments. In contrast, digital computers cannot operate at THz and, hence, digital-based NFT cannot utilize the full bandwidth of the fiber. Besides, in fiber optic networks, channels are multiplexed and demultiplexed at each node. If this multiplexing/demultiplexing is done linearly, there would be no advantage. To utilize the full advantage of NFT-based system, channels should be multiplexed/demultiplexed nonlinearly using INFT and NFT, respectively, which calls for the optical domain implementation of NFT.

In this chapter, we focus only on the continuous eigenvalues of the Zakharov–Shabat system, deferring the case of discrete eigenvalues to a future research work. If the system is quasi-linear, that is, nonlinear effects may be treated as a small perturbation to the linear system, Eq. (4.1) may have only continuous eigenvalues. However, the proposed approach is limited not only to quasi-linear systems but also to any nonlinear system. The order of the perturbation technique and number of stages can be tailored depending on the strength of nonlinearity.

This chapter is organized as follows. In Section 4.3, the theoretical background of the perturbation techniques is reviewed. Numerical computational of NFT of a raised cosine pulse is carried out using single stage second- and higher-order perturbation techniques. The

multistage perturbation technique is introduced in Section 4.4. In Section 4.5, we compare the accuracy of the single stage and multistage perturbation techniques. The FFT algorithm is modified to compute the NFT based on the multistage perturbation technique in Section 4.6.

4.3 Single Stage Perturbation Approach

To solve the nonlinear Schrödinger equation by the inverse scattering transform technique, the first step is to find the eigenfunctions of the Zakharov–Shabat system,

$$\begin{bmatrix} \frac{dv_1}{dt} \\ \frac{dv_2}{dt} \end{bmatrix} = \begin{bmatrix} -j\lambda & \alpha q(t) \\ -\alpha q^*(t) & j\lambda \end{bmatrix} \begin{bmatrix} v_1 \\ v_2 \end{bmatrix}. \tag{4.1}$$

In this chapter, we focus only on the continuous eigenvalues of Eq. (4.1). The solutions of Zakharov-Shabat system (4.1) are given by a regular perturbation series,

$$v_1 = e^{-j\lambda t}[1 + \alpha h_{11} + \alpha^2 h_{12} + \alpha^3 h_{13} + \ldots], \tag{4.2a}$$

$$v_2 = e^{j\lambda t}[\epsilon + \alpha h_{21} + \alpha^2 h_{22} + \alpha^3 h_{23} + \ldots], \tag{4.2b}$$

where $|\epsilon| \ll 1$ and α is a measure of perturbation. Substituting Eq. (4.2) into Eq. (4.1) and matching up powers of α, we obtain a hierarchy of equations for the unknown coefficients h_{nm}. If the optical signal power is small, i.e., $\alpha|q(t)| \ll 1$, a second-order perturbation theory can be used,

$$v_1 = e^{-j\lambda t}[1 + \alpha h_{11} + \alpha^2 h_{12}], \tag{4.3a}$$

$$v_2 = e^{j\lambda t}[\epsilon + \alpha h_{21} + \alpha^2 h_{22}]. \tag{4.3b}$$

Collecting the terms proportional to α, we find

$$h_{11}(t) = \epsilon \int_{-\infty}^{t} r(t')\, dt', \tag{4.4}$$

and

$$h_{21}(t) = -\int_{-\infty}^{t} r^*(t')\, dt', \tag{4.5}$$

where

$$r(t) = q(t)e^{j2\lambda t}. \tag{4.6}$$

The equations for the second-order terms are obtained by comparing the terms proportional to α^2,

$$h_{12}(t) = -\int_{-\infty}^{t} r(t_1) \int_{-\infty}^{t_1} r^*(t_2)\, dt_2\, dt_1, \tag{4.7}$$

and

$$h_{22}(t) = -\epsilon \int_{-\infty}^{t} r^*(t_1) \int_{-\infty}^{t_1} r(t_2)\, dt_2\, dt_1. \tag{4.8}$$

The nonlinear Fourier coefficients are given by (Eq. (3.17))

$$b(\lambda) = \lim_{t\to\infty} v_2 e^{-j\lambda t}, \tag{4.9}$$

and

$$a(\lambda) = \lim_{t\to\infty} v_1 e^{j\lambda t}. \tag{4.10}$$

Using Eq. (4.2) in Eqs. (4.9) and (4.10) and letting $\epsilon \to 0$, we find

$$b(\lambda) = -\alpha \int_{-\infty}^{+\infty} r^*(t')\, dt', \tag{4.11}$$

and

$$a(\lambda) = 1 - \alpha^2 \int_{-\infty}^{+\infty} r(t_1) \int_{-\infty}^{t_1} r^*(t_2)\, dt_2\, dt_1. \tag{4.12}$$

Using Eqs. (4.11) and (4.12), the continuous part of nonlinear Fourier transform of the input signal, $\alpha q(t)$, up to second-order is

$$\tilde{q}(\lambda) = \frac{b(\lambda)}{a(\lambda)} = \frac{-\alpha \int_{-\infty}^{+\infty} r^*(t')\, dt'}{1 - \alpha^2 \int_{-\infty}^{+\infty} r(t_1) \int_{-\infty}^{t_1} r^*(t_2)\, dt_2\, dt_1}. \tag{4.13}$$

It may be noted that if we ignore the second-order terms ($\propto \alpha^2$), Eq. (4.13) is simply the linear FT of $\alpha q^*(t)$. In other words, the first-order perturbation solution of Eq. (4.1) yields the linear FT. To simplify Eq. (4.13), let

$$I = \int_{-\infty}^{+\infty} r(t_1) \int_{-\infty}^{t_1} r^*(t_2)\, dt_2\, dt_1 = \int_{-\infty}^{+\infty} q(t_1) e^{j2\lambda t_1} \int_{-\infty}^{t_1} q^*(t_2) e^{-j2\lambda t_2}\, dt_2\, dt_1. \tag{4.14}$$

Setting $2\lambda = 2\pi f$ and $t_2 = t_1 + \tau$, Eq. (4.14) becomes

$$I = \int_{-\infty}^{0} s(\tau) e^{-j2\pi f \tau}\, d\tau, \tag{4.15}$$

where

$$s(\tau) = \int_{-\infty}^{+\infty} q(t_1) q^*(t_1 + \tau)\, dt_1. \tag{4.16}$$

In Eq. (4.16), $s(\tau)$ has the form of an auto-correlation function. The direct computation of $s(\tau)$ in Eq. (4.16) requires $O(N^2)$ operations. However, the cost can be significantly reduced if we use FTs.

Let

$$\hat{q}(f) = \mathcal{F}[q(t); t \to f] = \int_{-\infty}^{+\infty} q(t) e^{-j2\pi f t}\, dt, \tag{4.17}$$

$$q(t) = \mathcal{F}^{-1}[\hat{q}(f); f \to t] = \int_{-\infty}^{+\infty} \hat{q}(f) e^{j2\pi f t}\, df, \tag{4.18}$$

$$\hat{s}(f) = \mathcal{F}[s(\tau); \tau \to f] = \int_{-\infty}^{+\infty} s(\tau) e^{-j2\pi f\tau}\, d\tau = \int_{-\infty}^{+\infty} \int_{-\infty}^{+\infty} q(t_1) q^*(t_1+\tau) e^{-j2\pi f\tau}\, d\tau\, dt_1. \tag{4.19}$$

Let $t_2 = t_1 + \tau$,

$$\hat{s}(f) = \int_{-\infty}^{+\infty} q(t_1) e^{j2\pi f t_1}\, dt_1 \int_{-\infty}^{+\infty} q^*(t_2) e^{-j2\pi f t_2}\, dt_2 = \hat{q}(-f)\mathcal{F}[q^*(t); t \to f]. \tag{4.20}$$

From Eq. (4.17), we have

$$\hat{q}(-f) = \int_{-\infty}^{+\infty} q(t) e^{j2\pi f t}\, dt. \tag{4.21}$$

Complex-conjugating Eq. (4.21), we obtain

$$\hat{q}^*(-f) = \int_{-\infty}^{+\infty} q^*(t) e^{-j2\pi f t}\, dt = \mathcal{F}[q^*(t); t \to f]. \tag{4.22}$$

Substituting Eq. (4.22) in Eq. (4.20), we find

$$\hat{s}(f) = |\hat{q}(-f)|^2. \tag{4.23}$$

Using Eq. (4.18), we have

$$s(\tau) = \mathcal{F}^{-1}[\hat{s}(f); f \to \tau]. \tag{4.24}$$

Thus, to compute $s(\tau)$, we first take the FT of $q(t)$ to find $\hat{q}(-f)$ and calculate $\hat{s}(f)$ using Eq. (4.23). Finally, we take the inverse FT of $\hat{s}(f)$ to obtain $s(\tau)$. The computational cost of calculating $\hat{q}(-f)$ is $O(N \log_2 N)$. The calculation of the product in Eq. (4.23) is $O(N)$ and the calculation of the inverse FT is again $O(N \log_2 N)$. So, the total cost is $O(N \log_2 N)$.

Next, let us consider the third-order perturbation method by letting

$$v_1 = e^{-j\lambda t}[1 + \alpha h_{11} + \alpha^2 h_{12} + \alpha^3 h_{13}], \tag{4.25a}$$

$$v_2 = e^{j\lambda t}[\epsilon + \alpha h_{21} + \alpha^2 h_{22} + \alpha^3 h_{23}]. \tag{4.25b}$$

Inserting Eqs. (4.25) into Eq. (4.1), and comparing the terms proportional to α^3 results in equations for the third-order coefficients,

$$h_{13}(t) = \int_{-\infty}^{t} r(t_1) h_{22}(t_1)\, dt_1, \tag{4.26}$$

and

$$h_{23}(t) = \int_{-\infty}^{t}\int_{-\infty}^{t_1}\int_{-\infty}^{t_2} r^*(t_1) r(t_2) r^*(t_3)\, dt_3\, dt_2\, dt_1. \tag{4.27}$$

Now Eq. (4.11) is modified as

$$b(\lambda) = -\alpha \int_{-\infty}^{+\infty} r^*(t')\, dt' + \alpha^3 \int_{-\infty}^{+\infty}\int_{-\infty}^{t_1}\int_{-\infty}^{t_2} r^*(t_1) r(t_2) r^*(t_3)\, dt_3\, dt_2\, dt_1, \tag{4.28}$$

and $a(\lambda)$ is given by Eq. (4.12). The above result is first obtained by Prilepsky *et al.* (2013). Using Eqs. (4.28) and (4.12), we find

$$\begin{aligned}
\tilde{q}(\lambda) &= \frac{b(\lambda)}{a(\lambda)}, \\
&= \frac{-\alpha \int_{-\infty}^{+\infty} r^*(t')\, dt' + \alpha^3 \int_{-\infty}^{+\infty}\int_{-\infty}^{t_1}\int_{-\infty}^{t_2} r^*(t_1) r(t_2) r^*(t_3)\, dt_3\, dt_2\, dt_1}{1 - \alpha^2 \int_{-\infty}^{+\infty} r(t_1) \int_{-\infty}^{t_1} r^*(t_2)\, dt_2\, dt_1}, \\
&= -\alpha \int_{-\infty}^{+\infty} r^*(t')\, dt' - \alpha^3 \int_{-\infty}^{+\infty} r^*(t_1) \int_{t_1}^{+\infty} r(t_2) \int_{-\infty}^{t_2} r^*(t_3)\, dt_3\, dt_2\, dt_1 + O(\alpha^4).
\end{aligned} \tag{4.29}$$

Equations (4.13) and (4.29) are the NFT of $\alpha q(t)$ using the second- and third-order perturbation method, respectively.

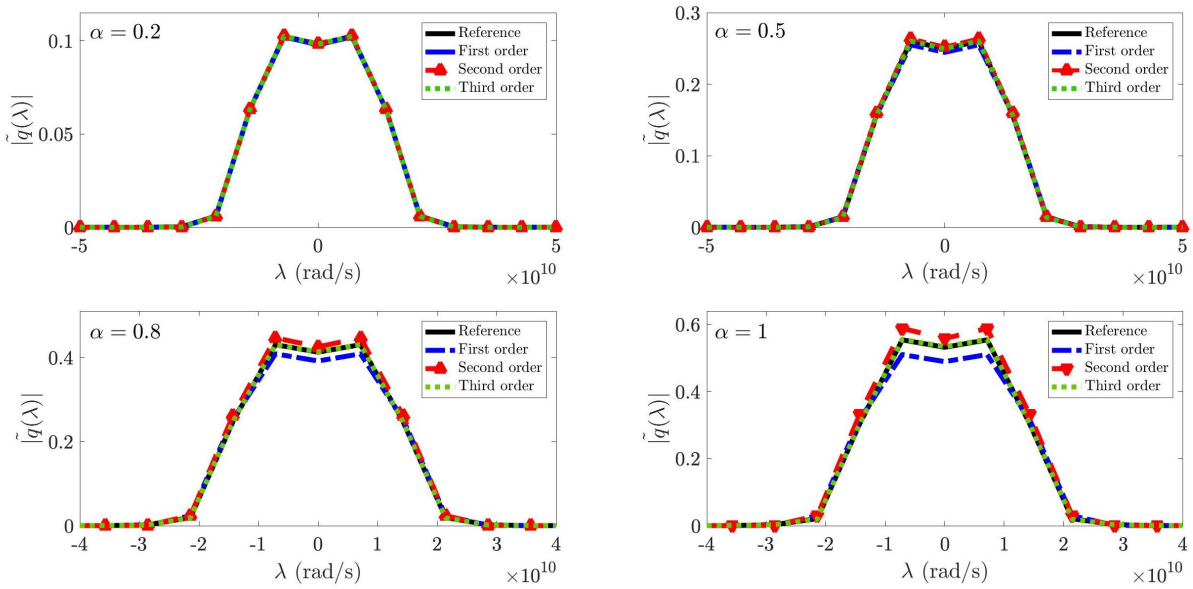

Figure 4.1: $|\tilde{q}(\lambda)|$ as a function of λ for different α. The signal is a raised-cosine pulse.

4.3.1 Simulation Results

Now we will examine the accuracy of the second- and third-order perturbation methods by comparing them with the solution obtained by solving Eq. (4.1) using the finite difference (FD) method. When we do the forward FD approximation, Eq. (4.1) becomes

$$\begin{bmatrix} v_{1,n+1} \\ v_{2,n+1} \end{bmatrix} = \begin{bmatrix} 1 - j\lambda\Delta t & \alpha q_n \Delta t \\ -\alpha q_n^* \Delta t & 1 + j\lambda\Delta t \end{bmatrix} \begin{bmatrix} v_{1,n} \\ v_{2,n} \end{bmatrix}, \tag{4.30}$$

where $v_{j,n} = v_j(n\Delta t), j = 1, 2$ and Δt is the step size for t.

Figure 4.1 shows the absolute value of $\tilde{q}(\lambda)$ as a function of λ for different α. We assume that the $q(t)$ is a raised-cosine pulse, given by

$$p(t) = \left(\frac{1}{2T_0}\right) \frac{\mathrm{sinc}\frac{\mathrm{t}}{\mathrm{T_0}} \cos\frac{\beta\pi\mathrm{t}}{\mathrm{T_0}}}{1 - (\frac{2\beta t}{T_0})^2}, \tag{4.31}$$

where $T_0 = 100$ ps, and $\beta = 0.5$. The solid line labeled as "Reference" in Fig. 4.1 shows the NFT $\tilde{q}(\lambda)$ obtained by solving Eq. (4.1) using the FD technique. λ is discretized from

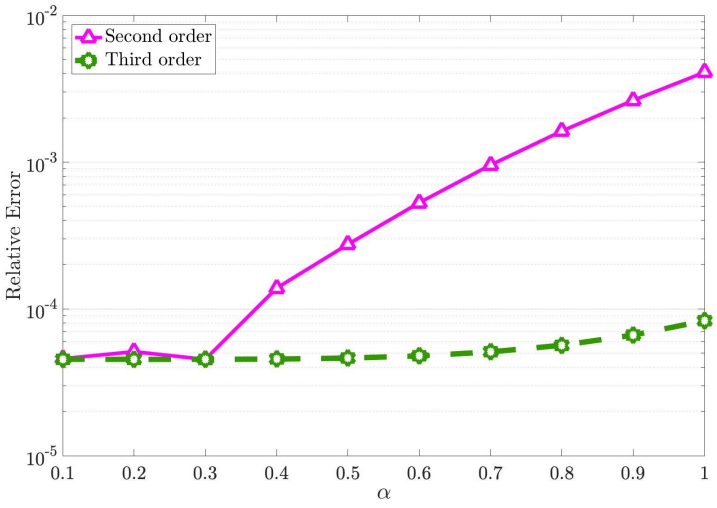

Figure 4.2: Relative error versus α for a raised cosine pulse for various single-stage perturbation techniques.

-4000 Grad/s to 4000 Grad/s with a step size of 7.8 Grad/s. The time t is discretized from -200 ps to 200 ps with a step size of 0.39 ps and the number of samples is 1024. Figure 4.1 shows that, for small α, the difference between the results of different perturbation methods and the reference spectrum is not large. As α increases, the results of first-order—that is, linear FT—and second-order approaches deviate from the reference; however, the third-order perturbation method achieves the best accuracy.

Figure 4.2 shows the relative error between the reference and nth-order perturbation theory, defined as

$$e = \int_{-\infty}^{+\infty} |\tilde{q}^{ref}(\lambda) - \tilde{q}^{n}(\lambda)|^2 \, d\lambda, \tag{4.32}$$

where $\tilde{q}^{ref}(\lambda)$ is the NFT obtained by the FD technique and $\tilde{q}^{n}(\lambda)$ is the NFT obtained by the nth-order perturbation techniques. From Fig. 4.2, we see that the relative error is roughly constant as a function of α for the third-order theory while it increases as a function of α for the second-order theory. The third-order theory provides the lower error for large α. However, the computational cost of the evaluation of triple integrals in Eq. (4.29) is extensive. Therefore, in the next section, we develop a multistage perturbation theory in which the first-order perturbation theory is used in each stage so that the accuracy of the

higher-order perturbation theory is achieved while the computational cost does not increase significantly.

4.4 Multistage Perturbation Approach

In this section, we introduce a multistage perturbation method in which the perturbation calculations are implemented recursively, that is, the output signal of the $(k-1)$th perturbation stage is used as the input signal of the kth perturbation stage. We suppose that the solution of Eq. (4.1) over the interval of $[t_{k-1}, t_k]$ (which we call kth perturbation stage) is given by the first-order perturbation technique,

$$v_1(t;\lambda) = e^{-j\lambda t}[h_{10}(\lambda) + \alpha h_{11}(t;\lambda)], \tag{4.33a}$$

$$v_2(t;\lambda) = e^{j\lambda t}[h_{20}(\lambda) + \alpha h_{21}(t;\lambda)], \tag{4.33b}$$

where h_{10} and h_{20} are constants to be determined later. Let the initial conditions be

$$v_1(t_{k-1};\lambda) = v_{10}(\lambda), \tag{4.34a}$$

$$v_2(t_{k-1};\lambda) = v_{20}(\lambda). \tag{4.34b}$$

Substituting Eqs. (4.33) into Eq. (4.1), and comparing the terms proportional to α^1, we obtain

$$\frac{dh_{11}(t;\lambda)}{dt} = qe^{j2\lambda t}h_{20}, \tag{4.35}$$

$$\frac{dh_{21}(t;\lambda)}{dt} = -q^*e^{-j2\lambda t}h_{10}. \tag{4.36}$$

Integrating Eq. (4.35) and (4.36), we find

$$h_{11}(t_k) - h_{11}(t_{k-1}) = h_{20}\int_{t_{k-1}}^{t_k} q(t)e^{j2\lambda t}\,dt, \tag{4.37}$$

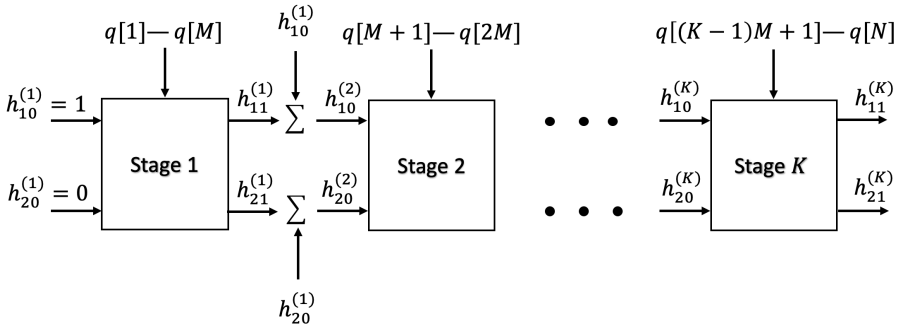

Figure 4.3: A block diagram of the NFT using the multistage perturbation technique.

$$h_{21}(t_k) - h_{21}(t_{k-1}) = -h_{10} \int_{t_{k-1}}^{t_k} q^*(t) e^{-j2\lambda t}\, dt. \tag{4.38}$$

Let

$$h_{11}(t_{k-1}) = 0, \tag{4.39a}$$

$$h_{21}(t_{k-1}) = 0. \tag{4.39b}$$

The computational window is divided into $K = N/M$ blocks. Now, we discretize time window with a step size of ΔT,

$$t_{k-1} = (k-1)M\Delta T,$$

$$t_k = kM\Delta T.$$

$2\lambda = 2\pi m \Delta f$, where m is the index for discrete frequencies. Equations (4.37) and (4.38) have the form of continuous FTs. The standard approach to convert the continuous FT to discrete Fourier transform (DFT) is by using Nyquist sampling, $\Delta f \Delta T = 1/N$. Now Eq. (4.37) becomes

$$h_{11}^m[kM] = h_{20}^m \Delta T \sum_{n=(k-1)M}^{kM-1} q[n] e^{j2\pi nm/N}, \tag{4.41}$$

where $h_{11}^m[kM]$ and h_{20}^m are the discrete form of $h_{11}(t_k;\lambda)$ and $h_{20}(\lambda)$, respectively. Similarly, from Eq. (4.38), we have

$$h_{21}^m[kM] = -h_{10}^m \Delta T \sum_{n=(k-1)M}^{kM-1} q^*[n] e^{-j2\pi nm/N}. \tag{4.42}$$

Using Eqs. (4.39a) and (4.39b) in Eq. (4.33), we find

$$h_{10}^m = v_{10}^m e^{j\pi m(k-1)M/N}, \tag{4.43}$$

and

$$h_{20}^m = v_{20}^m e^{-j\pi m(k-1)M/N}. \tag{4.44}$$

The main idea of the multistage perturbation method is to repeat this procedure for the next stage, $t_k < t \leq t_{k+1}$, and use

$$v_1^m[kM] = \big(h_{10}^m + \alpha h_{11}^m[kM]\big) e^{-j\pi mkM/N} = v_{10}^m \tag{4.45}$$

and

$$v_2^m[kM] = \big(h_{20}^m + \alpha h_{21}^m[kM]\big) e^{j\pi mkM/N} = v_{20}^m \tag{4.46}$$

as the initial conditions for the next stage.

The block diagram of the proposed technique is shown in Fig. 4.3. In each stage, h_{11} and h_{21} need to be evaluated. Equations (4.41) and (4.42) have the forms similar to DFT. Hence, each stage requires two DFTs for the evaluation of h_{11} and h_{21} and the NFT can be interpreted as the cascade of DFTs. The FFT algorithm can be adapted for this application, and we find that the computational cost of the evaluation of Eqs. (4.41) and (4.42) is $O(NK \log_2 N/K)$ complex multiplications (see Section 4.6.1).

It is well known that a conventional lens provides the two dimensional linear FT of a two-dimensional spatial signal located at the front focal plane, at the back focal plane. A

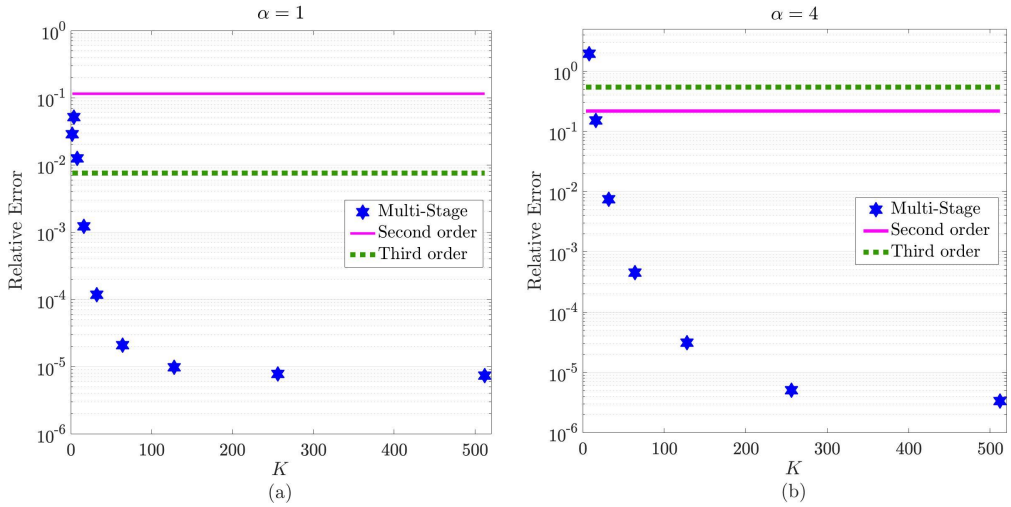

Figure 4.4: Relative error versus K for a single raised cosine pulse. Stepsize, ΔT of any perturbation schemes is 0.78 ps and number of samples is 512. For FD method, stepsize $\Delta t = 0.39$ ps and number of samples is 1024. L1-norms for $\alpha = 1$ and 4 are 0.65 and 2.58, respectively.

time lens is the time analogue of a space lens which provides the FT of a temporal signal (Lohmann and Mendlovic, 1992; Yang and Kumar, 2009). Replacing the diffraction by dispersion and the spatial phase modulation due to a space lens by a phase modulator, the FT of a temporal signal can be realized (Lohmann and Mendlovic, 1992; Yang and Kumar, 2009). The time domain Fourier transformation using a time lens has been experimentally demonstrated in (Hirooka and Nakazawa, 2006; Guan *et al.*, 2017). For the optical domain implementation of NFT, the linear FTs required in each stage can be realized using time lenses. The advantage of the optical domain realization of NFT is that the high speed digital signal processing needed for solving the Zakharov–Shabat problem is now replaced by optical signal processing using time lenses which have inherently high bandwidth.

Alternatively, DFT in the optical domain can be realized using interferometers and passive devices such as delay lines, directional couplers, Y-branches, and phase-shifters (Lee *et al.*, 2008; Hillerkuss *et al.*, 2010; Nejadriahi *et al.*, 2017). To realize Eq. (4.41), first $q(t)$ undergoes serial-to-parallel conversion. The signal corresponding to $q[n]$ undergoes a phase shift of $2\pi nk/N$, and then a power coupler combines the phase shifted signals [corresponding

to summation in Eq. (4.41)]. A convenient way to introduce the phase shift is by using delay lines. The optical path length of the delay line should be precisely adjusted to obtain the required phase shift. More details can be found in (Lee *et al.*, 2008). An all-optical DFT scheme has been experimentally demonstrated in (Hillerkuss *et al.*, 2010) enabling Tb/s real time optical signal processing. The design and sensitivity of integrated all-optical FFT in a silicon photonics chip are discussed in (Nejadriahi *et al.*, 2017).

4.5 Comparison of the Proposed Methods

In this section, the aforementioned techniques are evaluated by applying them for various cases. In Fig. 4.4, we assume the following parameters: $\Delta T = 0.78$ ps and $\Delta f = 2.5$ GHz. Initially, we consider the case of a single pulse with $q(t)$ given by Eq. (4.31). Figure 4.4a shows the relative error as a function of the number of blocks when $\alpha = 1$. For small K ($K \leq 8$), single stage third-order perturbation method provides a better accuracy than the multistage perturbation method. As K increases, the accuracy of multistage perturbation method improves and the error becomes roughly constant for $K > 128$. Figure 4.4b shows the error for the case of when $\alpha = 4$, which corresponds to the high energy signal. As can be seen, the error using single stage perturbation techniques is huge, whereas multistage perturbation technique leads to reasonably accurate results if $K \geq 64$. Comparing Figs. 4.4a and 4.4b, we see that the number of stages required to achieve the given accuracy increases with α.

Figure 4.5 compares the nonlinear spectrum of a single raised cosine pulse obtained using the FD scheme, layer peeling (Yousefi and Kschischang, 2014), and multistage perturbation scheme. Both layer peeling and FD methods have the number of samples $N = 1024$ and step size $\Delta t = 0.39$ ps. Comparing Figs. 4.1 and 4.5b, we see that the spectrum deviates significantly as α changes from 0.2 to 8. As can be seen from Fig. 4.5, the FD and layer peeling approaches provide nearly identical results. When $\alpha = 4$, multistage perturbation

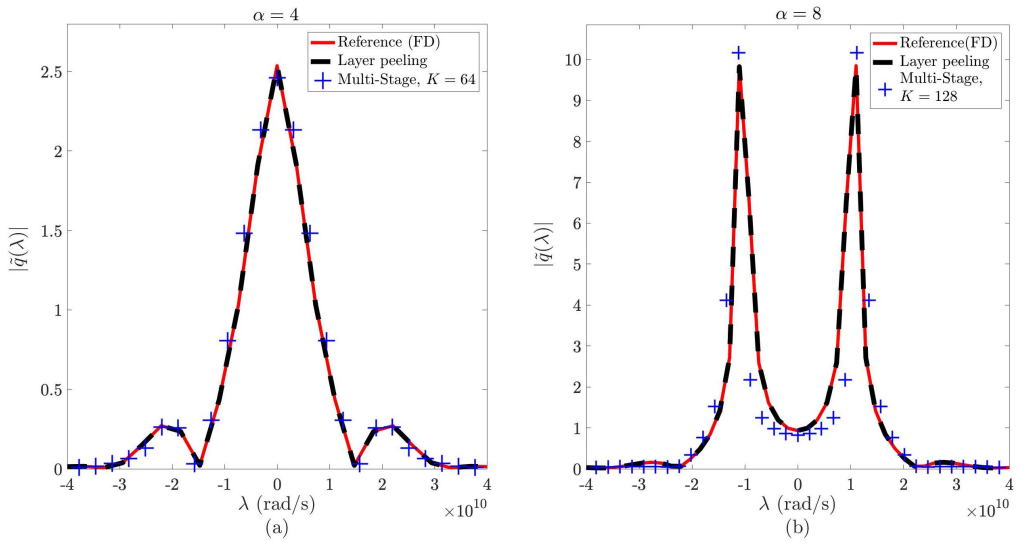

Figure 4.5: $|\tilde{q}(\lambda)|$ as a function of λ for a raised-cosine pulse. The parameters are the same as that of Fig. 4.4. L1-norms for $\alpha = 4$ and 8 are 2.6 and 5.2, respectively.

results are in good agreement with FD and layer peeling approaches. However, when $\alpha = 8$, the multistage technique deviates slightly from the other approaches.

The signal energy can be enhanced either by increasing the amplitude of the pulses (i.e., α) or by increasing the number of pulses. So, we consider the train of raised-cosine pulses given by

$$q(t) = \sum_{n=-4}^{3} a_n p(t - nT), \tag{4.47}$$

where $a_n = 11011111$, and the pulse shape function $p(t)$ is given by Eq. (4.31) with $T_0 = 50$ ps and $\beta = 0.5$.

Figure 4.6 shows the relative error as a function of the number of blocks of the multistage perturbation theory. When $\alpha = 2$, the relative error for the single stage second- and third-order perturbation techniques is 1.1 and 0.89, respectively, which is reduced to 8.88×10^{-3} and 9.38×10^{-4} for $K = 128$ and 256, respectively, when the multistage perturbation method is used.

Next, we consider an 8-bit long random bit pattern and find the mean and variances of error by averaging over 12 runs. Figures 4.7a and 4.7b show the mean and variance of error

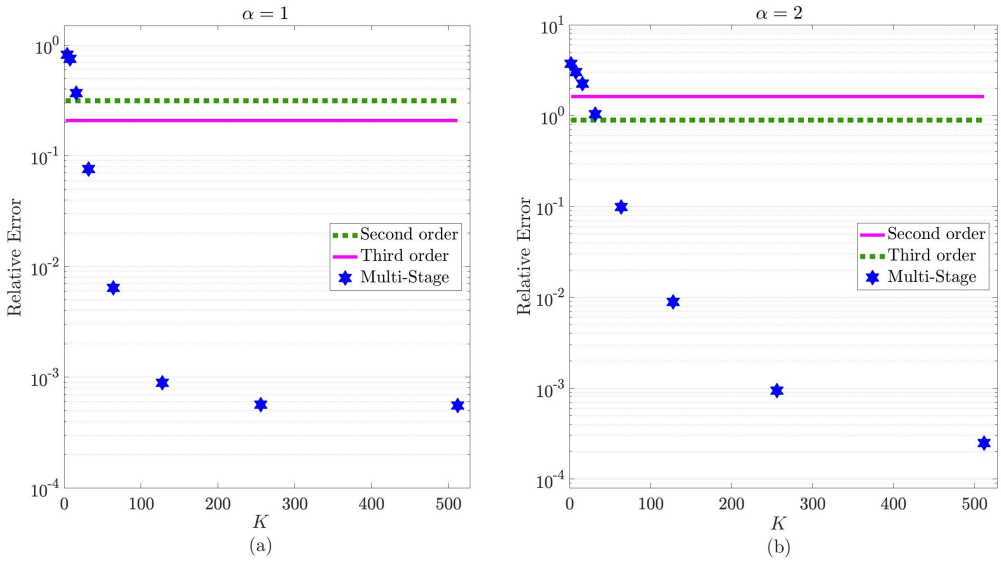

Figure 4.6: Relative error versus K, for bit pattern 11011111. The input pulses are raised cosine pulses. $\Delta T = 0.97$ ps, $\Delta f = 1$ GHz and $N = 1024$. For FD method, $\Delta t = 0.97$ ps and the number of samples is 1024. L1-norms for $\alpha = 1$ and 2 are 3.78 and 7.57 respectively.

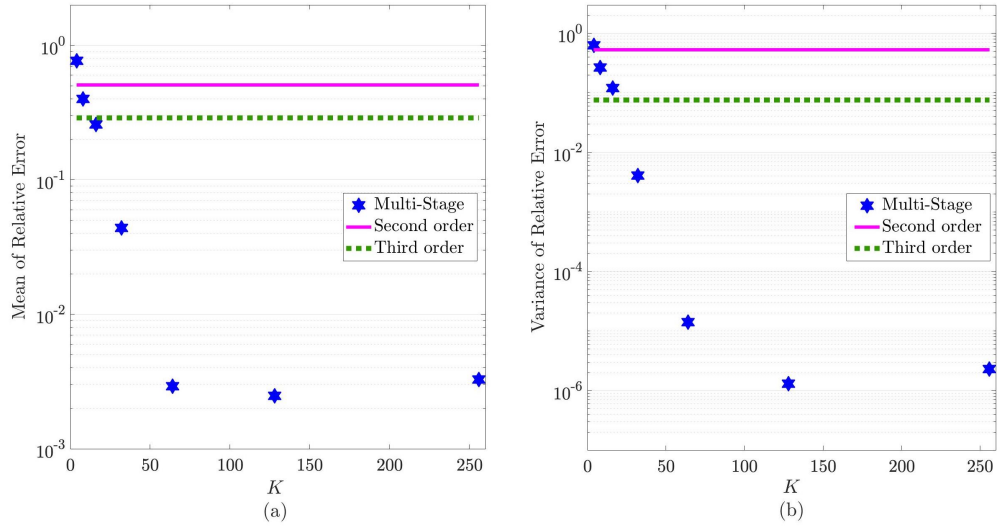

Figure 4.7: (a) Mean of Error (b) Variance of Error ($\alpha = 1$). The parameters are the same as Fig. 4.6a.

when $\alpha = 1$. Figure 4.7 shows the same trend as in Fig. 4.6a. The only difference is that the error decreases monotonically with K for large K in Fig. 4.6a whereas Fig. 4.7a shows that the optimum K is around 128.

4.6 Computational Complexity

The direct application of FFT algorithms to Eq. (4.41) or (4.42) leads to $O(N \log_2 N)$ complex multiplications per stage. If there are $K = N/M$ stages, the total cost is $O(NK \log_2 N)$. In this section, we develop a novel algorithm to reduce the cost to $O(NK \log_2 N/K)$ for $K < N$. When $K = N$, the computational cost is $O(N^2)$.

4.6.1 Modified FFT Algorithm

Let the summation in Eq. (4.42) be

$$\hat{h}_k[m] = \sum_{n=(k-1)M}^{kM-1} q^*[n] e^{-j2\pi nm/N}, \quad 0 \leq m \leq N-1. \tag{4.48}$$

In the multistage perturbation method, the signal $x[n]$ is divided into K blocks of M samples. Let

$$l = n - (k-1)M. \tag{4.49}$$

Substituting Eq. (4.49) in Eq. (4.48), we obtain

$$\hat{h}_k[m] = e^{-j2\pi(k-1)Mm/N} \sum_{l=0}^{M-1} q^*[n] e^{-j2\pi lm/N}. \tag{4.50}$$

The summation is over the kth block of $q^*[n]$ with the length M. If $q^*[n]$ is padded with zeros to make its length N, Eq. (4.50) may be represented as a DFT, that is,

$$x_k[l] = \begin{cases} q^*[l + (k-1)M], & 0 \leq l < M \\ 0 & \text{otherwise.} \end{cases} \tag{4.51}$$

Now the summation in Eq. (4.50) may be written as

$$\sum_{l=0}^{M-1} q^*[n] e^{-j2\pi lm/N} = \sum_{l=0}^{N-1} x_k[l] e^{-j2\pi lm/N} = \text{DFT}\{x_k[l]\} = X_k[m]. \tag{4.52}$$

Let $m = Km' + c$, where $c = 0, 1, 3, \ldots K-1$ and $m' = 0, 1, 2, \ldots M-1$. Now, Eq. (4.52) may be written as

$$X_k[Km' + c] = \sum_{l=0}^{M-1} x_k[l] e^{-j2\pi lm'/M} W^{cl}, \tag{4.53}$$

where $W = e^{-j2\pi/N}$ is the twiddle constant (Chassaing and Reay, 2008). As c changes from 0 to $K-1$, Eq. (4.53) may be broken down as

$$\begin{aligned} & W^0 x_k[l] \xrightarrow{M\text{-point FFT}} X_k[Km], \\ & W^l x_k[l] \xrightarrow{M\text{-point FFT}} X_k[Km+1], \\ & \vdots \\ & W^{(K-1)l} x_k[l] \xrightarrow{M\text{-point FFT}} X_k[Km + (K-1)]. \end{aligned} \tag{4.54}$$

The cost of M-point FFT is $O(M \log_2 M)$. Since there are K M-point FFTs in Eq. (4.54), the total computational cost of Eq. (4.54) is $O(N \log_2 M)$ for $K < N$. An advantage of the scheme shown in Eq. (4.54) is that these operations (i.e. M-point FFTs) are independent (i.e. any M-point FFT does not require input from the other) and hence, it can be processed simultaneously by multiple processors. Therefore, the computational cost per stage per processor is $O(M \log_2 M)$ for $K < N$.

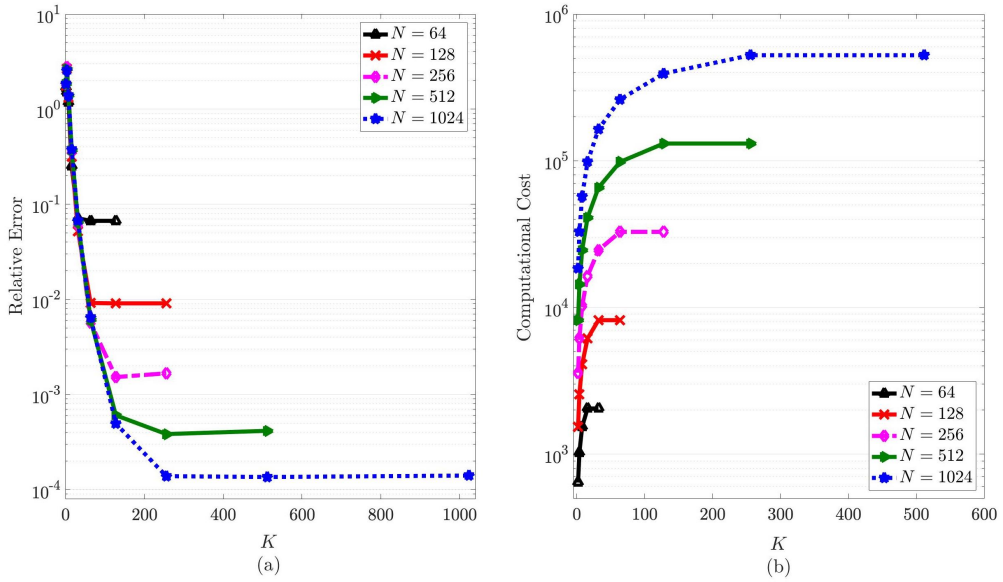

Figure 4.8: (a) Relative error of the multistage perturbation method versus number of blocks (K), (b) Complexity of the multistage perturbation method versus number of blocks. The other parameters are the same as that of Fig. 4.7a.

Table 4.1: Comparison of computational complexity of various perturbation techniques with $N = 512, \alpha = 1$ for a raised cosine pulse

	Number of complex multiplications	Relative Error
Finite difference ($N = 1024$)	1048576	—
Single stage second-order perturbation method	4608	1.15×10^{-1}
Single stage third-order perturbation method	134217728	7.58×10^{-3}
Multistage perturbation method ($K = 16$)	40960	1.23×10^{-3}
Multistage perturbation method ($K = 64$)	98304	2.1×10^{-5}

The parameters used in this calculation are the same as that of Fig. 4.4.

4.6.2 Complexity and Number of Stages

As discussed in previous sections, the accuracy of the multistage perturbation compared to the single stage method is higher if the number of stages (K) is larger. In addition, the computational cost of this technique increases with K. Therefore, the choice of the optimal K plays an important role. Figure 4.8a shows that the relative error decreases as N and/or K increases while Fig. 4.8b shows that the computational cost increases with N (and also with K). Thus, there is a trade-off between the computational cost and accuracy. The number of samples, N, is determined by the length of sequence $\{a_n\}$. For the given N, K is determined based on the accuracy requirements. Table 4.1 compares the computational cost and relative error of various perturbation schemes. It can be seen that the computational cost is the lowest for the single stage second-order perturbation scheme. However, the error is huge. In this example, the multistage perturbation technique provides good accuracy at modest computational cost.

4.7 Conclusion

NFT pairs can be used to multiplex and demultiplex the signals so that fiber nonlinear impairments can be significantly suppressed in fiber optic communication systems. Currently, in an NFT-based system, the data within a channel are nonlinearly multiplexed using INFT at the transmitter and the channels are multiplexed linearly using the wavelength-division multiplexer. Hence, the nonlinear impairments arising from the interaction with the other channels cannot be compensated in NFT-based systems. If wideband data ($\approx$ Tb/s) is nonlinearly multiplexed using INFT in the optical domain, nonlinear impairments can be significantly suppressed. However, it is hard to realize NFT/INFT in the optical domain. In this chapter, we have developed a technique to evaluate the NFT as a cascade of linear FTs. With the recent development of all-optical DFT operating at Tb/s on a silicon photonics chip, our proposed approach provides a promising way to realize NFT in the optical domain.

We have developed computational techniques to evaluate the NFT using single stage second-order and third-order perturbation techniques and found that the computational cost of the second-order perturbation technique is $O(N \log_2 N)$, whereas that of the third-order technique is significantly higher. However, the third-order technique provides a better accuracy than the second-order technique. Next, we developed a multistage perturbation technique in which the first-order perturbation technique is used in each stage. We found that the accuracy of the multistage perturbation technique is much higher than that of a single stage second-order or third-order technique. The structure of NFT in each stage has a form similar to DFT. We have developed novel FFT-like algorithms to evaluate NFT and found that the total computational cost of NFT is $O(NK \log_2 N/K)$, where K is the number of stages. The N-point FFT can be split into K M-point FFTs, which can be processed by K parallel processors. Hence, the computational cost per processor is $O(N \log_2 M)$.

Chapter 5

Enhanced-Power NFDM Transmission System with Midpoint Optical Phase Conjugation

5.1 Abstract

We investigate the combination of a nonlinear frequency division multiplexed (NFDM) transmission scheme with midpoint optical phase conjugation (OPC), and show that midpoint OPC introduces a power enhancement by compensating for nonlinear impairments. It offers a degree of freedom to have a flexible power normalization factor, P_n. Optimizing P_n helps minimize the signal-noise mixing in nonlinear Fourier transform processing for a specific launch power, resulting in improving the system performance significantly. Mid-OPC NFDM system can provide 4.5 dB and 5.6 dB advantage in Q-factor as compared to the conventional NFDM system when the transmission fiber is standard single-mode fiber and a fiber with the optimum dispersion, respectively. Mid-OPC NFDM can also offer higher spectral efficiency at longer transmission reach due to the shorter guard interval.

5.2 Introduction

Several techniques have been proposed to suppress the signal distortion due to the interplay between nonlinearity and dispersion such as digital back propagation (DBP) (Ip and Kahn, 2008), optical back propagation (OBP) (Bidaki and Kumar, 2020) and optical phase conjugation (OPC) (Pepper and Yariv, 1980). Nonlinear frequency division multiplexed (NFDM) transmission has attracted a great attention recently due to the multiplicative evolution of nonlinear (discrete and continuous) spectral modes over the lossless fiber channel (Hasegawa and Nyu, 1993; Turitsyna and Turitsyn, 2013; Yousefi and Kschischang, 2014; Turitsyn *et al.*, 2017).

It is well-known that midpoint OPC can mitigate fiber dispersion and nonlinear impairments (Pepper and Yariv, 1980) and it has been demonstrated experimentally (Minzioni *et al.*, 2006). In midpoint OPC systems, transmission fibers after the OPC mitigate the dispersion and nonlinearity effects of the fibers preceding the OPC, if there is a power symmetry about the point of phase conjugation. However, due to fiber loss, the power symmetry is broken and signal-signal nonlinear impairments cannot be fully compensated for by midpoint OPC. In (McKinstrie *et al.*, 2003; Kumar and Liu, 2007b), it is shown that the variance of signal-noise nonlinear interaction can be reduced by a factor of 4 using the midpoint OPC for soliton (McKinstrie *et al.*, 2003) and quasi-linear systems (Kumar and Liu, 2007b). In NFDM systems, non-integrable fiber channel due to the loss and noise introduces nonlinear signal-signal interaction and nonlinear signal-noise interaction, leading to system performance degradation. In other words, neither NFDM systems nor midpoint OPC systems are perfect in the presence of fiber loss and noise.

In this chapter, we combine NFDM with midpoint OPC and find that the midpoint OPC can improve significantly the performance of the NFDM system due to the fact that fiber launch power can be enhanced without increasing the nonlinear penalty. In NFDM systems without midpoint OPC, the power normalization factor, P_n is fixed, determined solely by the fiber parameters. However, midpoint OPC could partially compensate for nonlinear

effects and hence, it offers a degree of freedom to choose P_n over a wide range. In addition, midpoint OPC compensates for the fiber dispersion exactly and therefore, the NFDM system with midpoint OPC could have a guard interval (GI) much smaller than that of the NFDM system without OPC, which improves the spectral efficiency significantly for longer reach systems.

5.3 NFDM System with OPC

The block diagram of an NFDM transmission system with midpoint OPC is depicted in Fig. 5.1a. The data is directly encoded on the continuous spectrum (CS), $\tilde{q}_0(\lambda)$, in the nonlinear spectral domain. Next, inverse NFT (INFT) is applied to generate the time domain signal, $q_0(t)$. The fiber-optic link consists of two $N/2$-span subsystems of length $NL_a/2$, where L_a is the span length. The OPC is placed at the middle of the link. At the receiver, after applying digital phase conjugation (DPC) on the time domain signal, forward NFT is performed to recover the nonlinear spectrum. In contrast to conventional NFDM transmission, due to the presence of midpoint OPC, there is no need to remove the phase shift due to dispersion. This can be explained as follows: The evolution of nonlinear Fourier spectrum along the subsystem consisting of the first half of the fiber-optic link can be written as

$$\tilde{q}(\lambda, z) = \tilde{q}_0(\lambda) \exp(-j4\lambda^2 z), \tag{5.1}$$

where $\tilde{q}_0(\lambda)$ and z are the nonlinear spectrum at the transmitter and the normalized distance along the fiber, respectively. The continuous nonlinear spectrum after the OPC is

$$\tilde{q}(\lambda, z_m) = \tilde{q}_0^*(-\lambda) \exp(j4\lambda^2 z_m), \tag{5.2}$$

where $z_m = NL_a/(2L_0)$, distance scale, $L_0 = 2T_0^2/|\beta_2|$ and T_0 is a suitable time scale. Let the conjugated signal propagate through the second half of the fiber-optic link. The nonlinear

spectrum at the end of the link is

$$\tilde{q}_{out}(\lambda) = \tilde{q}(\lambda, z_m) \exp(-j4\lambda^2 z_m). \tag{5.3}$$

Substituting Eq. (5.2) in Eq. (5.3), we obtain the output nonlinear spectrum based on the nonlinear spectrum at the transmitter as

$$\tilde{q}_{out}(\lambda) = \tilde{q}_0^*(-\lambda). \tag{5.4}$$

Thus the nonlinear spectrum of the signal at the output of the link is identical to conjugated nonlinear spectrum of the input signal with $\lambda \to -\lambda$. By taking the complex conjugate of the received signal in the electrical domain at the receiver followed by power normalization and then performing NFT, the input nonlinear spectrum can be retrieved.

5.4 Signal Description and Simulation Results

At the transmitter, after serial to parallel conversion, for block k, the multiplexed continuous nonlinear spectrum in the normalized form is

$$\tilde{q}_k(\lambda) = A \sum_{m=-M/2}^{M/2} c_{m,k} \frac{\sin(\lambda T_s + m\pi)}{\lambda T_s + m\pi} e^{-2jk\lambda T_b}, \tag{5.5}$$

where A is the power control parameter, M is the number of subcarriers, $c_{m,k}$ is the symbol sequence, $T_s = T/T_0$, useful block duration is $T = 1/R_s$, R_s = baud rate per subcarrier, and normalized total block duration, $T_b = GI + T_s$. GI is the guard interval which is in general proportional to the normalized dispersion-induced channel memory, $2\pi\beta_2 B L_t/T_0$, where β_2 is the chromatic dispersion coefficient, B is the signal bandwidth and L_t is the total distance. Since signal propagation along the fiber-optic link with midpoint OPC is effectively non-dispersive, GI can be much smaller than that for a transmission system without OPC. For

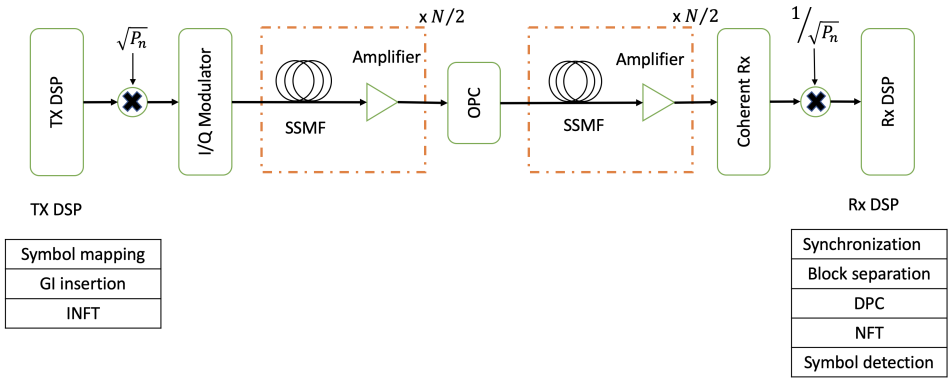

(a)

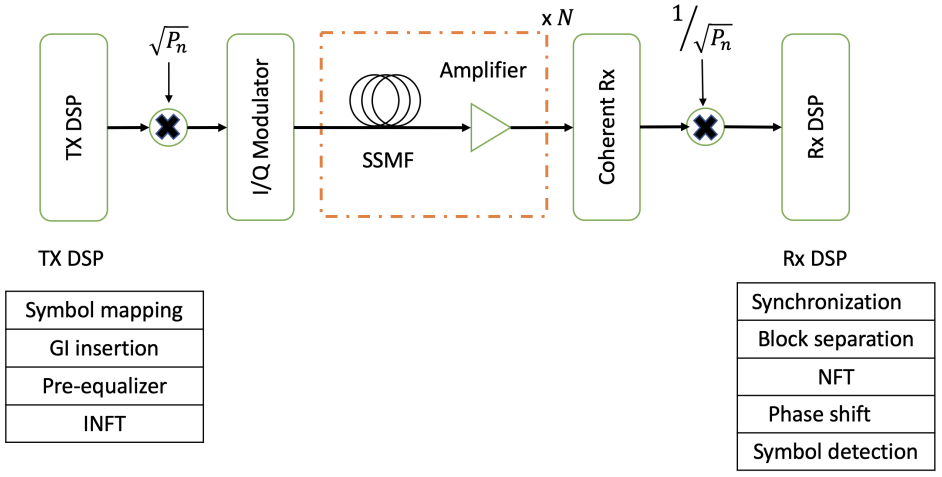

(b)

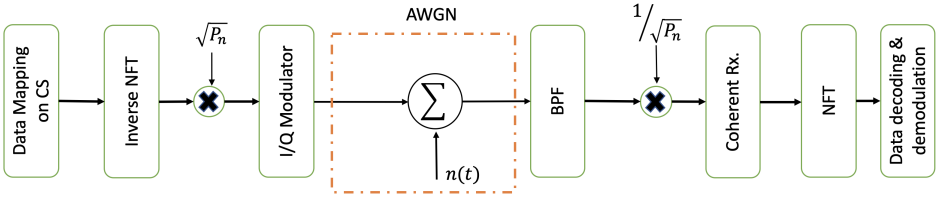

(c)

Figure 5.1: (a): A mid-OPC NFDM transmission system; (b): A conventional NFDM transmission system; (c) Linear channel with NFT-INFT. OPC: optical phase conjugator; DSP: digital signal processing; Rx: receiver; DPC: digital phase conjugator; SSMF: standard single-mode fiber; P_n : power normalization factor; BPF: band-pass filter; AWGN: additive white Gaussian noise.

mid-OPC NFDM system, to keep the impact of tail truncation through the NFT process insignificant, we keep $GI/T_s = 1$.

Figures 5.1b and 5.1c show a 50% dispersion pre-compensated NFDM system (conventional NFDM system) and a system consisting of INFT, linear channel and NFT, respectively. The linear channel is assumed to be additive white Gaussian noise (AWGN) with unity gain. The noise power, P_{noise} is $2\rho\Delta f$, where ρ is the white noise power spectral density, and Δf is the bandwidth of the band-pass filter (BPF). The power normalization factor P_n can be chosen arbitrarily for the linear channel (Fig. 5.1c), whereas it is a constant determined by the dispersion and system parameters for the conventional system (Fig. 5.1b). As for the NFDM system with midpoint OPC, P_n is adjusted to obtain the optimum performance. For the 50% dispersion pre-compensated NFDM system, the nonlinear spectrum is (Le *et al.*, 2018b)

$$\tilde{q}_k^{pre}(\lambda) = Ae^{2j\lambda^2 z_{tot}} \sum_{m=-M/2}^{M/2} c_{m,k} \frac{\sin(\lambda T_s + m\pi)}{\lambda T_s + m\pi} e^{-2jk\lambda T_b}, \tag{5.6}$$

where z_{tot} is the normalized transmission distance. The term $\exp(2j\lambda^2 z_{tot})$ corresponds to performing 50% TX-side digital compensation.

Three systems shown in Fig. 5.1 are simulated using the following parameters, unless otherwise specified. Number of subcarriers = 132, useful block duration, $T = 3.3$ ns, $T_0 = 1$ ns, modulation = 32 QAM. The transmission fiber is standard single-mode fiber (SSMF) whose dispersion, loss and nonlinear coefficients are $\beta_2 = -22$ ps^2/km, $\alpha = 0.2$ dB/km and $\gamma = 1.27$ W^{-1} km^{-1}, respectively. Fiber span length, $L_a = 81.3$ km. The noise figure of EDFA is 5.32 dB. The well-known split-step Fourier techniques is used to solve the NLS equation (Agrawal, 2012). NFT and INFT blocks are simulated using the FNFT toolbox (Wahls *et al.*, 2018).

We study the performance of the NFDM systems with and without OPC in terms of

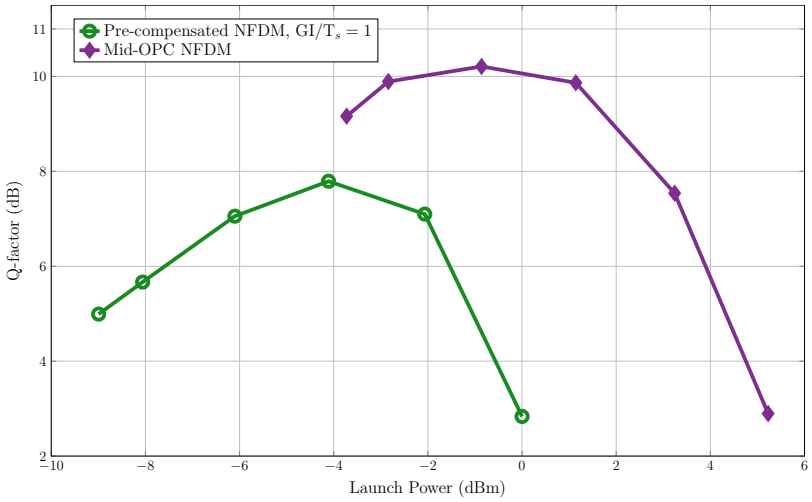

Figure 5.2: Q-factor versus launch power when the transmission distance is 975.6 km and the modulation format is 32 QAM.

Q-factor. The Q-factor is calculated using

$$Q = 20 \log_{10} \left[\sqrt{2}\, \text{erfcinv}(2 \times \text{BER}) \right], \tag{5.7}$$

where the BER is the bit error rate computed by the error counting.

The performance of a 132×0.303 Gbaud mid-OPC NFDM system is compared to a conventional 132×0.303 Gbaud NFDM system in Fig. 5.2 when the transmission distance is 975.6 km. The mid-OPC NFDM system provides 2.5 dB advantage in Q-factor as compared to pre-compensated NFDM. Guard interval, GI, is equal to T_s for both systems. The Q-factor decreases at higher launch powers for both systems which is due to the noise dependency on signal amplitude in nonlinear frequency domain (Yangzhang *et al.*, 2018; Tavakkolnia and Safari, 2017). Next, we extend the reach further. Figure 5.3 shows the Q-factor as a function of launch power when transmission distance is 2439 km. As the reach increases, the GI has to be increased for the conventional pre-compensated NFDM systems since the dispersion-induced channel memory scales linearly with transmission distance. In contrast, midpoint OPC compensates for dispersion and hence, GI need not be changed for a midpoint OPC based NFDM system with longer reach. We keep the $GI/T_s = 1$ for midpoint OPC

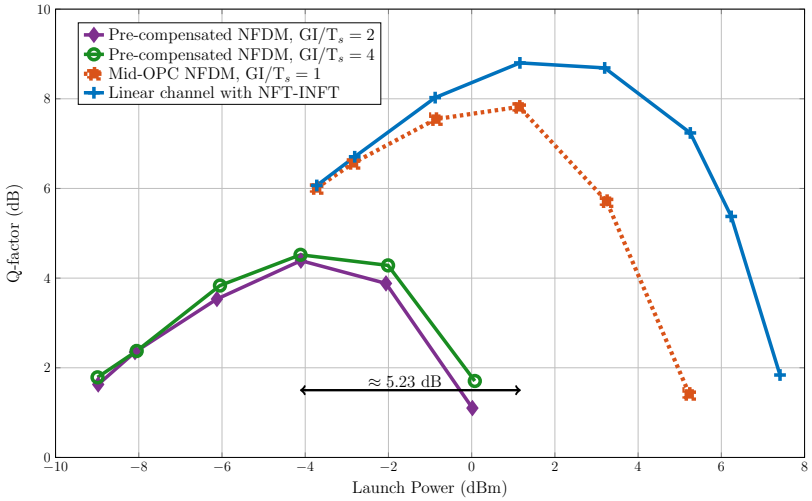

Figure 5.3: Q-factor versus launch power when transmission distance is 2439 km and modulation format = 32 QAM. For each curve, launch power is adjusted by changing the amplitude of nonlinear spectrum A while power normalization factor is fixed.

system and $GI/T_s = 2$ for pre-compensated NFDM system and find that the midpoint OPC provides 3.5 dB advantage in Q-factor as compared to pre-compensated NFDM. When $GI/T_s = 4$ for pre-compensated NFDM system, the performance gets slightly better (by 0.15 dB) which shows that the performance improvement brought by mid-point OPC is not due to its ability to compensate for dispersion. The reason for the performance improvement by midpoint OPC is discussed later. If $GI/T_s = 1$ for pre-compensated NFDM system, the performance degrades significantly with the highest Q-factor dropping to -4 dB due to dispersion-induced ISI between blocks. Although the signal tail grows with power (Turitsyn *et al.*, 2017), we kept the same GI for all the launch powers which is long enough to avoid the interference between the adjacent blocks. Since the overhead due to GI is minimum for the midpoint OPC system, it offers high spectral efficiency at longer transmission reach; spectrum efficiency of 2.5 bits/s/Hz in mid-OPC NFDM as compared to 1.66 bits/s/Hz in NFDM transmission system over 2439 km.

It is also noted in both Figs. 5.3 and 5.2 that the optimum power in mid-OPC NFDM is higher than that in conventional NFDM. It can be explained as follows: the average power

of the signal for focusing region can be written as

$$P = \frac{P_n E}{T} = \frac{P_n}{\pi T} \int \log(1 + |\tilde{q}(\lambda)|^2)\, d\lambda, \tag{5.8}$$

where E is the normalized signal energy. So, for a signal of given width and and also a given modulation format, the launch power can be changed either by changing the amplitude of nonlinear spectrum, A (see Eq. 5.5 or 5.6) or by power normalization factor, P_n. P_n is determined by the physical characteristics of the optical link and it can be different from one system to another. For a given system (in the absence of OPC), P_n is fixed and the fiber launch power can be changed only by changing the amplitude A of the nonlinear spectrum.

In Fig. 5.3, we see that the optimum launch power for the mid-OPC NFDM system is ≈ 5.23 dB higher than that of the conventional NFDM system. This power shift is due to the larger P_n for NFDM systems with midpoint OPC. Indeed, in all systems, signals have the same normalized energy E at their optimum launch powers. In conventional NFDM system, power normalization factor, $P_n = \frac{|\beta_2|}{\gamma_{eff} T_0^2}$, where $\gamma_{eff} = \gamma \frac{(1-e^{-\alpha L_a})}{\alpha L_a}$. In mid-point NFDM system, we found $P_n = F \frac{|\beta_2|}{\gamma_{eff} T_0^2}$, where F is the power enhancement factor for NFDM with OPC. The optimum value of the factor F is found to be 5.23 dB through simulations for the parameters of Fig. 5.3. In this figure, the launch power is changed by changing the amplitude A of the normalized nonlinear spectrum while keeping P_n constant. In Fig. 5.3, for linear channel with NFT-INFT, although P_n can be chosen freely, it is kept the same as that for mid-OPC NFDM system. The performance improvement in midpoint OPC system is attributed to the power enhancement factor, F of NFDM system. In mid-OPC NFDM, for a specific signal power, power control parameter A is smaller than that in pre-compensated NFDM system due to a larger power enhancement factor, which results in lower signal-noise mixing in NFT processing for NFDM systems based on midpoint OPC.

Figure 5.3 also shows Q-factor as a function of launch power for a linear channel with NFT-INFT system while keeping the noise power P_{noise} to be the same as that in the NFDM

system with nonlinear fiber channel (Figs. 5.1a and 5.1b). Although the channel is linear, the overall system is nonlinear due to the presence of NFT and INFT. In the linear channel case, as the launch power increases, Q-factor increases initially and then it starts decreasing at higher launch powers. Higher launch powers, in this figure, are associated with larger nonlinear spectrum amplitude, A, resulting in higher signal-noise mixing through NFT block. The optimum Q-factor of the NFDM system with midpoint OPC is 1 dB lower than that of the linear channel with NFT-INFT. However, in the nonlinear region (launch power $\geqslant 2$ dBm), there is a significant performance degradation for the mid-OPC NFDM system as compared to the linear channel with NFT-INFT. This is mainly attributed to the signal-noise nonlinear interactions which are absent in the linear channel. This signal-noise interaction was first studied by Gordon and Mollenauer (1990). The noise field alters the amplitude of the signal which is translated into phase fluctuations due to Kerr effect, leading to nonlinear phase noise (Gordon and Mollenauer, 1990).

It is well known that in the absence of propagation loss and in the absence of noise, midpoint OPC can mitigate fiber dispersion and nonlinear impairments perfectly. Hence, it leads to a flat channel response in nonlinear frequency domain. In general, if the system is symmetric with respect to the location of OPC, the OPC acts as a temporal mirror that produces an ideal image of the transmitted signal, $q^*(t, 0)$ at the receiver. The received signal passes through a digital phase conjugator (DPC) to get $q(t, 0)$. In this case, the fiber-optic channel is linear with its transfer function being unity. The received field amplitude after the DPC is proportional to $\sqrt{EP_n}$. If the signal is divided by $\sqrt{P_n}$ before passing through the receiver, it would be equivalent to placing INFT and NFT back-to-back. In the case of ideal OPC, the power normalization P_n is arbitrary which can be taken as large as needed to have the desired signal-to-noise-ratio (SNR) and E could be chosen to be relatively smaller so that the signal-noise mixing in NFT can be minimized. For example, we could choose A to be small so as to avoid signal-noise mixing in NFT at the receiver, but very large P_n so that the launch power to fiber is large leading to high OSNR.

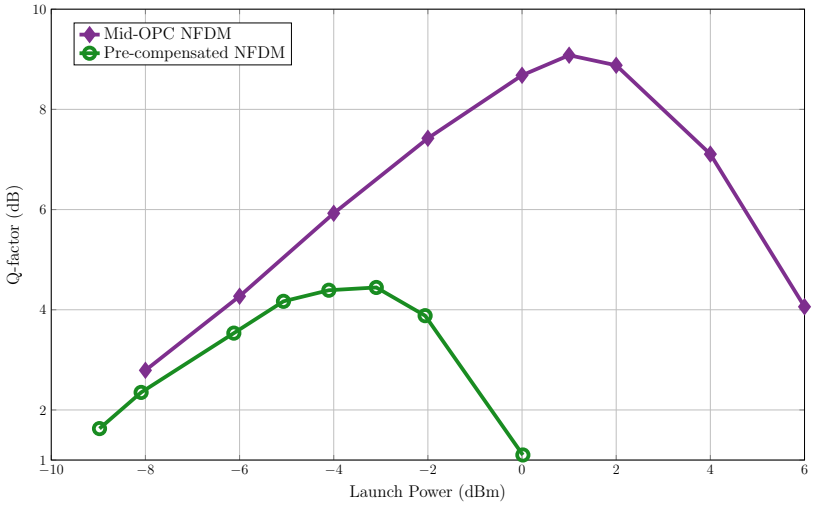

Figure 5.4: Q-factor versus launch power. For mid-point NFDM, launch power is adjusted by optimizing both P_n and A. The design parameters are the same as those of Fig. 5.3. $GI/T_s = 2$ for pre-compensated NFDM.

In the presence of loss, the channel response in nonlinear frequency domain is not perfectly flat. However, by using the path-averaged normalization rule, the flat channel filter is a good approximation (Yangzhang *et al.*, 2018). Indeed, the nonlinear fiber-optic channel with midpoint OPC behaves more like a linear channel. Hence, midpoint OPC can offer a degree of freedom to have a flexible P_n. The error between the exact model and the path-averaged approximation grows linearly with power (Yangzhang *et al.*, 2018) which can also explain the performance degradation at higher powers. The fiber launch power $P_{launch} \propto P_n E$. In Figs. 5.3 and 5.2, the launch power is varied by changing E while keeping P_n to be a constant. Figure 5.4 shows the Q-factor as a function of the launch power by optimizing both E and P_n for a specific launch power. As can be seen, the mid-point NFDM system provides 4.5 dB performance advantage over the conventional NFDM system. In contrast, the improvement in Q-factor is only 3.5 dB in Fig. 5.3.

So far we assumed that the transmission fiber is SSMF. Next, we would like to explore the performance of mid-OPC NFDM system when the dispersion is varied. Figure 5.5 shows the dependence of ΔQ on the fiber dispersion $|\beta_2|$. ΔQ is defined as ΔQ (dB) = Q (dB)$-$ Q_{ref} (dB), where Q_{ref} (dB) is the optimum Q-factor of the conventional NFDM system with

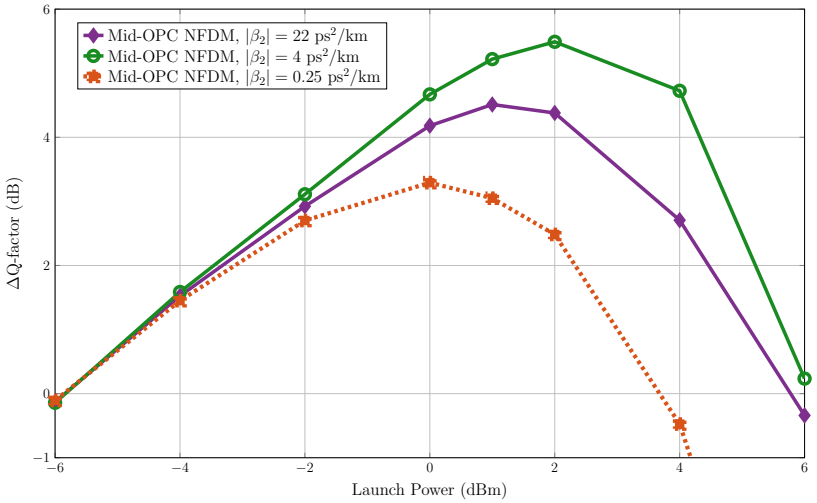

Figure 5.5: ΔQ-factor versus launch power when β_2 is varied. For mid-point NFDM, launch power is adjusted by optimizing both P_n and A. The other design parameters are the same as those of Fig. 5.4.

SSMF as the transmission fiber. This reference is chosen because if the absolute dispersion is further decreased, the performance only gets worse for conventional NFDM systems. The launch power shown in X-axis is obtained by optimizing both E and P_n for a specific launch power. As the absolute dispersion $|\beta_2|$ decreases, the optimum ΔQ (dB) increases initially and then it starts decreasing. This is because in the absence of dispersion, midpoint OPC compensates exactly for signal-signal nonlinear interactions even in the presence of fiber loss. However, if β_2 is close to zero, signal-noise nonlinear interaction increases (Gordon and Mollenauer, 1990) and as $|\beta_2|$ becomes large, it can be suppressed significantly (Kumar, 2005). From Fig. 5.5, we conclude that there exists a dispersion at which the sum of signal-signal nonlinear interaction and signal-noise nonlinear interaction are minimum for the mid-OPC NFDM system. In contrast, in conventional NFDM systems, the performance improves monotonically with $|\beta_2|$ because the power normalization factor P_n is proportional to $|\beta_2|$. In NFDM system with OPC, if A, P_n and β_2 are optimum, it provides a performance advantage of 5.6 dB over conventional NFDM system. Therefore, non-zero dispersion shifted fibers (NZDSF) are likely to show performance advantages for NFDM system with midpoint OPC as compared to SSMF.

5.5 Conclusion

In conclusion, we have analyzed the performance of a NFDM system with midpoint OPC and found that it gives a performance advantage of 4.5 dB in Q-factor over a NFDM system without OPC, if the transmission fiber is the SSMF. If the fiber dispersion is optimized, the performance improvement can be further improved up to 5.6 dB. Since the dispersion is fully compensated in NFDM system with midpoint OPC, the guard interval could be much smaller, which enhances spectral efficiency.

Chapter 6

Conclusion and Future Work

6.1 Conclusion

The main obstacle to improve the information-transmitting capacity of an optical fiber is the nonlinear impairments due to the interplay between dispersion, inherent nonlinearity of the fiber and noise. This thesis has focused on overcoming these limiting factors to enhance the capacity and/or transmission reach of the fiber-optic system by adopting two different approaches:

(i) In the first approach, this thesis dealt with an optical signal processing technique to suppress the dispersion and nonlinear effects of the transmission fiber in real time. An optical back propagation (OBP) scheme using distributed Raman amplification in dispersion compensating fibers (DCFs) was investigated. In OBP, virtual fibers of DBP are replaced by real fibers/photonic devices. Since optical fibers with negative nonlinear coefficient are not available, the conjugation of the transmission signals is needed before the OBP module. Therefore, an optical phase conjugator (OPC) is placed at the beginning of the OPB module, and then the conjugated signal passes through the OBP module which consists of amplifiers and a Raman pumped DCF. An analytical expression for the power profile required by the ideal OBP condition to fully compensate for the nonlinear effects (both intra-

and inter-channel nonlinearities) was derived. In order to suppress the nonlinear effects of the transmission fibers exactly, the loss coefficient of the OBP fiber has to be a negative constant or equivalently the power in the OBP fiber should increase exponentially with distance. This condition can be approximately fulfilled by using Raman pumping of the DCF. In the case of forward or backward power pumping, the power in the DCF deviates from that required by the ideal OBP due to the pump attenuation. Therefore, an OPB scheme based on bidirectional pumping which provides the closest power profile to the ideal power profile was proposed. To realize the OBP, two possible configurations were introduced and compared. The simulation results have shown that bidirectional pumping OBP scheme outperforms single-channel DBP and wideband DBP by 7.7 dB and 5 dB in Q-factor, respectively, when transmission distance is 5000 km for a 5-channel WDM system with QAM-64 and a baud rate of 28 GBaud/channel. Numerical simulations also have predicted that the proposed OBP technique can provide more than a ten-fold enhancement in the transmission reach as compared to single-channel DBP.

(ii) As the second approach, this thesis adopted nonlinear Fourier transform (NFT) as a promising framework to embrace the fiber nonlinearity as an essential design element. This part has been carried out through different parts, starting from the mathematical and theoretical framework, going though the development of computational algorithms, and finally the investigation of a nonlinear frequency division multiplexed (NFDM) transmission system.

- After an overview on integrable PDEs and the NFT, the theoretical aspects of the NFT for optical communication purpose regarding the NLSE with vanishing boundary conditions—essential for the realization of NFDM—was studied. It has been shown that nonlinear spectrum keeps invariant and nonlinear spectral amplitudes evolve multiplicatively without mutual interaction as the optical signal propagates down the fiber. Finally, NFDM transmission systems which use the NFT to encode data on the nonlinear spectra were discussed.

- Computational techniques to compute the NFT were developed and the accuracy and

computational cost of single stage second-order and third-order perturbation techniques were compared. As the order of the perturbation technique is increased, the accuracy can be improved, but at the cost of computational complexity. Hence, for the first time to our knowledge, a multistage perturbation technique to realize the NFT was proposed. In each stage, a first-order perturbation technique is used and the output of the current stage is used as the input of the next stage. The accuracy of the multistage perturbation technique has been found to be much higher than that of single stage technique. A new fast Fourier transform (FFT)-like algorithm was developed to reduce the computational complexity of the multistage perturbation technique. The digital implementation of the proposed technique can also be processed on parallel processors, resulting in the computational cost reduction.

In NFT-based multi-channel systems, the inter-channel nonlinear impairments can be compensated if channels are multiplexed/demultiplexed nonlinearly using the INFT and NFT, respectively, in the optical domain. Linear Fourier transform (FT) can be easily implemented in the optical domain using a time lens or discrete photonic components. The proposed multistage technique provides a promising way to realize the NFT in optical domain since the structure of NFT in each stage has a form similar to linear FT.

- An NFDM transmission scheme in which an NFT pair is employed to multiplex and demultiplex the data, with midpoint OPC was investigated. The beauty of NFDM theory is spoiled in practice by non-integrable fiber channel due to the loss and noise which introduce nonlinear interactions. Currently, NFDM systems slightly outperform (≈ 1 dB) their linear counterparts, OFDM. For a given system, to increase the signal power, one should increase the energy of the normalized field E since the power normalization factor P_n which depends on fiber parameters is fixed. However, the larger value of E leads to penalty due to signal-noise mixing in NFT at the receiver which degrades the system performance.

The proposed mid-OPC NFDM system provides some flexibility in terms of optimization. The OPC acts as a temporal mirror that gives the phase-conjugated temporal "image" of the transmitted signal at the receiver if the system is symmetric with respect to the location of OPC. The received signal passes through a digital phase conjugator (DPC) to get the input signal. In this case (and in the absence of noise), the fiber optic channel is linear with its transfer function being unity, that is, it would be equivalent to placing INFT and NFT back-to-back. In the case of ideal OPC, the power normalization P_n is arbitrary which can be chosen as large as needed to have the desired signal-to-noise-ratio (SNR) and E could be relatively small so that the signal-noise mixing in NFT can be minimized. Although, in practice, the OPC does not produce the ideal "image" due to the loss and noise and the channel is not fully linear, it still offers a flexibility to choose P_n over a wide range. Simulation results have shown that using mid-OPC NFDM and standard single-mode fiber (SSMF), the performance can be improved by 4.5 dB relative to the conventional NFDM system without OPC.

The performance of the proposed scheme was compared with that of a linear channel (with signals multiplexed/demultiplexed nonlinearly using INFT/NFT) which provides an upper bound on the achievable performance of a realistic mid-OPC NFDM system. It has been also investigated how dispersion map can help to improve the performance of the system.

Another important contribution of this work is that mid-OPC NFDM extends the transmission reach without having to increase the guard interval which enables higher spectral efficiency.

6.2 Future Work

This thesis provided theoretical analysis and simulation results for the optical back propagation scheme. The experimental validation of the proposed OBP is of considerable interest

which can measure the performance of the OBP to compensate for nonlinear impairments.

To develop an OBP scheme, we have focused on proposing the concept with dominant effects and neglecting other impairments. We expect that the impairments such as single/double Rayleigh back scattering may cause a couple of dBs penalty, although the improvement due to optical backpropagation with bidirectional pumping would still be significant. To consider the impact of these impairments, further analytical/numerical simulations should be done to find the optimum design parameters and minimize the penalty due to these impairments.

Another interesting research topic is to investigate advanced pumping schemes such as higher-order Raman pumping in order to achieve the ideal power profile in OBP module with reduced noise figure.

The results obtained in this thesis together with several excellent researches conducted by other research groups in the last few years, are the first important steps towards understanding NFDM systems. In spite of the potential of NFDM to offer advantages in terms of nonlinearity resilience, it is still far from being a mature technology. There are many challenges and interesting topics about NFDM that need to be studied: The development of optical NFT/INFT is crucial to effectively utilize the full bandwidth of the optical fiber in NFT-based systems. The experimental demonstration of the proposed NFT as the cascade of linear FTs using discrete photonic components or in silicon photonics will be of significant importance.

The huge performance improvement in NFDM provided by midpoint OPC in this thesis suggests that developing techniques to reduce signal-noise mixing in NFT block can be a fruitful line of investigation. In addition, to avoid the approximation error from the path-average model, further fundamental models that describe noise interaction together with loss, which make the NLSE non-integrable, on nonlinear spectrum are essential in order to mitigate these non-ideal effects.

Furthermore, the range of power enhancement factor F in mid-OPC NFDM in general

depends on the fiber parameters and also the energy of the normalized signal. It is a challenging task to obtain an analytical expression for the range of F which can be the subject of a future work.

Bibliography

Ablowitz, M. J. and Herbst, B. M. (1990). On homoclinic structure and numerically induced chaos for the nonlinear Schrödinger equation. *SIAM Journal on Applied Mathematics*, **50**(2), 339–351.

Ablowitz, M. J. and Ladik, J. F. (1976). Nonlinear differential-difference equations and Fourier analysis. *Journal of Mathematical Physics*, **17**(-), 1011–1018.

Ablowitz, M. J. and Segur, H. (1981). Solitons and the inverse scattering transform. *Siam, Studies in Applied Mathematics, Philadelphia, PA*, **4**.

Ablowitz, M. J., Prinari, B., and Trubatch, A. D. (2003). *Discrete and Continuous Nonlinear Schrödinger Systems*. London Mathematical Society Lecture Note Series. Cambridge University Press.

Ablowitz, M. J., Prinari, B., and Trubatch, A. D. (2004). Integrable nonlinear Schrödinger systems and their soliton dynamics. *Dynamics of PDE*, **1**(3), 239–299.

Agrawal, G. P. (2012). *Nonlinear Fiber Optics*. Academic Press, 5th edition.

Antos, A. J. and Smith, D. K. (1994). Design and characterization of dispersion compensating fiber based on the LP/sub 01/ mode. *Journal of Lightwave Technology*, **12**(10), 1739–1745.

Aref, V., Bulow, H., Schuh, K., and Idler, W. (2015). Experimental demonstration of nonlinear frequency division multiplexed transmission. In *2015 European Conference on Optical Communication (ECOC)*, pages 1–3.

Aref, V., Le, S. T., and Buelow, H. (2016). Demonstration of fully nonlinear spectrum modulated system in the highly nonlinear optical transmission regime. In *ECOC 2016 - Post Deadline Paper; 42nd European Conference on Optical Communication*, pages 1–3.

Aref, V., Le, S. T., and Bulow, H. (2017). Does the cross-talk between nonlinear modes limit the performance of NFDM systems? In *European Conf. on Opt. Commun.*, pages 1–3.

Aref, V., Le, S. T., and Buelow, H. (2018). Modulation over nonlinear Fourier spectrum: Continuous and discrete spectrum. *Journal of Lightwave Technology*, **36**(6), 1289–1295.

Asif, R., Lin, C.-Y., and Schmauss, B. (2011). *Digital Backward Propagation: A Technique to Compensate Fiber Dispersion and Non-Linear Impairments.* Applications of Digital Signal Processing, InTech, InTech-Book Publisher 2011.

Bajaj, V., Chimmalgi, S., Aref, V., and Wahls, S. (2020). Exact NFDM transmission in the presence of fiber-loss. *Journal of Lightwave Technology*, **38**(11), 3051–3058.

Bidaki, E. and Kumar, S. (2018). Multi-stage perturbation technique based nonlinear Fourier transform for fiber optic systems. In *2018 Photonics North (PN)*, pages 1–2.

Bidaki, E. and Kumar, S. (2018). Nonlinear Fourier transform using multistage perturbation technique for fiber-optic systems. *Journal of the Optical Society of America B*, **35**(9), 2286–2293.

Bidaki, E. and Kumar, S. (2020). Enhanced-power NFDM transmission system with mid-point optical phase conjugation. *Optics Letters*, **45**(17), 4682–4685.

Bidaki, E. and Kumar, S. (2020). A Raman-pumped dispersion and nonlinearity compensating fiber for fiber optic communications. *IEEE Photonics Journal*, **12**(1), 1–17.

Buelow, H., Aref, V., and Idler, W. (2016). Transmission of waveforms determined by 7 eigenvalues with PSK-modulated spectral amplitudes. In *ECOC 2016; 42nd European Conference on Optical Communication*, pages 1–3.

Bulow, H. (2014). Experimental assessment of nonlinear Fourier transformation based detection under fiber nonlinearity. In *2014 The European Conference on Optical Communication (ECOC)*, pages 1–3.

Bulow, H. (2015). Experimental demonstration of optical signal detection using nonlinear Fourier transform. *Journal of Lightwave Technology*, **33**(7), 1433–1439.

Burtsev, S., Camassa, R., and Timofeyev, I. (1998). Numerical algorithms for the direct spectral transform with applications to nonlinear Schrödinger type systems. *Journal of Computational Physics*, **147**(1), 166–186.

Cartledge, J. C., Guiomar, F. P., Kschischang, F. R., Liga, G., and Yankov, M. P. (2017). Digital signal processing for fiber nonlinearities [invited]. *Opt. Express*, **25**(3), 1916–1936.

Chassaing, R. and Reay, D. S. (2008). *Digital Signal Processing and 523 Applications with the TMS320C6713 and TMS320C6416 DSK 524*. Wiley, 2nd edition.

Civelli, S., Forestieri, E., and Secondini, M. (2017). Why noise and dispersion may seriously hamper nonlinear frequency-division multiplexing. *IEEE Photonics Technology Letters*, **29**(16), 1332–1335.

Civelli, S., Forestieri, E., and Secondini, M. (2018). Decision-feedback detection strategy for nonlinear frequency-division multiplexing. *Opt. Express*, **26**(9), 12057–12071.

Derevyanko, S. A., Prilepsky, J. E., and Turitsyn, S. K. (2016). Capacity estimates for optical transmission based on the nonlinear Fourier transform. *Journal of Lightwave Technology*, **7**(12710), 662–701.

Dong, Z., Hari, S., Gui, T., Zhong, K., Yousefi, M. I., Lu, C., Wai, P. A., Kschischang, F. R., and Lau, A. P. T. (2015). Nonlinear frequency division multiplexed transmissions based on NFT. *IEEE Photonics Technology Letters*, **27**(15), 1621–1623.

Du, L. B. and Lowery, A. J. (2010). Improved single channel backpropagation for intra-channel fiber nonlinearity compensation in long-haul optical communication systems. *Opt. Express*, **18**(16), 17075–17088.

Emori, Y., Akasaka, Y., and Namiki, S. (1998). Broadband lossless DCF using Raman amplification pumped by multichannel WDM laser diodes. *Electron. Lett.*, **34**(22), 2145–2146.

Essiambre, R. . and Winzer, P. J. (2005). Fibre nonlinearities in electronically pre-distorted transmission. In *2005 31st European Conference on Optical Communication, ECOC 2005*, volume 2, pages 191–192 vol.2.

Essiambre, R. ., Mikkelsen, B., and Raybon, G. (1999). Intra-channel cross-phase modulation and four-wave mixing in high-speed TDM systems. *Electronics Letters*, **35**(18), 1576–1578.

Essiambre, R., Kramer, G., Winzer, P. J., Foschini, G. J., and Goebel, B. (2010). Capacity limits of optical fiber networks. *Journal of Lightwave Technology*, **28**(4), 662–701.

FaddeevLeon, L. D. and Takhtajan, A. (2007). *Hamiltonian Methods in the Theory of Solitons*. Springer, Berlin, Heidelberg.

Fisher, R. A., Suydam, B. R., and Yevick, D. (1983). Optical phase conjugation for time-domain undoing of dispersive self-phase-modulation effects. *Opt. Lett.*, **8**(12), 611–613.

Fludger, C. R. S., Handerek, V., and Mears, R. J. (2001). Pump to signal RIN transfer in Raman fiber amplifiers. *J. Lightwave Technol.*, **19**(8), 1140–1148.

Foo , B., Corcoran , B., Zhu, C., and Lowery, A. J. (2016). Distributed nonlinear compensation of dual-polarization signals using optoelectronics. *IEEE Photon. Technol. Lett.*, **28**(20), 2141–2144.

Foo, B., Corcoran, B., and Lowery , A. J. (2018). Distributed nonlinear compensation using optoelectronic circuits. *J. Lightw. Technol.*, **36**(6), 1326–1339.

Frumin, L. L., Belai, O. V., Podivilov, E. V., and Shapiro, D. A. (2015). Efficient numerical method for solving the direct Zakharov-Shabat scattering problem. *J. Opt. Soc. Am. B*, **32**(2), 290–296.

Galdino, L., Semrau, D., Lavery, D., Saavedra, G., Czegledi, C. B., Agrell, E., Killey, R. I., and Bayvel, P. (2017). On the limits of digital back-propagation in the presence of transceiver noise. *Opt. Express*, **25**(4), 4564–4578.

Gao, Y., Karar, A. S., Cartledge, J. C., Yam, S. S. ., O'Sullivan, M., Laperle, C., Borowiec, A., and Roberts, K. (2014). Simplified nonlinearity pre-compensation using a modified summation criteria and non-uniform power profile. In *OFC 2014*, pages 1–3.

Gardner, C. S., Greene, J. M., Kruskal, M. D., and Miura, R. M. (1967). Method for solving the Korteweg-deVries equation. *Phys. Rev. Lett.*, **19**, 1095–1097.

Gordon, J. P. and Mollenauer, L. F. (1990). Phase noise in photonic communications systems using linear amplifiers. *Opt. Lett.*, **15**(23), 1351–1353.

Gu, C., Hu, H., and Zhou, Z. (2005). *Darboux Transformations in Integrable Systems*. Mathematical Physics Studies. Springer Netherlands.

Guan, P., Røge, K. M., Lillieholm, M., Galili, M., Hu, H., Morioka, T., and Oxenløwe, L. K. (2017). Time lens-based optical Fourier transformation for all-optical signal processing of spectrally-efficient data. *J. Lightwave Technol.*, **35**(4), 799–806.

Gui, T., Lu, C., Lau, A. P. T., and Wai, P. K. A. (2017). High-order modulation on a single discrete eigenvalue for optical communications based on nonlinear Fourier transform. *Opt. Express*, **25**(17), 20286–20297.

Gui, T., Zhou, G., Lu, C., Lau, A. P. T., and Wahls, S. (2018). Nonlinear frequency division multiplexing with b-modulation: shifting the energy barrier. *Opt. Express*, **26**(21), 27978–27990.

Hansen, P. B., Jacobovitz-Veselka, G., Gruner-Nielsen, L., and Stentz, A. J. (1998). Raman amplification for loss compensation in dispersion compensating fibre modules. *Electron. Lett.*, **34**(11), 1136–1137.

Hasegawa, A. and Kodama, Y. (1990). Guiding-center soliton in optical fibers. *Opt. Lett.*, **15**(24), 1443–1445.

Hasegawa, A. and Matsumoto, M. (2003). *Optical solitons in fibers*. Springer, 3th edition.

Hasegawa, A. and Nyu, T. (1993). Eigenvalue communication. *Journal of Lightwave Technology*, **11**(3), 395–399.

Hasegawa, A. and Tappert, F. (1973). Transmission of stationary nonlinear optical pulses in dispersive dielectric fibers. I. anomalous dispersion. *Applied Physics Letters*, **23**(3), 142–144.

Hill, K. O., Bilodeau, F., Malo, B., Kitagawa, T., Thériault, S., Johnson, D. C., Albert, J., and Takiguchi, K. (1994). Chirped in-fiber Bragg gratings for compensation of optical-fiber dispersion. *Opt. Lett.*, **19**(17), 1314–1316.

Hillerkuss, D., Winter, M., Teschke, M., Marculescu, A., Li, J., Sigurdsson, G., Worms, K., Ezra, S. B., Narkiss, N., Freude, W., and Leuthold, J. (2010). Simple all-optical FFT scheme enabling Tbit/s real-time signal processing. *Opt. Express*, **18**(9), 9324–9340.

Hirooka, T. and Nakazawa, M. (2006). Optical adaptive equalization of high-speed signals using time-domain optical Fourier transformation. *J. Lightwave Technol.*, **24**(7), 2530.

Inoue, K., Nakanishi, K., Oda, K., and Toba, H. (1994). Crosstalk and power penalty due to fiber four-wave mixing in multichannel transmissions. *Journal of Lightwave Technology*, **12**(8), 1423–1439.

Ip, E. and Kahn, J. M. (2008). Compensation of dispersion and nonlinear impairments using digital backpropagation. *Journal of Lightwave Technology*, **26**(20), 3416–3425.

Iqbal, M. A., Tan, M., and Harper, P. (2018). On the mitigation of RIN transfer and transmission performance improvement in bidirectional distributed Raman amplifiers. *J. Lightwave Technol.*, **36**(13), 2611–2618.

Isoe, G. M., Muguro, K. M., and Waswa, D. W. (2013). Noise figure analysis of distributed fibre Raman amplifier. *J. Sci Technol. Research*, **2**(11), 375–378.

Jones, R. T., Gaiarin, S., Yankov, M. P., and Zibar, D. (2018). Noise robust receiver for eigenvalue communication systems. In *2018 Optical Fiber Communications Conference and Exposition (OFC)*, pages 1–3.

Kamalian, M., Prilepsky, J. E., Le, S. T., and Turitsyn, S. K. (2016a). Periodic nonlinear Fourier transform for fiber-optic communications, part I: theory and numerical methods. *Opt. Express*, **24**(16), 18353–18369.

Kamalian, M., Prilepsky, J. E., Le, S. T., and Turitsyn, S. K. (2016b). Periodic nonlinear Fourier transform for fiber-optic communications, part II: eigenvalue communication. *Opt. Express*, **24**(16), 18370–18381.

Kamalian, M., Prilepsky, J. E., Le, S. T., and Turitsyn, S. K. (2017). On the design of NFT-based communication systems with lumped amplification. *Journal of Lightwave Technology*, **35**(24), 5464–5472.

Kaminski, P. M., Da Ros, F., Da Silva, E. P., Clausen, A. T., Forchhammer, S., Oxenløwe, L. K., and Galili, M. (2019). Unrepeatered transmission reach extension by receiver-side all-optical back-propagation. In *2019 24th OptoElectronics and Communications Conference (OECC) and 2019 International Conference on Photonics in Switching and Computing (PSC)*, pages 1–3.

Kazakopoulos, P. and Moustakas, A. L. (2008). Nonlinear schrödinger equation with random Gaussian input: Distribution of inverse scattering data and eigenvalues. *Phys. Rev. E*, **78**, 016603.

Kumar, S. (2001). Intrachannel four-wave mixing in dispersion managed RZ systems. *IEEE Photonics Technology Letters*, **13**(8), 800–802.

Kumar, S. (2005). Effect of dispersion on nonlinear phase noise in optical transmission systems. *Opt. Lett.*, **30**(24), 3278–3280.

Kumar, S. and Deen, M. J. (2014). *Fiber Optic Communications: Fundamentals and Applications*. John Wiley & Sons.

Kumar, S. and Liu, L. (2007a). Reduction of nonlinear phase noise using optical phase conjugation in quasi-linear optical transmission systems. *Opt. Express*, **15**(5), 2166–2177.

Kumar, S. and Liu, L. (2007b). Reduction of nonlinear phase noise using optical phase conjugation in quasi-linear optical transmission systems. *Opt. Express*, **15**(5), 2166–2177.

Kumar, S. and Shao, J. (2013). Optical back propagation with optimal step size for fiber optic transmission systems. *IEEE Photon. Technol. Lett.*, **25**(5), 523–526.

Kumar, S. and Yang, D. (2011). Optical backpropagation for fiber-optic communications using highly nonlinear fibers. *Opt. Lett*, **36**(7), 1038–1040.

Lamb, G. (1980). *Elements of Soliton Theory*. A Wiley-Interscience publication. Wiley.

Lax, P. D. (1968). Integrals of nonlinear equations of evolution and solitary waves. *Communications on Pure and Applied Mathematics*, **21**(5), 467–490.

Le, S. T. (2019). Nonlinear frequency division multiplexing: from single polarization to dual polarization. In *2019 24th OptoElectronics and Communications Conference (OECC) and 2019 International Conference on Photonics in Switching and Computing (PSC)*, pages 1–3.

Le, S. T. and Buelow, H. (2017). 64 x 0.5 Gbaud nonlinear frequency division multiplexed transmissions with high order modulation formats. *J. Lightwave Technol.*, **35**(17), 3692–3698.

Le, S. T., Prilepsky, J. E., and Turitsyn, S. K. (2014). Nonlinear inverse synthesis for high spectral efficiency transmission in optical fibers. *Opt. Express*, **22**(22), 26720–26741.

Le, S. T., Prilepsky, J. E., and Turitsyn, S. K. (2015). Nonlinear inverse synthesis technique for optical links with lumped amplification. *Opt. Express*, **23**(7), 8317–8328.

Le, S. T., Philips, I. D., Prilepsky, J. E., Harper, P., Ellis, A. D., and Turitsyn, S. K. (2016a). Demonstration of nonlinear inverse synthesis transmission over transoceanic distances. *Journal of Lightwave Technology*, **34**(10), 2459–2466.

Le, S. T., Philips, I. D., Prilepsky, J. E., Kamalian, M., Ellis, A. D., Harper, P., and Turitsyn, S. K. (2016b). Equalization-enhanced phase noise in nonlinear inverse synthesis transmissions. In *ECOC 2016; 42nd European Conference on Optical Communication*, pages 1–3.

Le, S. T., Aref, V., and Buelow, H. (2017). Nonlinear signal multiplexing for communication beyond the Kerr nonlinearity limit. *Nature Photonics*, **11**, 570–576.

Le, S. T., Schuh, K., Buchali, F., and Buelow, H. (2018a). 100 Gbps b-modulated nonlinear frequency division multiplexed transmission. In *2018 Optical Fiber Communications Conference and Exposition (OFC)*, pages 1–3.

Le, S. T., Aref, V., and Buelow, H. (2018b). High speed pre-compensated nonlinear frequency-division multiplexed transmissions. *Journal of Lightwave Technology*, **36**(6), 1296–1303.

Lee, K., Thai, C. T., and Rhee, J.-K. K. (2008). All optical discrete Fourier transform processor for 100 Gbps OFDM transmission. *Opt. Express*, **16**(6), 4023–4028.

Li, G. (2009). Recent advances in coherent optical communication. *Adv. Opt. Photon.*, **1**(2), 279–307.

Li, X., Chen, X., Goldfarb, G., Mateo, E., Kim, I., Yaman, F., and Li, G. (2008). Electronic post-compensation of WDM transmission impairments using coherent detection and digital signal processing. *Opt. Express*, **16**(2), 880–888.

Liang, X. and Kumar, S. (2014). Multi-stage perturbation theory for compensating intra-channel nonlinear impairments in fiber-optic links. *Opt. Express*, **22**(24), 29733–29745.

Liang, X. and Kumar, S. (2015). Correlated digital back propagation based on perturbation theory. *Opt. Express*, **23**(11), 14655–14665.

Liang, X. and Kumar, S. (2016). Optical back propagation for compensating nonlinear impairments in fiber optic links with ROADMs. *Opt. Express*, **24**(20), 22682–22692.

Liang, X. and Kumar, S. (2017). Optical back propagation for fiber optic networks with hybrid EDFA Raman amplification. *Opt. Express*, **25**(5), 5031–5043.

Liang, X., Kumar, S., and Shao, J. (2013). Ideal optical backpropagation of scalar NLSE using dispersion-decreasing fibers for WDM transmission. *Opt. Express*, **21**(23), 28668–28675.

Liang, X., Kumar, S., Shao, J., Malekiha, M., and Plant, D. V. (2014). Digital compensation of cross-phase modulation distortions using perturbation technique for dispersion-managed fiber-optic systems. *Opt. Express*, **22**(17), 20634–20645.

Lohmann, A. W. and Mendlovic, D. (1992). Temporal filtering with time lenses. *Appl. Opt.*, **31**(29), 6212–6219.

Mateo, E., Zhu, L., and Li, G. (2008). Impact of XPM and FWM on the digital implementation of impairment compensation for WDM transmission using backward propagation. *Opt. Express*, **16**(20), 16124–16137.

Mateo, E. F., Yaman, F., and Li, G. (2010). Efficient compensation of inter-channel nonlinear

effects via digital backward propagation in WDM optical transmission. *Opt. Express*, **18**(14), 15144–15154.

Mateo, E. F., Zhou, X., and Li, G. (2011). Improved digital backward propagation for the compensation of inter-channel nonlinear effects in polarization-multiplexed WDM systems. *Opt. Express*, **19**(2), 570–583.

McKinstrie, C. J., Radic, S., and Xie, C. (2003). Reduction of soliton phase jitter by in-line phase conjugation. *Opt. Lett.*, **28**(17), 1519–1521.

Mecozzi, A. (1994). Limits to long-haul coherent transmission set by the kerr nonlinearity and noise of the in-line amplifiers. *Journal of Lightwave Technology*, **12**(11), 1993–2000.

Mecozzi, A., Clausen, C. B., and Shtaif, M. (2000). System impact of intra-channel nonlinear effects in highly dispersed optical pulse transmission. *IEEE Photonics Technology Letters*, **12**(12), 1633–1635.

Minzioni, P., Cristiani, I., Degiorgio, V., Marazzi, L., Martinelli, M., Langrock, C., and Fejer, M. M. (2006). Experimental demonstration of nonlinearity and dispersion compensation in an embedded link by optical phase conjugation. *IEEE Photon. Technol. Lett.*, **18**(9), 995–997.

Mollenauer, L. F. and Evangelides, S. G. (1990). Wavelength division multiplexing with solitons in ultralong distance transmission using lumped amplifiers. In *Conference on Lasers and Electro-Optics*, page CFI1. Optical Society of America.

Mollenauer, L. F. and Smith, K. (1988). Demonstration of soliton transmission over more than 4000 km in fiber with loss periodically compensated by Raman gain. *Opt. Lett.*, **13**(8), 675–677.

Mollenauer, L. F., Stolen, R. H., and Gordon, J. P. (1980). Experimental observation of Picosecond pulse narrowing and solitons in optical fibers. *Phys. Rev. Lett.*, **45**, 1095–1098.

Morshed, M., Du, L. B., Foo, B., Pelusi, M. D., and Lowery, A. J. (2013). Optical phase conjugation for nonlinearity compensation of 1.21-Tb/s Pol-Mux coherent optical OFDM. In *18th OptoElectronics and Communications Conference, (OECC/PS, 2013)*. Paper PD3-4.

Nakazawa, M., Yamada, E., Kubota, H., and Suzuki, K. (1991). 10 Gbit/s soliton data transmission over one million kilometres. *Electronics Letters*, **27**(14), 1270–1272.

Namiki, S., Tsukiji, N., and Emori, Y. (2004). Pump laser diodes and WDM pumping. In M. N. Islam, editor, *Raman Amplifiers for Telecommunications 1: Physical Principles*, pages 121–160. Springer New York, New York, NY.

Nejadriahi, H., HillerKuss, D., George, J. K., and Sorger, V. J. (2017). Integrated all-optical fast Fourier transform: Design and sensitivity analysis.

Nicholson, J. W. (2003). Dispersion compensating Raman amplifiers with pump reflectors for increased efficiency. *J. Lightw. Technol.*, **21**(8), 1758–1762.

Oyama, T., Nakashima, H., Oda, S., Yamauchi, T., Tao, Z., Hoshida, T., and Rasmussen, J. C. (2014). Robust and efficient receiver-side compensation method for intra-channel nonlinear effects. In *OFC 2014*, pages 1–3.

Paré, C., Villeneuve, A., Bélanger, P.-A., and Doran, N. J. (1996). Compensating for dispersion and the nonlinear Kerr effect without phase conjugation. *Opt. Lett.*, **21**(7), 459–461.

Pelusi, M. D. (2013). WDM signal all-optical pre-compensation of the fiber nonlinearity in dispersion-managed links. *IEEE Photon. Technol. Lett.*, **25**(1), 71–74.

Pepper, D. and Yariv, A. (1980). Compensation for phase distortions in nonlinear media by phase conjugation. *Opt. Lett.*, **5**(2), 59–60.

Poggiolini, P. (2012). The GN model of non-linear propagation in uncompensated coherent optical systems. *Journal of Lightwave Technology*, **30**(24), 3857–3879.

Prilepsky, J. E., Derevyanko, S. A., and Turitsyn, S. K. (2013). Nonlinear spectral management: Linearization of the lossless fiber channel. *Opt. Express*, **21**(20), 24344–24367.

Prilepsky, J. E., Derevyanko, S. A., Blow, K. J., Gabitov, I., and Turitsyn, S. K. (2014). Nonlinear inverse synthesis and eigenvalue division multiplexing in optical fiber channels. *Phys. Rev. Lett.*, **113**, 013901.

Rahbarfam, S. and Kumar, S. (2019). Nonlinear phase noise reduction using digital back propagation and midpoint optical phase conjugation. *Opt. Express*, **27**(6), 8968–8982.

Roberts, K., Li, C., Strawczynski, L., O'Sullivan, M., and Hardcastle, I. (2006). Electronic precompensation of optical nonlinearity. *IEEE Photon. Technol. Lett.*, **18**(2), 403–405.

Russel, J. S. (1838). *Report of the committee on waves*, volume 3. Report of the 7th Meeting of British Association for the Advancement of Science.

Ryczkowski, P., Narhi, M., Billet, C., Merolla, J.-M., Genty, G., and Dudley, J. M. (2018). Real-time full-field characterization of transient dissipative soliton dynamics in a mode-locked laser. *Nature Photonics*, **12**(-), 221–227.

Saavedra, G., Semrau, D., Galdino, L., Killey, R. I., and Bayvel, P. (2017). Digital back-propagation for nonlinearity mitigation in distributed Raman amplified links. *Opt. Express*, **25**(5), 5431–5439.

Savory, S. J., Gavioli, G., Torrengo, E., and Poggiolini, P. (2010). Impact of interchannel nonlinearities on a split-step intrachannel nonlinear equalizer. *IEEE Photonics Technology Letters*, **22**(10), 673–675.

Shannon, C. E. (1948). A mathematical theory of communication. *The Bell System Technical Journal*, **27**(3), 379–423.

Shao, J. and Kumar, S. (2012). Optical backpropagation for fiber-optic communications using optical phase conjugation at the receiver. *Opt. Lett*, **37**(15), 3012–3014.

Shao, J., Kumar, S., and Liang, X. (2013). Digital back propagation with optimal step size for polarization multiplexed transmission. *IEEE Photon. Technol. Lett.*, **25**(23), 2327–2330.

Shepelsky, D., Vasylchenkova, A., Prilepsky, J. E., and Karpenko, I. (2020). Nonlinear Fourier spectrum characterization of time-limited signals. *IEEE Transactions on Communications*, **68**(5), 3024–3032.

Solis-Trapala, K., Inoue, T., and Namiki, S. (2014). Nearly-ideal optical phase conjugation based nonlinear compensation system. In *OFC 2014*, pages 1–3.

Sugavanam, S., Kamalian, M., Peng, J., Prilepsky, J. E., and Turitsyn, S. K. (2017). Experimentally characterized nonlinear Fourier transform of a mode-locked fibre laser. In *2017 Conference on Lasers and Electro-Optics Europe European Quantum Electronics Conference (CLEO/Europe-EQEC)*, pages 1–1.

Tao, Z., Dou, L., Yan, W., Li, L., Hoshida, T., and Rasmussen, J. C. (2011). Multiplier-free intrachannel nonlinearity compensating algorithm operating at symbol rate. *J. Lightwave Technol.*, **29**(17), 2570–2576.

Tavakkolnia, I. and Safari, M. (2015). Signaling over nonlinear fibre-optic channels by utilizing both solitonic and radiative spectra. In *2015 European Conference on Networks and Communications (EuCNC)*, pages 103–107.

Tavakkolnia, I. and Safari, M. (2016). Dispersion pre-compensation for NFT-based optical fiber communication systems. In *Conference on Lasers and Electro-Optics*, page SM4F.4. Optical Society of America.

Tavakkolnia, I. and Safari, M. (2017). Capacity analysis of signaling on the continuous spectrum of nonlinear optical fibers. *Journal of Lightwave Technology*, **35**(11), 2086–2097.

Terauchi, H. and Maruta, A. (2013). Eigenvalue modulated optical transmission system based on digital coherent technology. In *2013 18th OptoElectronics and Communications*

Conference held jointly with 2013 International Conference on Photonics in Switching (OECC/PS), pages 1–2.

Tkach, R. W., Chraplyvy, A. R., Forghieri, F., Gnauck, A. H., and Derosier, R. M. (1995). Four-photon mixing and high-speed WDM systems. *Journal of Lightwave Technology*, **13**(5), 841–849.

Tsang, M., Psaltis, D., and Omenetto, F. G. (2003). Reverse propagation of femtosecond pulses in optical fibers. *Opt. Lett.*, **28**(20), 1873–1875.

Turitsyn, S. K., Prilepsky, J. E., Le, S. T., Wahls, S., Frumin, L. L., Kamalian, M., and Derevyanko, S. A. (2017). Nonlinear Fourier transform for optical data processing and transmission: advances and perspectives. *Optica*, **4**(3), 307–322.

Turitsyna, E. G. and Turitsyn, S. K. (2013). Digital signal processing based on inverse scattering transform. *Opt. Lett.*, **38**(20), 4186–4188.

Vasilyev, M., Szalabofka, B., Tsuda, S., Grochocinski , J. M., and Evans , A. F. (2002). Reduction of Raman MPI and noise figure in dispersion-managed fibre. *Electron. Lett.*, **38**(6), 271–272.

Wahls, S. (2017). Generation of time-limited signals in the nonlinear Fourier domain via b-modulation. In *2017 European Conference on Optical Communication (ECOC)*, pages 1–3.

Wahls, S. and Poor, H. V. (2015). Fast numerical nonlinear Fourier transforms. *IEEE Transactions on Information Theory*, **61**(12), 6957–6974.

Wahls, S., Chimmalgi, S., and Prins, P. (2018). FNFT: A Software Library for Computing Nonlinear Fourier Transforms. *The Journal of Open Source Software*, **3**, 597.

Wai, P. K. A. and Menyak, C. R. (1996). Polarization mode dispersion, decorrelation,

and diffusion in optical fibers with randomly varying birefringence. *Journal of Lightwave Technology*, **14**(2), 148–157.

Wang, H. M., Shih, W. T., and Taga, H. (2008). Single fiber based 10.66 Gb/s bidirectional long reach WDM-PON supported by distributed Raman amplifier. In *OECC/ACOFT 2008 - Joint Conference of the Opto-Electronics and Communications Conference and the Australian Conference on Optical Fibre Technology*, pages 1–2.

Watanabe, S. (1994). Cancellation of four-wave mixing in a single-mode fiber by midway optical phase conjugation. *Opt. Lett.*, **19**(17), 1308–1310.

Watanabe, S. and Shirasaki, M. (1996). Exact compensation for both chromatic dispersion and Kerr effect in a transmission fiber using optical phase conjugation. *J. Lightwave Technol.*, **14**(3), 243–248.

Xia, T. J., Wellbrock, G. A., Ming-Fang Huang, Shaoliang Zhang, Yue-Kai Huang, Do-il Chang, Burtsev, S., Pelouch, W., Zak, E., de Pedro, H., Szeto, W., and Fevrier, H. (2014). Transmission of 400G PM-16QAM channels over long-haul distance with commercial all-distributed Raman amplification system and aged standard smf in field. In *OFC 2014*, pages 1–3.

Y. Fan, L. Dou, Z. Tao, Hoshida, T., and Rasmussen, J. C. (2014). A high performance nonlinear compensation algorithm with reduced complexity based on XPM model. In *OFC 2014*, pages 1–3.

Yamazaki, E., Sano, A., Kobayashi, T., Yoshida, E., and Miyamoto, Y. (2011). Mitigation of nonlinearities in optical transmission systems. In *2011 Optical Fiber Communication Conference and Exposition and the National Fiber Optic Engineers Conference*, pages 1–3.

Yang, D. and Kumar, S. (2009). Realization of optical OFDM using time lenses and its comparison with optical OFDM using FFT. *Opt. Express*, **17**(20), 17214–17226.

Yangzhang, X., Aref, V., Le, S. T., Bülow, H., and Bayvel, P. (2018). 400 Gbps dual-polarisation non-linear frequency division multiplexed transmission with b-modulation. In *2018 European Conference on Optical Communication (ECOC)*, pages 1–3.

Yangzhang, X., Lavery, D., Bayvel, P., and Yousefi, M. I. (2018). Impact of perturbations on nonlinear frequency-division multiplexing. *Journal of Lightwave Technology*, **36**(2), 485–494.

Yangzhang, X., Aref, V., Le, S. T., Buelow, H., Lavery, D., and Bayvel, P. (2019a). Dual-polarization non-linear frequency-division multiplexed transmission with b-modulation. *Journal of Lightwave Technology*, **37**(6), 1570–1578.

Yangzhang, X., Le, S. T., Aref, V., Buelow, H., Lavery, D., and Bayvel, P. (2019b). Experimental demonstration of dual-polarization NFDM transmission with b-modulation. *IEEE Photonics Technology Letters*, **31**(11), 885–888.

Yousefi, M. and Yangzhang, X. (2020). Linear and nonlinear frequency-division multiplexing. *IEEE Transactions on Information Theory*, **66**(1), 478–495.

Yousefi, M. I. and Kschischang, F. R. (2014). Information transmission using the nonlinear Fourier transform, part I-III: Mathematical tools. *IEEE Transactions on Information Theory*, **60**(7), 4312–4369.

Zabusky, N. J. and Kruskal, M. D. (1965). Interaction of "solitons" in a collisionless plasma and the recurrence of initial states. *Phys. Rev. Lett.*, **15**, 240–243.

Zaharov, V. and Shabat, A. (1972). Exact theory of two-dimensional selffocusing and one-dimensional selfmodulation of waves in nonlinear media. *Sov. Phys. JETP*, **34**, 62–69.

Zhang, Q. and Chan, T. H. (2015). A spectral domain noise model for optical fibre channels. In *2015 IEEE International Symposium on Information Theory (ISIT)*, pages 1660–1664.